7-2015

Fabrication of Sub-10 nm Metallic Structures via Nanomasking Technique for Plasmonic Enhancement Applications

Stephen Joseph Bauman
University of Arkansas, Fayetteville

Fabrication of Sub-10 nm Metallic Structures via Nanomasking Technique for Plasmonic Enhancement Applications

A thesis submitted in partial fulfillment
of the requirements for the degree of
Master of Science in Microelectronics-Photonics

by

Stephen J. Bauman
Southeast Missouri State University
Bachelor of Science in Engineering Physics, 2013
Southeast Missouri State University
Bachelor of Science in Physics, 2013

July 2015
University of Arkansas

This thesis is approved for recommendation to the Graduate Council.

Dr. Joseph B. Herzog
Thesis Director

Dr. Omar Manasreh
Committee Member

Dr. Ryan Tian
Committee Member

Dr. Rick Wise
Ex-Officio Member

The following signatories attest that all software used in this thesis was legally licensed for use by Stephen Bauman for research purposes and publication.

_____ _____

Mr. Stephen Bauman, Student Dr. Joseph B. Herzog, Thesis Director

This thesis was submitted to http://www.turnitin.com for plagiarism review by the TurnItIn company's software. The signatories have examined the report on this thesis that was returned by TurnItIn and attest that, in their opinion, the items highlighted by the software are incidental to common usage and are not plagiarized material.

_____ _____

Dr. Rick Wise, Program Director Dr. Joseph B. Herzog, Thesis Director

Abstract

One area of nanoscience that has become popular in recent years is the study of optics at the nanoscale. Due to enhanced fabrication techniques, new geometries and improved dimensional resolutions have been allowing the creation of nanostructures for use in this area. Nanoscale geometries cause unique optical effects such as enhancement of the signal's electric field strength at the surface of a substrate. Specifically, structures separated by nanogaps (10 nm and smaller) have been shown to exhibit strong field enhancement within the gaps. This has opened up the potential for surface enhanced spectroscopies, enhanced absorption for photovoltaics, and improved sensing and detection technologies. This work discusses a new fabrication technique to create nanostructures and nanogaps below the resolution limit of the lithography system used, down to sub-10 nm dimensions. This involves a sacrificial mask, and thus has been dubbed the "nanomasking" technique. This technique increases the previously demonstrated capabilities by enabling fabrication of many nanogaps that are below the resolution limit of the lithography system over a wafer-scale area. It also provides the unique ability to create sub-lithography limited nanostructures both with and without adjacent nanogaps. Various geometries have been fabricated using the technique, demonstrating its versatility. Results show promise for the possibility of using nanomasking to create optical enhancement devices. The broad range of fabrication capabilities of the technique may allow it to be useful in many other areas of nanotechnology as well. It makes it easier to fabricate nanostructures across a greater surface area. This is crucial for newly developed nanofabrication methods if they are to benefit future technology or manufacturing processes.

Acknowledgements

I would like to express my gratitude toward my principal investigator and research adviser, Dr. Joseph Herzog, for giving me the opportunity to be a part of and help establish the Plasmonic Nano-optics research group here at the University of Arkansas. He has continued to be a motivational advisor and helpful teacher, and his hard work here has been inspirational.

I would like to thank Dr. Tian, Dr. Manasreh, Dr. Wise, and Ken Vickers for serving on my thesis committee and for the words of advice and laboratory usage that have helped me reach this point. The constant support and wealth of knowledge and experience from Errol Porter, Dick Penhallegon, Brandon Rogers, and Renee Jones-Hearon are also greatly appreciated.

I am grateful for having a great group of graduate and undergraduate students with whom to perform research. I would especially like to thank Desalegn Debu, Avery Hill, and Eric Novak for their collaborative efforts on research and publications. My thanks also go to Gabrielle Abraham for keeping a lighthearted spirit alive in the group and Jonathan Mishler for his motivational talks prior to conference presentations.

I will always be thankful for my family back home for being proud of everything that I have achieved and helping me along the way and my friends at home as well as here in Fayetteville for giving me the support and more often the distractions that I need to keep me sane through graduate school.

This work was supported with start-up funding provided by the University of Arkansas through the Department of Physics, the Fulbright College of Arts and Sciences, and the Vice Provost for Research and Economic Development. Stephen J. Bauman has been supported by the Doctoral Academy Fellowship through the University of Arkansas Graduate School. This work has also been funded in part by the National Science Foundation award number: 1359306.

Dedication

This thesis is dedicated to Courtney, Matt, Mom, and Dad. Thanks for everything. ☺

"If we knew what it was we were doing, it wouldn't be called 'research,' would it?"

- Albert Einstein

Table of Contents

List of Figures

Chapter 1. INTRODUCTION

1.1 Motivation

Nanoscale fabrication techniques are on the forefront of human technological innovation. New methods continue to push the limits of the possible in terms of how small humans can create things that cannot even be seen with an optical microscope. Controllably creating smaller and smaller features over the past five decades has made possible many advances to semiconductor technology [1]–[5], photovoltaics and other light-based electronics [6]–[11], biomedical technology [12]–[15], and materials science [16]–[20]. To truly appreciate the scale of current advancement, one must consider the unit of the nanometer.

Nanotechnology is the science, engineering, and technology that occurs in the range from one to 100 nanometers. A nanometer is one billionth of a meter, a difference of nine orders of magnitude. Take this illustrative example: if a marble had a diameter of one nanometer, planet Earth would be on the order of one meter. This means that extreme precision is required for macroscopic-scale humans to manipulate objects at the nanoscale. Through advances in controlled and self-assembling chemical processes [21]–[23], control of accelerated ions and particles [24]–[27], as well as deposition and etch techniques [28]–[31], humans have been able to extend their scale of precision and technology to this level. This has led to improved scientific understanding of nanoscale phenomena and improved technologies as previously mentioned [32], [33].

At this level, quantum effects tend to take over as opposed to the classical effects seen in macroscopic features. Some material properties such as optical interactions and electrical conductivity change when confined to such small particles and structures. Nanoscale features have been required for the furthering of Moore's law, in which semiconductor transistor

technology continues to decrease in size, allowing for faster and more powerful computing by reducing the necessary path length for device electrons [1], [34], [35]. Creating objects on the scale of biological cells, blood vessels, and proteins opens doors to advanced drug delivery systems and other biomedical technologies [12], [15], [36], [37].

Many recent advances have come from the field of nano-optics or nanophotonics, where the size of nanofeatures (< 100 nm) is smaller than that of the wavelength of visible light (~300 – 700 nm). The interaction of light with solid features at the nanoscale brings about interesting and useful phenomena including overcoming the diffraction limit at this scale. Nanoscale features have been proven capable of increasing the optical signal or absorption in various technologies including photovoltaics [11], [38]–[45], surface-enhanced Raman and other spectroscopies [46]–[52], single molecule detection, , and biosensing. Some such optical effects are increased as nanostructures and nanogaps approach the smaller end of the nanoscale (< 15 nm) [53]–[61].

The increasing number of applications for nanoscale structures and features means that methods of fabrication need to continue to improve. There are various limitations with existing techniques. Self-assembling processes tend to lack control of structure geometry. Lithographic methods are typically limited by the resolution limit of the machine and optics used. Some advanced techniques also tend to require many process steps in order to obtain a single structure on a substrate surface [29], [30], [62]. Many existing methods do not hold much promise for mass production scale fabrication, which is needed in order to be useful for fields that require nanofeatures across a macroscopic area (> mm^2), such as photovoltaics for solar energy generation. There is a strong need for a wafer-scale fabrication technique that allows users to overcome the resolution limit of the lithography technique used with a high degree of geometric

variation at the nanoscale. A versatile technique will involve many possible materials, structure geometries, reduction of process steps, and truly nanoscale features. This will allow scientists and engineers to make advances to nanotechnology and the understanding of nanoscale phenomena as well as to make such advances more economically, quickly, and reliably.

1.2 Photolithography

There are many fabrication techniques used today across the broad field of nanotechnology. Top-down lithographic techniques have become some of the most widely used fabrication techniques in the micro and nanoelectronics industry as well as others. This is largely due to the repeatability and simultaneous patterning capabilities of such methods.

Photolithography uses light, typically ultraviolet (UV) or extreme ultraviolet, along with a predefined mask to pattern a photoresist material. Light shines directly down onto the surface of the sample that has been spin-coated with photoresist. The mask will let light shine through areas of specific shapes so that the resist below will be exposed to light in areas with these same shapes. The resist is sensitive to the exposing light such that chemical changes occur in the material where it has been hit by incoming light. A positive photoresist material is cross-linked prior to exposure, and exposed areas are thus unlinked, allowing these regions to be removed in a development step. This is useful for creating holes with specific shapes in the resist so that a later evaporation step can fill the holes with a metal or other material. Negative resists begin unlinked, and the light causes exposed areas to become cross-linked. This allows for the creation of posts of resist material so that holes may be created in a subsequently evaporated material.

The resolution of photolithography is limited by the diffraction limit of the light being used for exposure. This is demonstrated by the Equation 1.2.1 which gives the minimum feature

dimension that can be resolved with an optical system depending on the wavelength and material parameters. This Abbe diffraction limit is given by,

$$d = \frac{\lambda}{2n \sin \theta} \qquad \text{Equation (1.2.1)}$$

where d is the minimum feature size that can be resolved, λ is the wavelength used, n is the refractive index of the material in which the focusing system is working, and θ is the converging angle of the light. Thus, shorter wavelength light is desired. After extreme UV light, however, x-rays become too difficult to control with conventional lens systems and can be expensive, requiring access to a synchrotron radiation facility [63]–[65]. Shorter wavelength light than this is simply too energetic and can damage samples and equipment typically used in electronics today. Such high energy light can also be dangerous to those who would use the lithography equipment regularly.

1.3 Electron Beam Lithography

The resolution of an imaging or photolithography patterning system may be improved by using electrons as the source of exposure in place of light. This is due to the fact that the wavelength of an electron depends upon its energy as demonstrated by,

$$\lambda_e = \frac{h}{\sqrt{2meV_{acc}}} \qquad \text{Equation (1.3.1)}$$

for the DeBroglie wavelength, λ_e in meters, h is Planck's constant, m is the electron mass, and e is the electron charge, with a known accelerating voltage, V_{acc}. [66]

The DeBroglie wavelength of an electron is in the range of three orders of magnitude less than the wavelength of light of the same energy. Visible light is around 600 nm while an electron's wavelength is closer to 0.006 nm (6 picometers) when accelerated to 200 keV. Thus, accelerating electrons to tens or hundreds of keV gives them wavelengths that allow for imaging

and patterning at much higher resolution than that of even extreme ultraviolet light. This is the premise behind both electron microscopy techniques and electron beam lithography (EBL) [25], [67].

An electron beam lithography system is essentially a scanning electron microscope (SEM) where the microscope beam is controlled by a computer to which a computer-aided design (CAD) file has been uploaded. EBL works without need of a mask unlike photolithography. Electrons are ejected from a filament at one end of an evacuated column and they are accelerated to the other end of the column by a voltage difference between the cathode and an anode positioned down the column, similar to the method used in large linear particle accelerators. Magnetic lenses help to steer and focus the beam within the column.

The electron beam is controlled by the magnets in the column to raster across the areas desired for exposure and the sample stage can be moved mechanically to cover distances to which the beam cannot be shifted. To pattern a 1x1 μm area takes on the order of a second with electron beam lithography. Thus, the electron beam lithography process is slow when patterning a large area (mm^2 and greater) compared to photolithography's instantaneous exposure of an entire sample. The benefit lies in the resolution of the smallest features that can be patterned, which is commonly below 100 nm. While many EBL systems today are capable of producing electron beam spot sizes on the order of single nanometers, the lithography resolution is limited by the developed e-beam resist. Scattering of electrons in the resist material can cause widening of the linewidths of developed patterns, as more of the resist becomes exposed than the area to which the beam is focused [67]–[69].

The most commonly used resist material for electron beam lithography is polymethylmethacrylate (PMMA), which is a positive type of resist. Upon exposure by an

accelerated beam of electrons, the cross-linked monomers are broken apart so that the affected areas can be washed away using a chemical development process. The common developer for use with PMMA is a 1:3 methyl-isobutyl-ketone (MIBK): isopropanol (IPA) solution.

Figure 1.3.1 depicts the electron beam lithography process. First, the electron beam resist is spin coated onto the sample surface, as in Figure 1.3.1(a). The sample is then exposed by the electron beam in the desired pattern shape(s), as in Figure 1.3.1(b). The sample is developed so that the affected area of the resist is washed away (in the case of positive e-beam resist), as in Figure 1.3.1(c). A subsequent etch, or in the case of Figure 1.3.1(d), deposition step affects only the area of the wafer that no longer contains resist. The resist is lifted off, leaving a sample surface with the desired etch or deposition in only the desired areas (Figure 1.3.1(e-f)).

The electron beam is focused into the smallest cone possible so that it comes to a point at the sample surface. In an ideal system, the beam would be only a single electron in width. Since this is not possible to achieve due to the beam spreading, the beam dose becomes an important factor to consider during EBL. The electron beam dose is essentially a measure of the number of electrons that strike a linear path or an area on the surface. Beam dose is measured in nC/cm for a line dose where the electron beam is not rastered, but passes once in a single direction. When the beam is rastered back and forth over an area of resist, the dose is measured in $\mu C/cm^2$. For a given beam diameter, accelerating voltage, and focus on the sample, the beam dose can be increased merely by causing the beam to spend more time exposing each individual point on the sample. The time of exposure at each point in a pattern is referred to as the dwell time, and is commonly in the μs range.

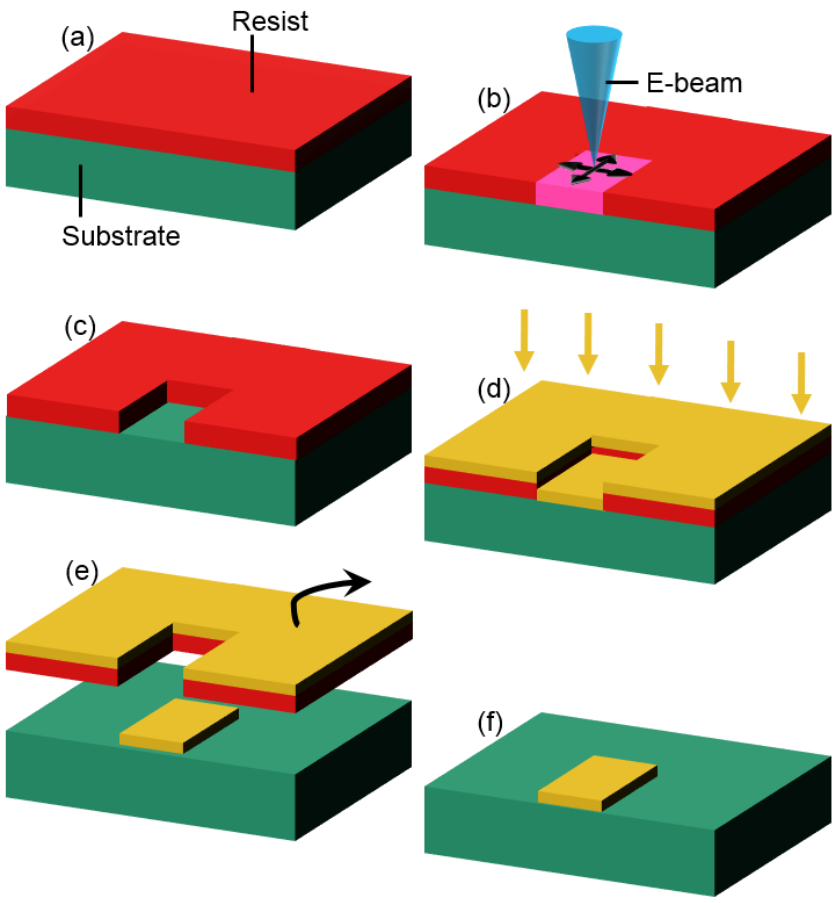

Figure 1.3.1: Major process steps for EBL.

Optimizing the beam dose is important to obtaining the most accurate patterns with respect to the designed geometries. Too little of a dose may underexpose the resist, resulting in dimensions below those designed. Overexposing the resist results in larger than planned dimensions and, often, rounding of corners that should be square. Dose tests are an important calibration for any EBL process, as the necessity for high resolution features is often the motivation for using EBL.

The proximity effect is another limiting factor in the production of nanoscale features via EBL. As the name implies, the proximity effect is a result of the spacing between adjacent features being patterned during the lithography process. For small patterns that are positioned close to larger patterns, and for areas of densely packed patterns, the electron dose does not

necessarily stay confined to the designed areas. Some patterns may receive an extra dose from the scattered electrons from neighboring regions, thus causing linewidth increases beyond the designed dimensions. Figure 1.3.2 shows an SEM image of nanowires fabricated at different spacing via EBL, where some wires have merged into a single pattern due to the proximity effect [67]–[70]. Due to this effect, the smallest gap between two individual wires fabricated using the described EBL process was measured to be 36 nm. See Section 4.1 for a discussion of the dose test for which the Figure 1.3.2 image was taken.

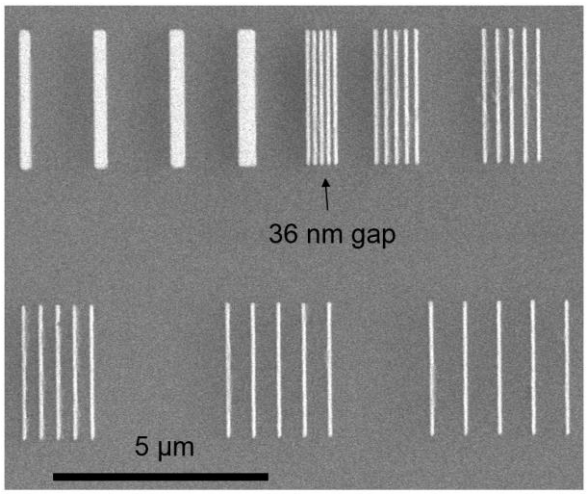

Figure 1.3.2: Merging of nanowires into a single pattern due to the proximity effect.

The ability to create nanoscale structures with a purely lithographic process makes electron beam lithography attractive to various areas of nanotechnology. If some of the feature resolution limitations can be overcome, EBL may be able to make a larger impact on future fabrication processes for useful nanodevices. Plasmonics and nano-optics are such areas that study nanoscale structures fabricated via advanced techniques due to the unique interactions of the structures with incident light at this sub-wavelength scale.

1.4 Plasmonics Background

Plasmonics is a major area of study that makes use of nanostructures, therefore, it is important to understand the plasmon. This requires at least a conceptual understanding of the interaction between light and matter.

When a conducting material is placed within a constant electric field, the material is polarized. This means that the many free electrons in the conductor shift to one side, leaving a region of positive ions on the opposite side so that the internal field established between these separated regions of charge completely cancels the external field. The charges are held in these respective positions until the external field is removed, at which point the charges, being attracted to one another, shift back to neutralize all of the regions of the material. There is some overshoot, due to the electrons' inertia, when the charges experience this restoring force, and thus a damped oscillation of charges occurs. This can be thought of as similar to the damped oscillation of a stretched spring after being released. The charge density oscillation is known as a *plasmon*. Just like a photon is a quantum of light and a phonon is a quantum of mechanical vibration, a plasmon is a quantum of charge density oscillation.

For a spherical metallic nanoparticle, the charges can be visualized as shown in Figure 1.4.1. The electrons shift to one side upon exposure to an external electric field, and upon removal of the field shift back to the other side and oscillate back and forth until the energy is lost due to collisions between the electrons and atoms in the metal, generating heat. Charges move from one surface to the other, oscillating through the entire volume of the conducting material. In such cases, the charge oscillation is known as a bulk plasmon.

Light is a propagating electromagnetic wave. That is, it is made up of electric and magnetic fields that oscillate as a light wave travels through space. Thus, when light interacts

with a material, its electric field is capable of causing an oscillating force on the free electrons and/or ions present in the material.

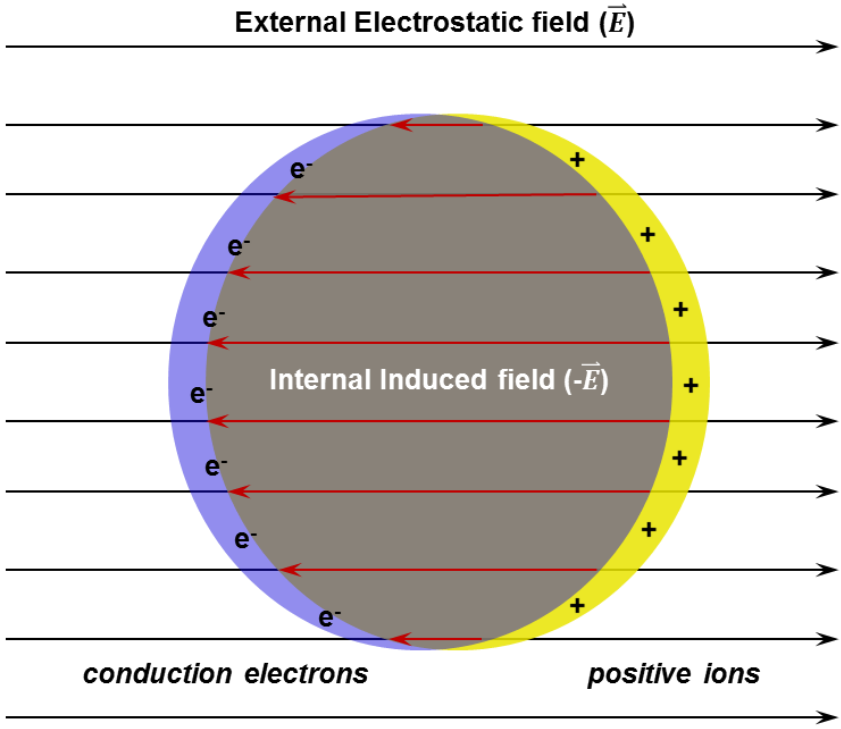

Figure 1.4.1: A bulk plasmon in a metallic nanoparticle due to an external electric field.

For conducting solids, and thus most metals, there are many free electrons present at the surface that can be affected by an incident light wave's electric field. If light of a given frequency is incident upon the surface of a metal, the oscillating field tangent to the surface moves electrons back and forth along the surface of the metal, causing longitudinal charge density waves. These oscillating charge density waves are known as surface plasmons because they propagate along the surface of the conducting material.

Accelerating charges generate light, therefore plasmons create a local electric field (light) near the metal surface. This local field is concentrated to a smaller wavelength than that of the incident light wave, meaning that the same energy is concentrated in a smaller volume in the near field of the interaction surface. This field enhancement is typically strongest near the edges

of metallic structures or in gaps between structures. Metallic nanostructures with dimensions on the order of the incident light's wavelength allow for some control over the spectral response. Various shapes and dimensions of metallic structures can cause different bulk and surface plasmon responses upon incident light irradiation. Plasmons can thus be coupled to light in order to increase the electric field strength in desired regions of a device for the purpose of increasing absorption of the light or the signal strength from a sample.

It has been demonstrated that metallic structures with nanoscale features can improve the plasmonic response of an irradiated sample surface containing the structures [49], [52], [71]–[76]. This type of light-matter interaction has sparked much research into the potential applications of sub-100 nm (and smaller) geometries on substrate surfaces [9], [51], [57], [77]–[81]. Nanogaps between features have been shown to provide even further enhancement of the optical intensity in the near field [47], [52], [82]–[94]. Section 2.3 of this thesis contains an example of simulation results demonstrating optical enhancement within a nanogap structure.

Thus, the importance of furthering nanofabrication techniques also depends on the benefits of plasmonic enhancement applications. Plasmonics is just one area that benefits from the ability to fabricate structures and devices at the nanoscale. Other material properties are affected by the creation and control of truly nanoscale features as well, providing plenty of areas of application for improved nanofabrication.

1.5 Sub-10 nm Fabrication Review

In order to continue pushing the limits of technology and research, improved methods of fabricating structures below current limits will become increasingly crucial. Top down photolithographic methods are continually limited by the resolution limits of the technology. Self-assembling fabrication methods tend to lack some degree of control over device geometry.

Some methods continue to require an increasing number of fabrication steps in order to pattern simple structures. Despite limitations, there exist techniques that are capable of producing features below 10 nanometers. One must appreciate the fact that it has become possible to control the physical locations of hundreds and even tens of atoms with some degree of repeatability [95], [96].

The nanoscale fabrication method known as molecular beam epitaxy (MBE) has been used since the 1960's and is a common method for growing crystal layers on substrates for semiconductor applications. It is a form of bottom-up deposition in which layers of atoms are grown one by one on the substrate surface. MBE is so widely used because of its ability to provide ordered crystalline structure throughout the deposited layer, but also for the ability to deposit sub-nm thin layers. Other methods such as chemical and physical vapor deposition (CVD and PVD) are also widely used today for their shared ability to deposit layers with angstrom level precision. These bottom up techniques are commonly used to build up layers of materials for specific integrated circuit components and other devices [29].

These types of deposition techniques, while maintaining a superior level of control over the vertical thickness of grown material layers, are typically unable to provide such control in the other two dimensions of the surface plane. Thus, other techniques have been relied upon for the fabrication of structures with nanoscale features beyond just layer thicknesses.

Nanoskiving is a technique that makes use of an ultramicrotome to physically shave off extremely thin slices of a material for the purpose of later reapplying them to a substrate. This technique allows for some nanoscale fabrication capabilities by allowing a vertical thickness from a deposition to become a lateral dimension or vice versa after a sample has been skived [97], [98].

Focused ion beam (FIB) milling is a subtractive fabrication technique capable of creating nanoscale features. FIB advances have allowed for nanoscale and even angstrom precision control. This method provides some control over structure geometry, but is a serial fabrication technique. It must pattern structure areas one by one, scanning the beam across the desired areas as in electron beam lithography [99]–[102].

Nanogaps have been fabricated successfully using break junction methods to essentially pull apart nanowires resulting in a space between two nanowires. Chemical etching can be used for this purpose. Electromigration is the movement of ions in a conducting material due to momentum transfer between the atoms and high velocity electrons. This potentially harmful effect in some circuits has been taken advantage of in order to allow the fabrication of gaps in metal nanowires [47], [50], [83], [103]. Mechanical break junctions make use of extremely fine precision mechanical systems in order to physically snap a nanowire in two [104]–[106]. These techniques tend to lack control over the geometry and possibly even the width of the gaps.

Colloidal self-assembly has been used to create a variety of nanoparticles, nanospheres, and other nanoscale structures. It has been found that colloidally grown structures can be deposited onto a surface to be used as a mask [107]–[109]. This technique is limited by the chemical processes of colloidal self-assembly as well as the lithography stage.

Glancing angle deposition (GLAD) is a clever variation on deposition techniques that allows for the fabrication of micro and nanostructures. The sample is tilted in the deposition chamber to allow for different geometrical capabilities than normal vertical deposition. This typically requires fabrication of structures prior to the glancing angle step [110]–[116].

Lithography combined with deposition techniques allows for some unique multistep processes capable of nanoscale resolution. Computer-aided sample alignment has increased the

precision of lithography systems so that masks and CAD designs can be aligned with nanometer precision in some cases. One method that takes advantage of the alignment capabilities of such systems is the self-aligned technique, which makes use of a clever material interaction to obtain nanoscale gaps between metallic electrodes. This technique is introduced and the process explained in detail in Chapter 2.

Chapter 2. BACKGROUND

A previous technique, called the self-aligned technique, is a method used to obtain a linear sub-10 nm gap between two electrodes that has been used for electrical measurements and plasmonic studies [85], [117]. The lithography-based method makes use of a two-step lithography and deposition process to obtain this gap resolution between electrodes. The large aspect ratio and ability to overcome lithography resolution limitations are made possible by a sacrificial metal layer that serves as a mask during subsequent process steps.

2.1 Process Description

The self-aligned fabrication technique involves performing photolithography or electron beam lithography and evaporation of metals in a strategic order for the benefit of overcoming the lower dimensional limit of the lithography device used. The process steps are depicted in Figure 2.1.1 as described in [85]. The left column shows a cross sectional view of the process, the middle column shows a top view, and the right column shows colorized SEM images corresponding to the steps in the drawings. All lithography steps used in the creation of the SEM images were EBL using PMMA electron beam resist.

After a standard initial lithography step, metal is deposited on the surface to create the first electrode. As shown in Figure 2.1.1(a), Au (gold) and Cr (gray) are deposited via electron beam evaporation with Ti as an adhesion layer between the silicon substrate and thin SiO_2 layer between the Au and Cr as a diffusion barrier (both not shown). The key step of the technique, shown in Figure 2.1.1(b), is the oxidation of the Cr layer. As the Cr is oxidized, it expands so that some width of Cr_xO_y will overhang the edge of the Au layer beneath [85]. The overhanging Cr_xO_y layer is able to act as a mask in the second lithography and evaporation steps, preventing the deposited metal from reaching an area of the substrate surface that is roughly the same size as

the Cr_xO_y overhang. This masking during the secondary Au and Cr evaporation is shown in Figure 2.1.1(c). After the second metallization is complete, the Cr is etched away chemically, resulting in Au structures that are separated by a gap roughly the same size as the Cr_xO_y overhang. The key benefit of this process if that the width of the resulting gap can be below the typical resolution limit of the lithography system used. This is shown in Figure 2.1.1(d).

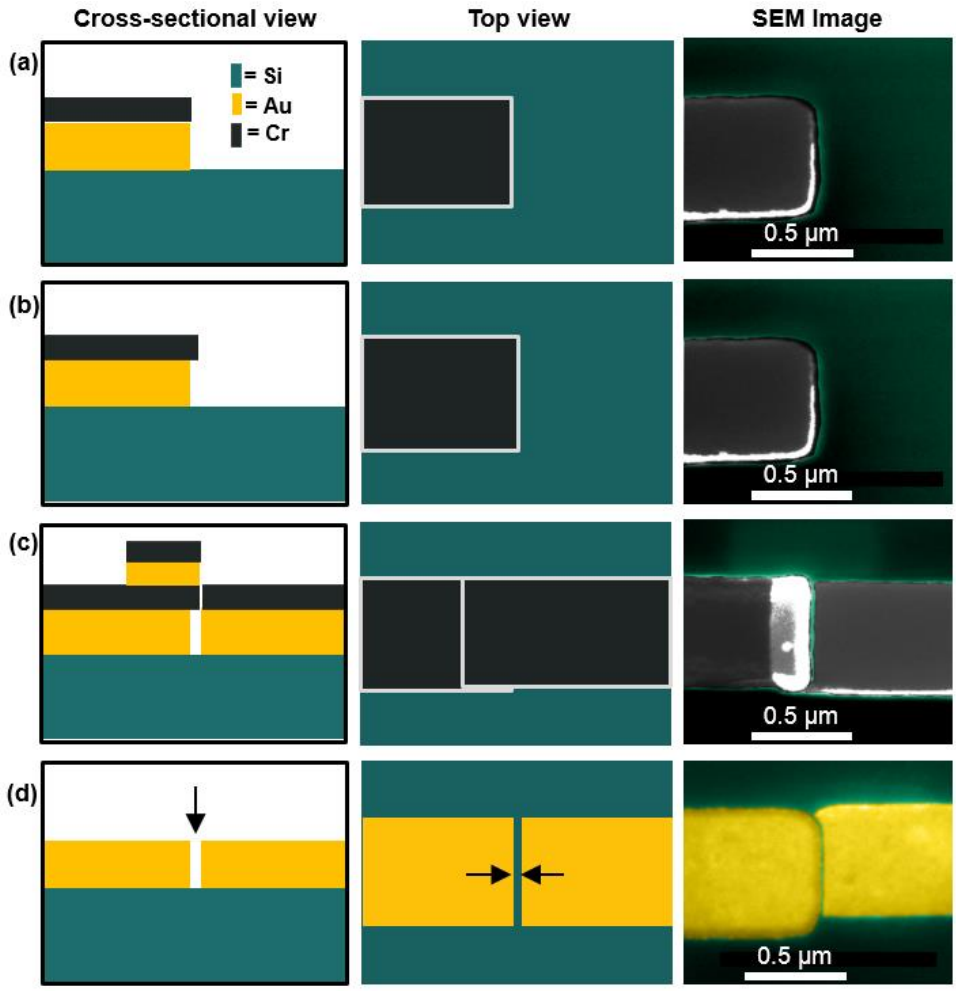

Figure 2.1.1: Major process steps for the self-aligned technique.

The first step of this thesis project successfully reproduced the self-aligned process, as outlined in Figure 2.1.1, here at the University of Arkansas Nano-Bio Materials Characterization Facility using the FEI XL30 Environmental Scanning Electron Microscope (ESEM) prior to conducting research toward advancing the technique. Both the EBL process steps and SEM

imaging used to obtain the images in Figure 2.1.1 were performed using the ESEM. Electron beam evaporation was used to deposit the following layers of materials: 1.4 nm Ti, 14 nm Au, 1.4 nm SiO_2, and 14 nm Cr. The result of this process can be seen in the inset of Figure 2.2.1 in Section 2.2.

2.2 Gap Size vs. Cr Thickness

The ability of the self-aligned technique to create nanogaps between structures is useful in itself. The ability to control the thickness of those nanogaps is what makes the method especially intriguing. In previous work, it was demonstrated that the thickness of the resulting nanogaps between electrodes is related to the thickness of the masking Cr layer [85], [117]. Figure 2.2.1 shows a plot of gap width versus vertical Cr layer thickness taken from different samples created via the self-aligned technique.

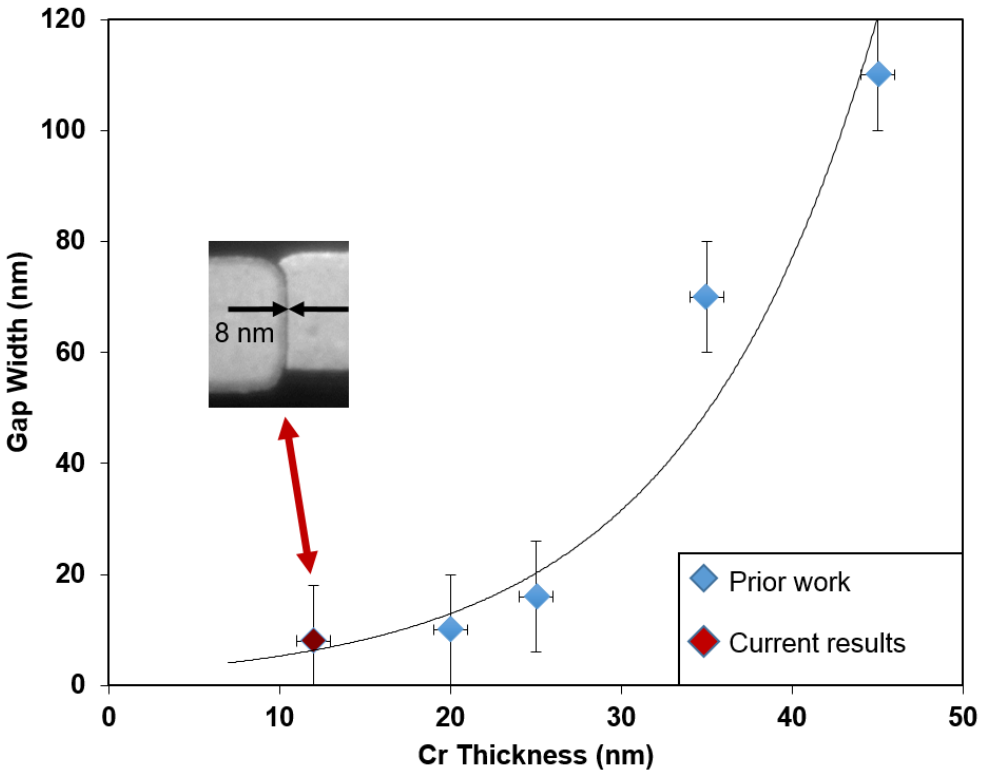

Figure 2.2.1: Plot of gap width versus Cr layer thickness for the self-aligned process. Data points in blue are from Fursina et al. [85].

The result was plotted (red) with data from Fursina et al. [85] (blue) to show that the gap width lies within the expected range. The inset is an SEM image of a nanogap structure with an approximately 8 nm gap between two metal structures that was fabricated by Bauman at the University of Arkansas.

The plot in Figure 2.2.1 shows a definite increase in gap width as the thickness of the Cr layer is increased. This means that designers have some control over the size of gaps that are created because the Cr thickness can be controlled with angstrom precision using current evaporation technology.

2.3 Optical Enhancement in Nanogaps

The benefit of fabricating nanostructures, specifically nanogaps, typically stems from the ability of the features to change properties of a material surface or the way in which the material interacts with other physical entities such as light. Metallic structures separated by nanogaps, as fabricated via the self-aligned technique, are perfect examples of such devices. The gap allows structures to couple to incident light to cause a change in the local field strength due to the plasmons excited at the surfaces adjacent to the gap. In such gap structures, it has been shown that there is an increase in the local electric field strength, and thus the intensity of the light, within the nanogap compared to the field of the incident light [52], [84], [87], [91].

A computational electromagnetic simulation of nanogap structures is shown in Figure 2.3.1 as discussed by Bauman et al. [118]. The simulation was performed as a cross section of two infinitely long rectangular nanowires of 140 nm width, 15 nm height, and varying gap size with a constant incident wavelength of 875 nm. The incident light was polarized transverse to the nanowire width with the electric field vector pointing across the gap. Insets show some of the simulated geometries with gap widths of 1, 5, 10, 25, and 50 nm. The electric field strength is

shown via color scale where dark red is the highest and dark blue is the lowest. There was zero field within the conducting structures.

The plot in Figure 2.3.1 shows optical enhancement versus gap width. The optical enhancement, G_{local}, is given by,

$$G_{local} = \left|\frac{E}{E_0}\right|^2 \tag{2.3.1}$$

where E is the average local electric field strength in the gap and E_0 is the field strength of the incident light. This is essentially a comparison of intensities, as the intensity of light is proportional to the square of the electric field strength in a location. A more detailed description of the optical simulation parameters used to obtain this data can be found in Appendix I.2 Optical Simulation Details.

The plot in Figure 2.3.1 was found to display a nearly exponential relationship between the width of a gap between nanostructures and the enhancement of the electric field within that gap. As the gap width was decreased, the optical enhancement continually increased with a sharper increase for gaps below 10 nm. These areas of high electric field enhancement near plasmonically active structures are commonly referred to as plasmonic *hotspots*.

This result is promising for the field of nano-optics and plasmonics in conjunction with these advanced fabrication techniques. This increased enhancement within nanogaps has been reported as discussed earlier in this section as well as in Section 1.4. The field strength enhancement obtained via such gap devices can be used to increase a light signal such as in SERS or sensing applications [86], [119]–[122], to increase absorption for photovoltaics [40], [43], [123], or to aid in various optical antenna designs. Structures such as those in the simulation are now possible to fabricate, as previously shown in Figure 2.1.1 and Figure 2.2.1

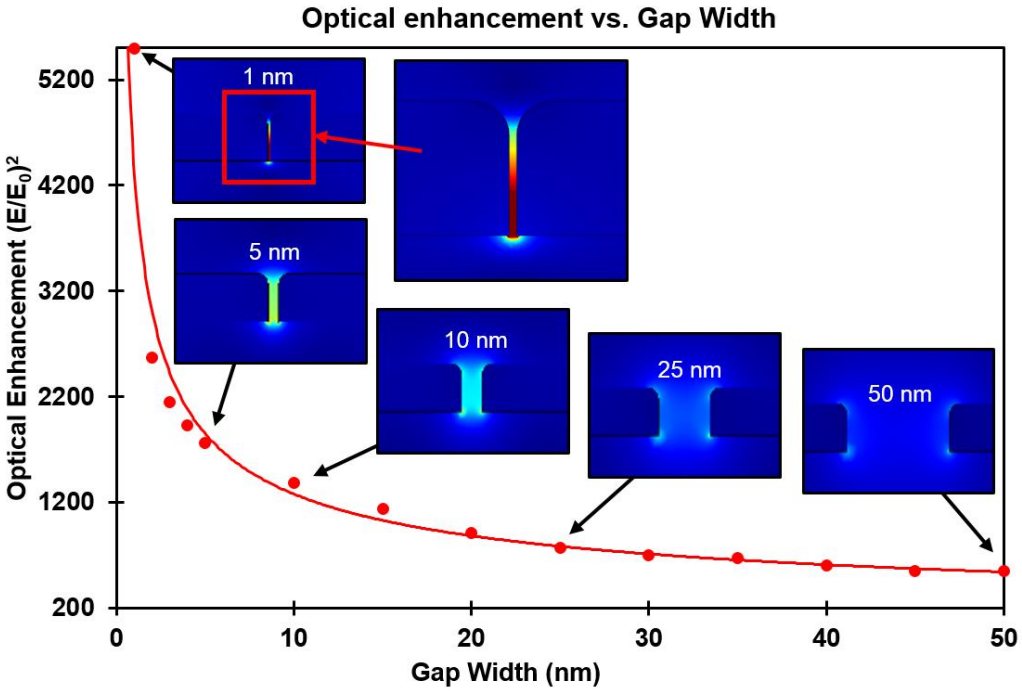

Figure 2.3.1: Plot of simulated optical enhancement versus gap width [118].

Chapter 3. NANOMASKING TECHNIQUE

The benefit of being able to fabricate nanostructures and especially nanogaps with sub-10 nm dimensions has been discussed in Chapter 1 and Chapter 2. All of the previously discussed methods of nanofabrication have been somewhat limited either in terms of geometrical design control or in the number of usable devices that can be created within a reasonable amount of process steps. Surface-enhancing devices used in sensing and spectroscopy can be useful when an entire surface has been modified as opposed to a nanoscale or microscale area. Photovoltaic cells are a very visible example of the need for wafer-scale active-device surface areas. These applications, if ever they will make use of nanodevice optical enhancement technology, will require a swift, repeatable fabrication method that can produce useful devices across a relatively large area.

Research into the plasmonic enhancement within nanogaps has been limited to studies of single gaps. The true benefit of this type of device will become realizable when many such light-enhancing gaps are fabricated across the surface area of a whole wafer so that localized gap enhancement occurs across an entire substrate.

This work expands upon the aforementioned methods used in the self-aligned fabrication technique. The focus of this master's thesis work was to prove the feasibility of the fabrication technique that has been called *nanomasking*, which is a new advanced development of the self-aligned process. This advancement has a U.S. patent pending [124], and results from this thesis have been accepted for publication: Bauman et al. [125].

3.1 Multi-gap Fabrication

The first advancement of nanomasking in this work was the production of a high-density of nanogaps over a wafer-scale area. The technique uses the same underlying principle of two-

step lithography and a sacrificial metal layer that can be oxidized and etched for the purpose of overcoming the resolution limit of the lithography method utilized. This method allows for the fabrication of multiple nanogaps between multiple structures across a substrate surface without increasing the number of steps required in the process.

This technique was found to be capable of producing variations of multi-gap patterns depending on the designs of the primary and secondary lithography steps. The major nanomasking process steps to create a grid type geometry with many nanogaps between many metallic structures are shown in Figure 3.1.1. In this process, the initial metal nanowires are deposited after a lithography and development step, resulting in structures as shown in Figure 3.1.1(a). In this figure, metal 1 is shown in gold and metal 2 in gray. For the purposes of this and following process explanations, metal 1 is shown to be Au and metal 2 to be Cr/Cr_xO_y. The materials used for metals 1 and 2 are not absolutely critical provided that the top layer can be controllably oxidized and etched. The Cr layer then oxidizes under ambient or controlled conditions. The Cr_xO_y overhangs the Au layer on both sides as shown in Figure 3.1.1(b). This masks many areas from subsequent material deposition. The sample is aligned in the lithography system so that the secondary nanowires will be patterned over the existing structures. Figure 3.1.1(c) shows the result of the metal 3 evaporation (also taken to be Au). Again, the metal 3 material used in this step is not crucial, provided that it will not be etched using the same chemical as the metal 2 etchant. Etching the Cr layer reveals Au structures separated by multiple nanogaps across the sample surface, as shown in Figure 3.1.1(d).

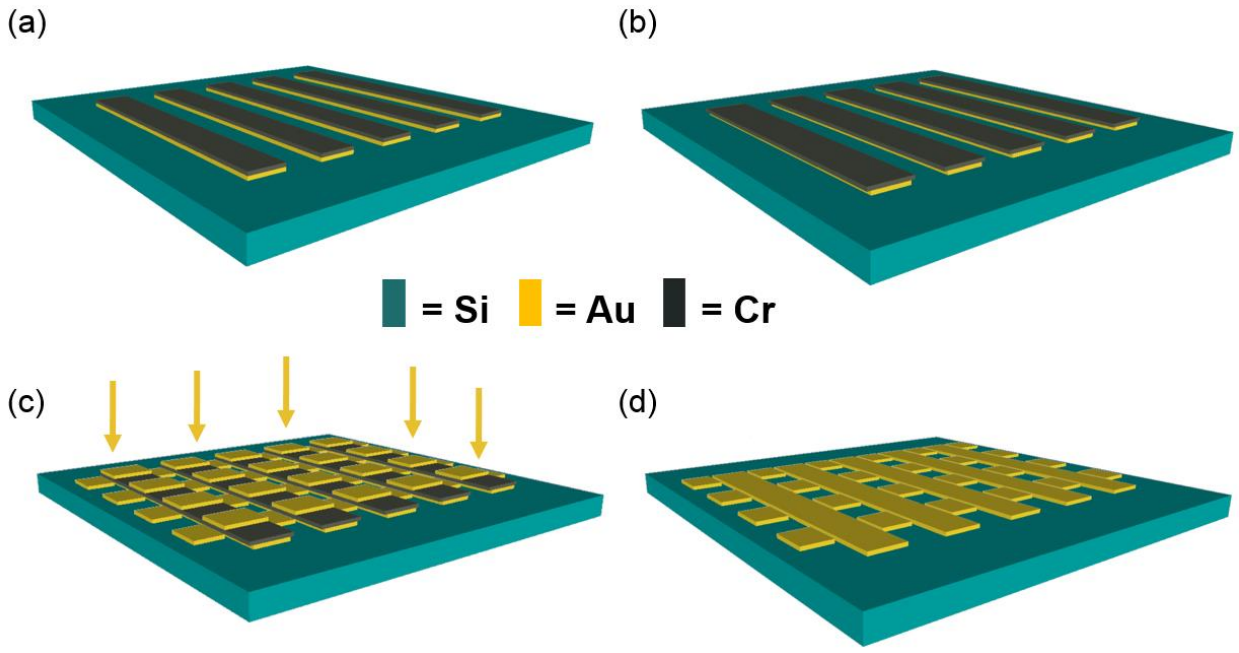

Figure 3.1.1: Nanomasking fabrication of many nanogaps over a large area.

The benefit of this type of pattern comes from the usefulness of nanogaps as plasmonic hotspots. Due to the high density of hotspots, the field strength of an incident optical signal is likely to be greatly enhanced across the entire surface on a sample like that in Figure 3.1.1(d). This large area plasmonic enhancement could prove extremely useful in applications such as photovoltaics or photodetector arrays, where absorption and light detection are increased with increasing field strength.

3.2 Sub-lithography Resolution Nanostructures

It was hypothesized in the early stages of testing the feasibility of sub-lithography resolution multi-gap fabrication that specially chosen pattern alignments could allow for the creation of physical structures below the lithography resolution limit, in addition to just nanogaps. Figure 3.2.1 illustrates the process steps for this with an example that creates a pattern of concentric squares where the larger square and smaller square are separated by the characteristic nanogap. Previous work has only produced nanogaps below the lithography

fabrication limit. The advancement in this work shows that one can *simultaneously* produce *both* nanogaps *and* nanostructures below the traditional fabrication limit.

In Figure 3.2.1(a), the Au (gold) and Cr (gray) are shown to have been deposited in a square and the Cr has been oxidized. The Cr layer thus overhangs all four edges of the Au structure below. This first step utilizes standard lithography practices, and thus the first square structure can only be as small as the minimum dimensions capable of being patterned. Figure 3.2.1(a_i–e_i) is a 3D sketch of the process and Figure 3.2.1(a_{ii}–e_{ii}) is a cross-sectional view.

Figure 3.2.1(b) displays the sample after a resist layer has been spin-coated and the sample has been aligned, patterned, and developed. The lithography for the second square is shown to have been directly over the primary structure with the secondary pattern extending over the edge slightly beyond the Cr overhang.

Figure 3.2.1(c) shows the sample after the second Au evaporation. Au is deposited on the entire sample. Where the Cr overhang covers the substrate, the Au does not reach the surface. Extending beyond the Cr layer, but before reaching the undeveloped resist, Au does deposit on the substrate.

Figure 3.2.1(d) displays the result after lift-off of the resist. All of the Au on top of the resist is lifted off as well. The sample still contains the primary Cr layer and secondary Au layer.

Figure 3.2.1(e) displays the final result of the process after the Cr layer has been etched away, removing the secondary Au on top as well. The primary Au square remains adhered to the substrate, as well as the secondary Au ring that has been deposited between the Cr layer overhang and the resist layer.

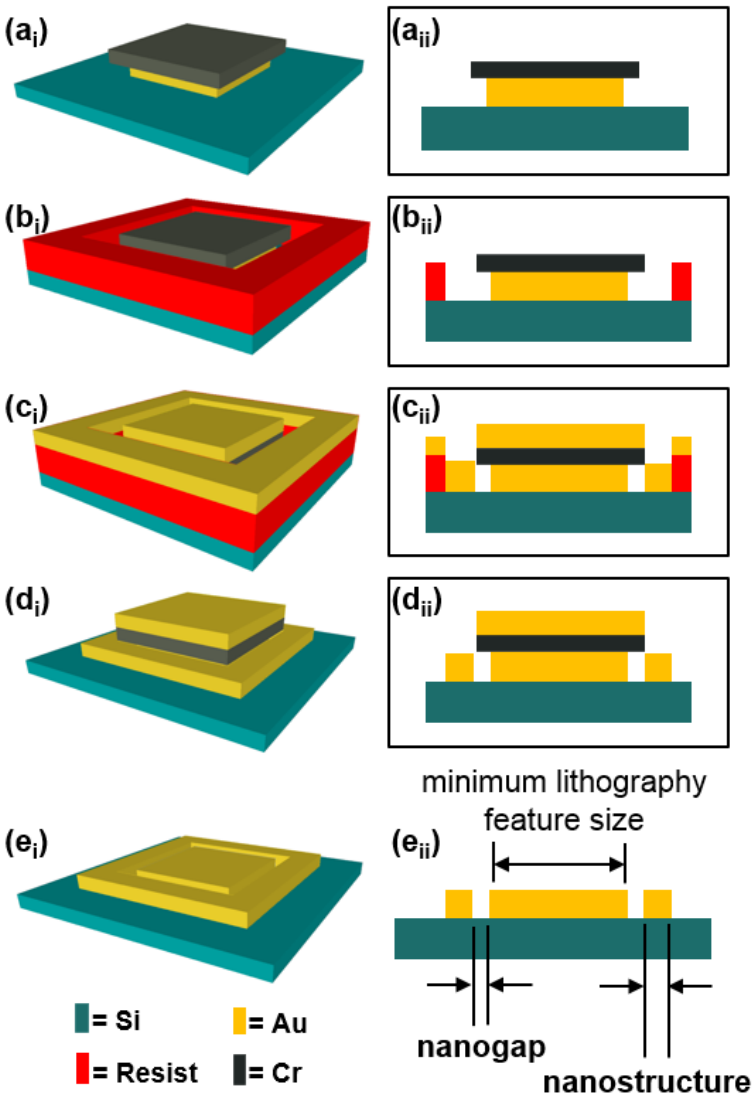

Figure 3.2.1: Nanomasking process step showing (a) Cr oxidation, (b) development after alignment and lithography, (c) the second metal deposition, (d) resist lift-off, (e) and the resulting gaps and structures after the Cr etch [125].

The result is a structure with adjacent nanostructure and nanogap that are both below the resolution limit of the machine used for patterning. This is noted in Figure 3.2.1(e_{ii}). The nanogap is achieved through the Cr deposition masking, and the nanostructure through the strategic overlap of the secondary pattern with the primary structures.

Another advancement of nanomasking creates sub-lithography limited structures without need for the nanogaps by directly depositing the mask metal onto the substrate during the first

lithography. This type of process is depicted for rectangular and circular patterns in Figure 3.2.2. The Cr (dark gray) is shown to have been deposited on the substrate in the cross-sectional view in Figure 3.2.2(a). The top view is shown for a rectangular geometry in Figure 3.2.2(a_i) and circular in Figure 3.2.2(a_{ii}); both share the same cross-section. Figure 3.2.2(b) shows the second metal (light gray) deposited as in previously discussed process flows for nanomasking. The width from one outer edge to the opposite outer edge of the deposited structures is the same as the diameter of the larger secondary circle as shown by the cross section in Figure 3.2.2(b). In this variation of the technique, the only metal remaining after the Cr etch is where it was deposited outside of the initial Cr structure and thus adhered to the substrate surface. Figure 3.2.2(c) shows the resulting structure(s) based on the chosen geometry. Figure 3.2.2(c_i) shows two small rectangular structures (nanorods) with no nanogaps, and Figure 3.2.2(c_{ii}) is an isolated ring structure. The widths of the rectangular structures and the ring are shown to be equal based on the cross-sectional view in Figure 3.2.2(c).

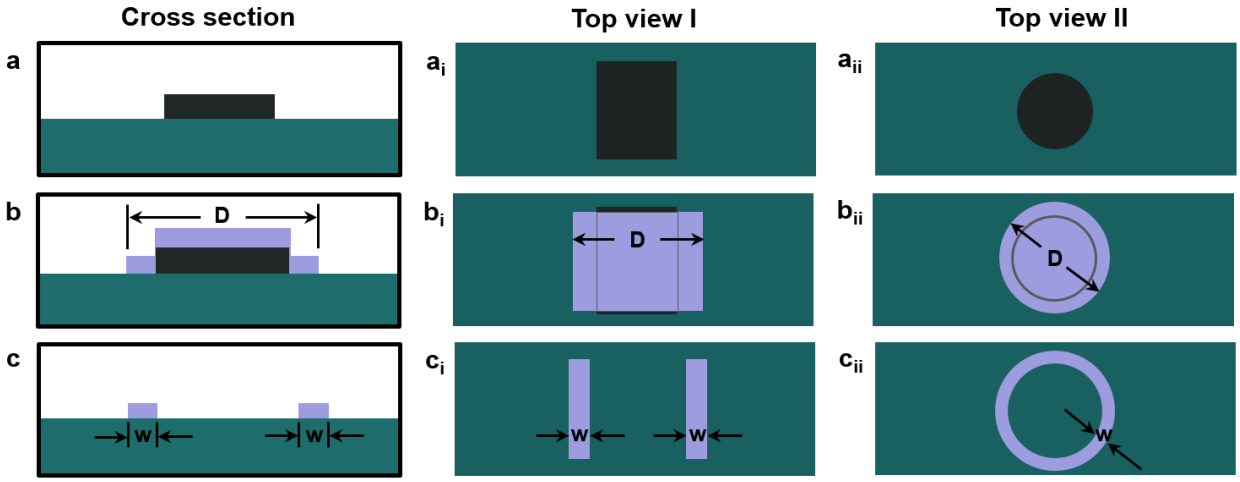

Figure 3.2.2: Nanomasking process steps for fabrication of gapless nanostructures [124].

This fabrication advancement could be useful for the creation of multiple structures that overcome the limitations of lithography systems. Various nanotechnology applications can

benefit from structures with dimensions below what can be easily created using lithography. Those applications that do not require the presence of nanogaps may especially have need of a process such as this. Versatility of geometrical variation over such a patterning technique may offer a robust solution to the fabrication needs of a wide range of applications.

A similar process to that of Figure 3.2.2 is shown in Figure 3.2.3 for more specific types of structure fabrication. The initial step shown in Figure 3.2.3(a) is identical to that of Figure 3.2.2(a). In Figure 3.2.3(b), however, the second metal (gold) is shown to be offset from the Cr (gray) layer. Thus, as shown in Figure 3.2.3(c), the second metal only adheres to the substrate on one side of the Cr. Upon etching, the result is a single rectangular structure as in Figure 3.2.3(c_i) or a crescent shape as in Figure 3.2.3(c_{ii}).

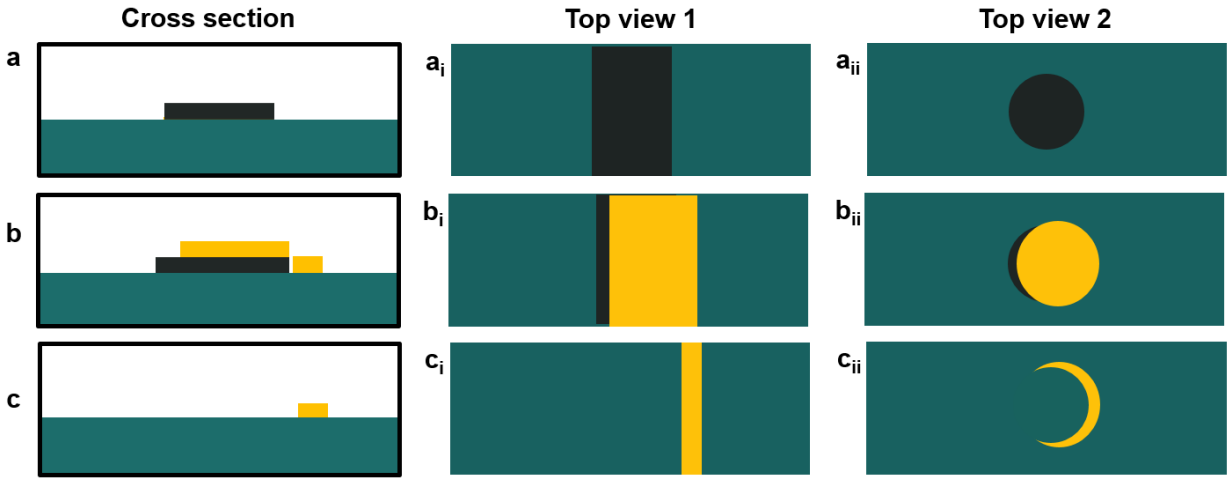

Figure 3.2.3: Nanomasking process steps for fabrication of isolated nanostructures [124].

This level of control over the overlap of structures is a significant benefit for defining unique geometries for various applications. The crescent shape could be used as a split-ring resonator, for example. One thing to note about these techniques that make use of the alignment of a sample in a lithography system is that the dimensional control will be limited to the alignment capabilities of the machine. Computer aided alignment systems are common today,

and thus error due to human intervention is reduced so that many machines are capable of alignment precision less than ten nanometers.

3.3 Elimination of Secondary Lithography Step

The procedures that have been described in sections 3.1 and 3.2 all involve two lithography steps. One of the criteria for a mass production fabrication technique is that many patterns be created simultaneously in as few process steps as possible. While the described processes in this work only have two lithographic steps, the potential exists for elimination of one of the lithography steps, to improve the efficiency of the fabrication process. Figure 3.3.1 shows the process flow for a specific geometrical case, a checkered square pattern, in which the second lithography step is not required in order to obtain the desired result.

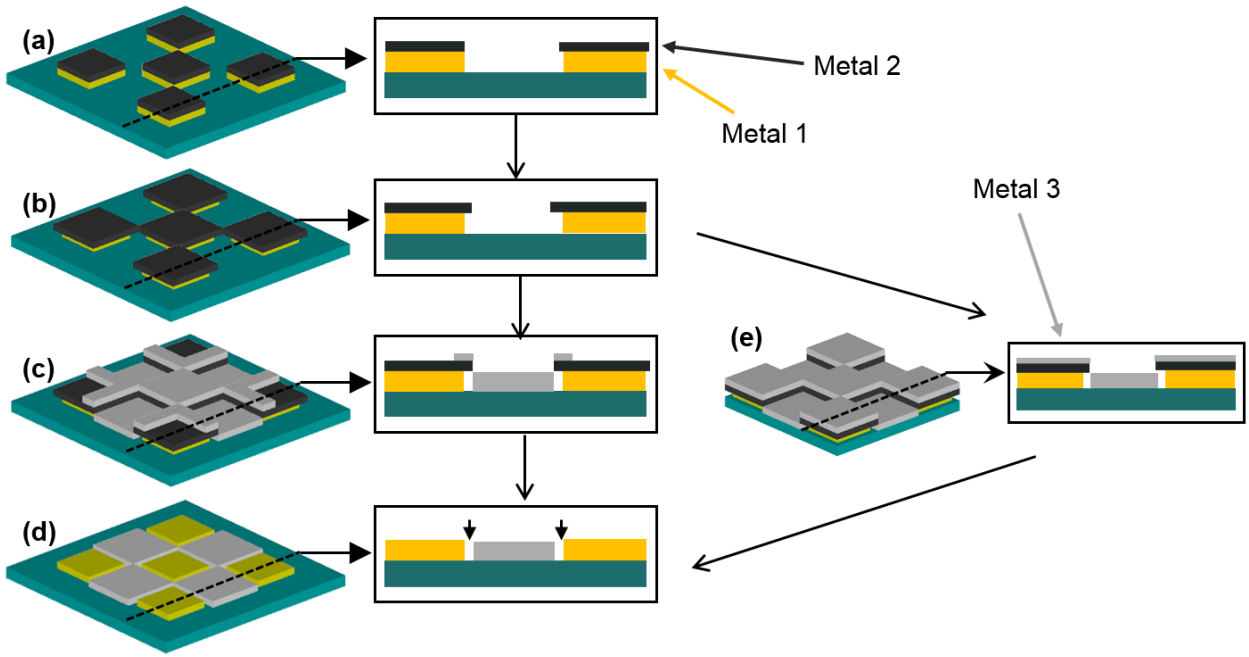

Figure 3.3.1: Checker pattern example showing nanomasking process steps for removal of the secondary alignment and lithography step [124].

The standard process shown in Figure 3.3.1(a) – (d) is similar to previously described process flows. In (a), square layers of Au (gold) and Cr (dark gray) are deposited. In (b), the Cr

layers are shown to have oxidized. In (c), alignment and lithography are required to deposit the desired overlapping pattern of metal 3 (light gray). Figure 3.3.1(d) shows the resulting checkered pattern made from metals 1 and 3 after the Cr (metal 2) has been lifted off.

The second lithography step between (b) and (d) can be removed by following the process step shown in Figure 3.3.1(e). Here, metal 3 is deposited over the entire sample after the Cr has been oxidized. Just as in (c), metal 3 adheres to the substrate surface where it is not masked by Cr. Everywhere else, metal 3 is deposited on top of the Cr layer. This achieves the same result as performing the secondary alignment, lithography, and development for a deposition that slightly overlaps the primary Au and Cr layers.

The lithography pattern designs required for the two process variations shown in Figure 3.3.1 are depicted in Figure 3.3.2.

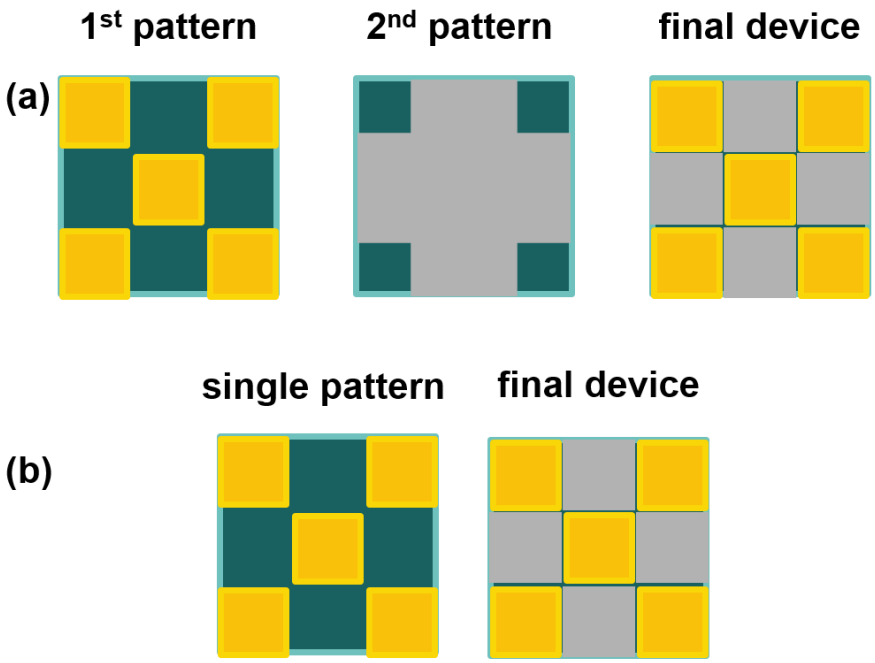

Figure 3.3.2: Eliminating the second lithography step from the checker pattern with the nanomasking process [124].

The two patterns and the resulting device for the process requiring two lithography steps is shown in Figure 3.3.2(a). The first pattern is shown in gold, and the second pattern in light gray

to match the metal colors used in Figure 3.3.1. For the modified process, only the first pattern is required to obtain the same final device, as shown in Figure 3.3.2(b).

The elimination of the secondary lithography step essentially halves the number of required steps in the nanomasking process, making it an even more attractive candidate for mass production level fabrication of nanogap-separated structures.

Chapter 4. FABRICATION RESULTS

The nanomasking technique was utilized as discussed in Chapter 3 to determine its feasibility for the creation of various nanostructure geometries. The fabrication processes were carried out using the FEI XL30 Environmental scanning electron microscope (ESEM) through the University of Arkansas Nano-Bio Materials Characterization Facility. SEM images were obtained for various structures using the ESEM and the FEI Nova Nanolab 200 high resolution scanning electron microscope through the same facility.

The ESEM was operated at an accelerating voltage of 30 kV with a beam current of 10 $\pm$ 0.5 pA for all fabrication procedures. The typical resolution limit when fabricating structures with the ESEM system was 60 $\pm$ 5 nm under standard conditions. Advancements of this work were able to produce features below this limit. See Appendix H: Manuals and Direction Sheets Developed for the detailed operating procedures that were followed during the imaging and fabrication processes.

4.1 Dose Tests

Tests were performed in order to determine the optimal electron beam dose to use for the fabrication processes in this work. The dose tests involved patterning specific designs at different electron beam doses and spacings. Gold was deposited on the samples via electron beam evaporation. By subsequently imaging the resulting patterns (also using the ESEM) and measuring the dimensions of the designs, it was possible to obtain plots of the resulting structure width versus beam dose.

4.1.1 Line Dose Test

The first design was a series of parallel lines as those shown in Figure 1.3.2. In this dose test, a varying line dose was used. This means that the beam was not rastered back and forth, but

was moved in a single straight-line path for each line. The dose was varied from 20% to 160% of a 3 nC/cm dose, from 0.6 to 4.8 nC/cm, with ten equal percentage increments in between. Lines were designed to have a center-to-center spacing of a = 45, 60, 75, 100, 200, 300, 400, 500, 750, and 1000 nm. Since a line dose is used, there is no specified design-width (lines have no width). The width, w, was affected by the dose and the line-spacing. A larger dose typically resulted in a greater width due to a larger area of resist being exposed. Smaller line spacing also increased line-width due to the proximity effect as discussed in Section 1.3. Figure 4.1.1 shows the results of the experiment, as a plot of measured line width, w, versus the beam dose for the various designed line spacings, a.

It should be noted that there are not 100 data points, as the experiment had been set up to measure. All groups of lines spaced by less than 200 nm were merged together due to the proximity effect, so no data are included for these line spacings. No lines were successfully patterned for the six sets of doses below 3.4 nC/cm, so it is likely that this was too small of an exposure to allow for complete removal of the resist upon development. Of the remaining data points taken, three spacings were chosen for clarity in the plot. Figure 4.1.1 shows the relationship between w and beam dose for line spacings a = 200, 400, and 1000 nm while the inset plot displays w versus a for the line dose values of 4.8, 4.3, and 3.4 nC/cm. The inset images are SEM images of these spacings taken from Figure 1.3.2.

The proximity effect can also be seen in the lines spaced beyond 200 nm: the closer that the lines were together, the larger their measured width. There is also a trend towards larger line widths with increasing line dose. The smallest lines were an average of 100 nm in width, and appeared for larger line spacings of 400 nm and 1 μm. As previously stated, no lines were successfully fabricated at a dose below 3.4 nC/cm. This result was an indication that a dose of at

least 3.4 nC/cm should be utilized when trying to fabricate lines with a single beam pass. This was the determined optimal line dose in order to achieve the smallest possible linewidths while providing enough exposure to fully pattern the resist.

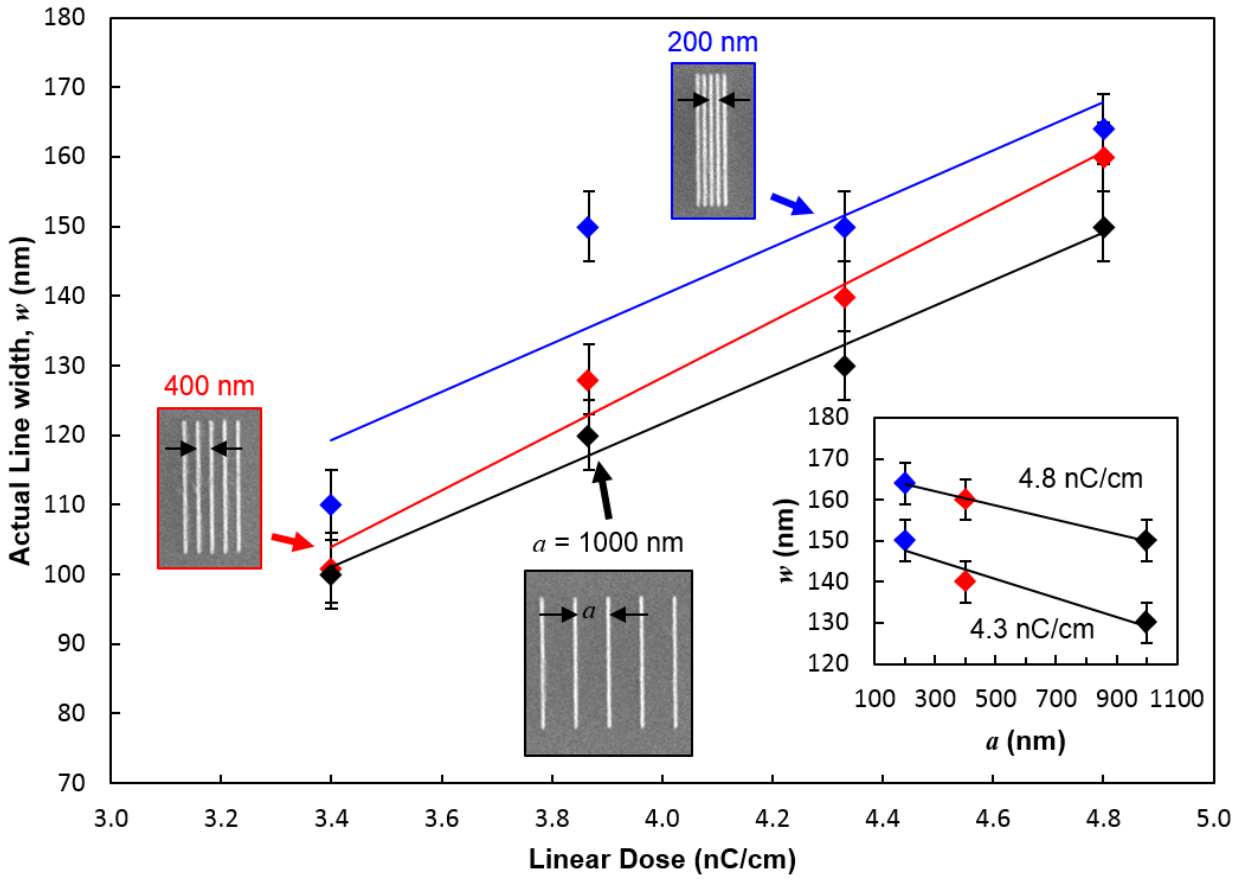

Figure 4.1.1: Plot of measured structure width vs. electron beam line dose for different line spacings, *a*. The design pattern was a straight line (no width). Width is a function of dose and line spacing. The inset plots the resulting width as a function of line spacing.

4.1.2 Area Dose Test

The most common patterns were not fabricated by a single pass of the beam, but involved an area beam dose or areal raster of the beam for the desired geometries. A separate dose test was conducted to determine the optimal areal dose. The dose was varied from 200 to 800 μC/cm^2 by 10 equal increments. Rectangles were designed at w_0 = 30, 50, 100, 200, and 400 nm in width, and all were 5 μm in length and had a center-to-center spacing of a = 1 μm.

The resulting pattern widths were measured for each of the varied designs. The data obtained from the area dose tests are shown in the plot in Figure 4.1.2, and displays measured width versus beam dose. The plot shows data for 400, 200, 100, and 50 nm wide designs, as no patterns designed at 30 nm were successfully created. The data again showed the result that below a certain dose, there was too little exposure and no patterns were created. None of the designed 30 nm wires were present, and only two of the 50 nm patterns were present, both at the highest doses tested. The error bars are ± 5 nm for w.

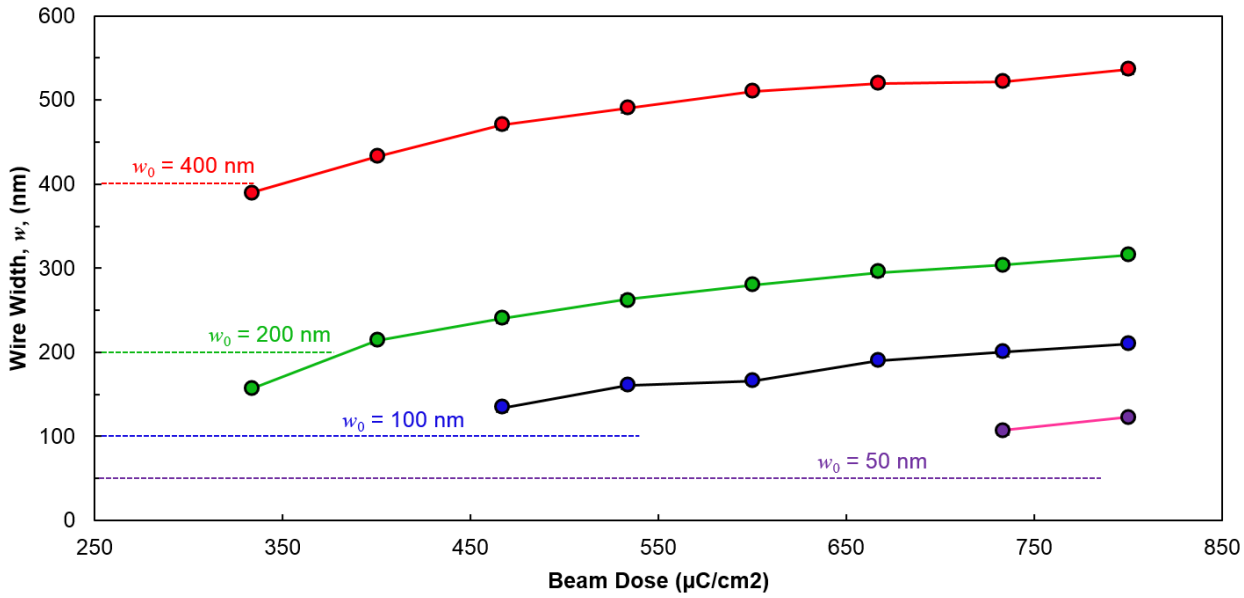

Figure 4.1.2: Plot of measured structure width vs. electron beam area dose for different nanowire design widths.

One result of the data was the determination of a beam dose near 400 µC/cm^2 as the optimal area dose. This dose was capable of producing structures closest to the designed width at w_0 = 200 nm, and within 25 nm at w_0 = 400 nm. The trend for the 50 and 100 nm wires was that they were either not present or they were overexposed and results were wider than designed. There was not a high need for fabrication of structures at or below 100 nm widths throughout the

remainder of this work. Thus, a dose of 400 μC/cm^2 was determined to be sufficient for producing the most accurate patterns without underexposing the resist.

The dose tests were used in determining the beam doses for patterns fabricated throughout this work. Knowing the capabilities of the machine and processes used was key in obtaining successful fabrication results.

4.2 Nanomasking Fabrication of Nanogaps

To validate the feasibility of simultaneous multi-gap fabrication, different structure designs were implemented. One method of the nanomasking process was used for the creation of a grid pattern as outlined in Figure 3.1.1 and reproduced in Figure 4.2.1(a). In this process, a 1.4 nm layer of Ti was used for adhesion to the Si/SiO_2 substrate. This was followed by 14 nm of Au, 1.4 nm of SiO_2 for a diffusion barrier, and 14 nm of Cr. The second evaporation step was performed in the same manner. The Cr etch was performed using a solution containing 9 percent ceric ammonium nitrate and 6 percent perchloric acid both by weight after a dilution in DI water (1:2 :: Cr Etch:DI Water). The SiO_2 layer was etched using a buffered oxide etch solution with an etch rate of 100 nm/min. See Appendix H.3 Electron Beam Lithography with FEI XL30 ESEM for Nanomasking Process for the detailed procedure that was created and followed for the fabrication tests reported in this work. A colorized SEM image of the resulting pattern is shown in Figure 4.2.1(b). The inset displays a higher magnification view of a nanogap between the crisscrossed wires.

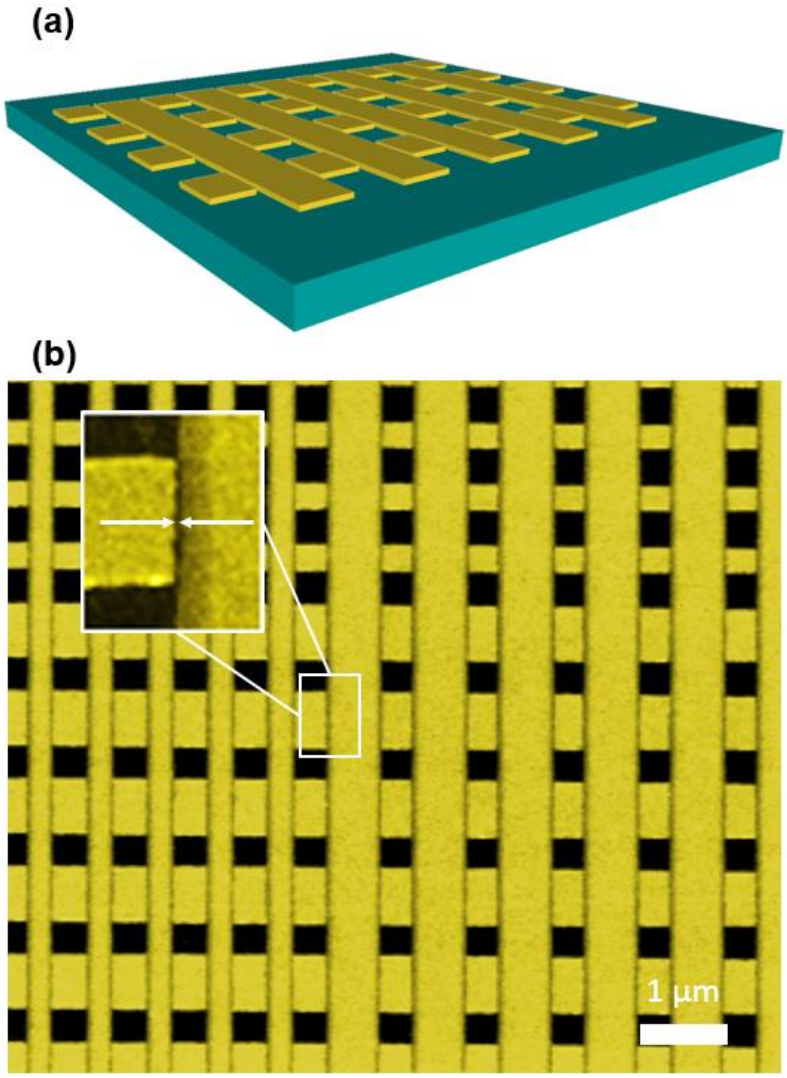

Figure 4.2.1: Grid pattern fabricated as shown in Figure 3.1.1 [125].

The SEM image in Figure 4.2.1(b) demonstrates the success of the technique in creating many nanogaps at once through this type of overlapping grid pattern. Between the vertical nanowires and every overlapping horizontal nanowire section, there are nanogaps on the order of less than 10 nm. A preliminary measurement of the gap density on this type of device was found to be greater than 500 million gaps/cm^2.

Another unique nanogap design was successfully fabricated in which the first step was a large pad with spaced nanowire fingers protruding from one side. The second step design was a

similar pad with fingers protruding the opposite way so that they overlapped with the gaps between the fingers from the first lithography step. The result of this process was two larger pads with interdigital fingers separated by a long continuous nanogap around 5 nm in width. This result is shown in Figure 4.2.2. The larger gaps visible to the left of the image were present due to the designed length of the fingers in the second pattern. Had the fingers been designed to extend all the way to the left pad, the nanogap would appear as on the right side of the image.

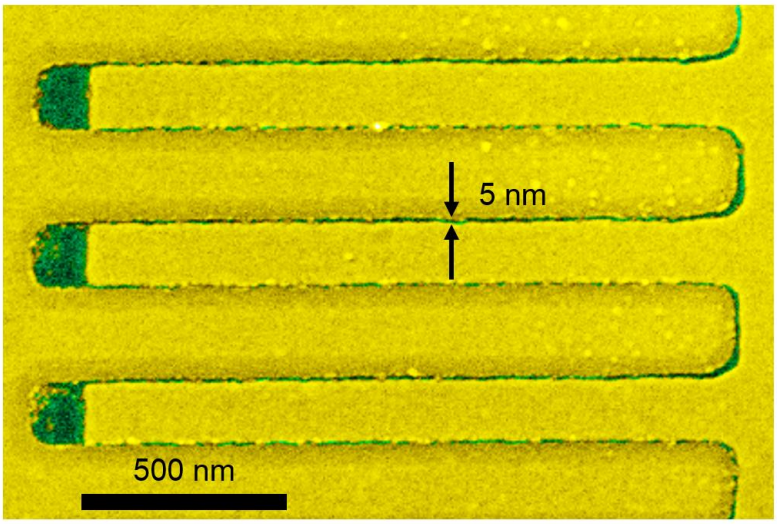

Figure 4.2.2: Interdigital fingers fabricated via nanomasking [125].

Interdigital patterns such as this but with gaps on the order of hundreds of nanometers have been studied for the presence of plasmonic activity [126]–[129]. It was found in these previous studies that this type of structure has the potential to act as a photodetector. The pads allow for electrical measurements to be made under different incident light conditions. The optical enhancement obtained from reducing the interdigital gaps to below 10 nm as in Figure 4.2.2 could provide improved signal strength at the surface of the device. This could help improve the signal detection or increase the photocurrent in such a device.

Another device fabricated via nanomasking is a pad separated from multiple leads by nanogaps as shown in Figure 4.2.3. This device was fabricated by first patterning the leads and

then the pad. This had the result of increasing the gap area between the leads and the pad versus the straight vertical gaps that would have been present if the pad were to have been created first.

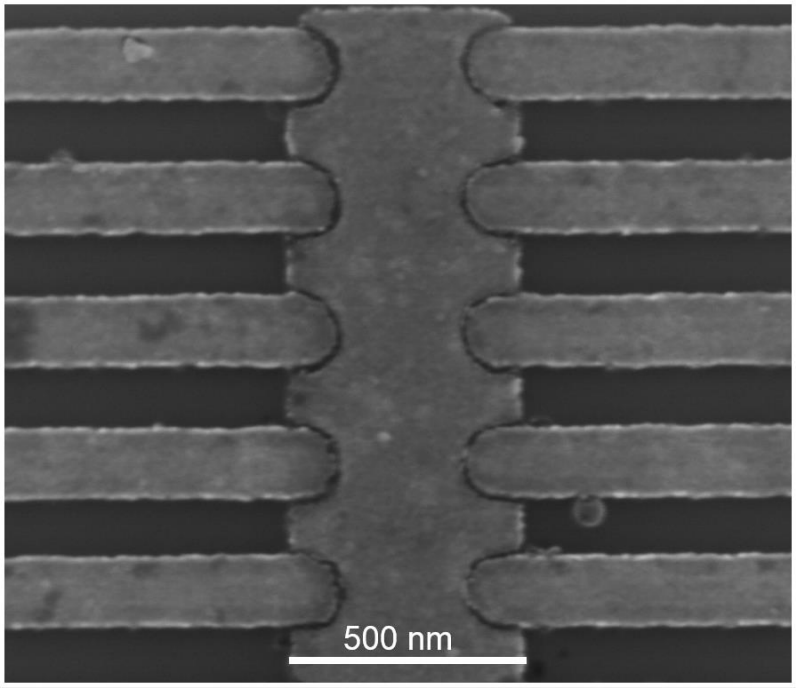

Figure 4.2.3: Pad type pattern separated from leads by nanogaps via nanomasking.

The types of structures fabricated as shown in Figure 4.2.1, Figure 4.2.2, and Figure 4.2.3 demonstrate the versatility of the nanomasking technique in the creation of multiple sub-10 nm gaps simultaneously. These geometries and others may prove useful for various applications making use of nanogaps. One clear advantage is that this expands the benefit of the optical enhancement capabilities of sub-10 nm nanogaps potentially across a full substrate area by increasing the number of plasmonic hotspots.

4.3 Nanomasking Fabrication of Nanostructures

Having demonstrated the success of the technique in fabricating many nanogaps at once, the ability to create sub-lithography limited nanostructures (in addition to nanogaps) was achieved. One design method produced different widths of nanostructures adjacent to primary

structures. The first pattern was a simple array of squares. The second pattern, a similarly simple array of rectangles was aligned with the squares so that the degree of overlap between the rectangles and squares was varied as shown Figure 4.3.1. In some samples, the widths of the squares were changed, as is also shown in Figure 4.3.1.

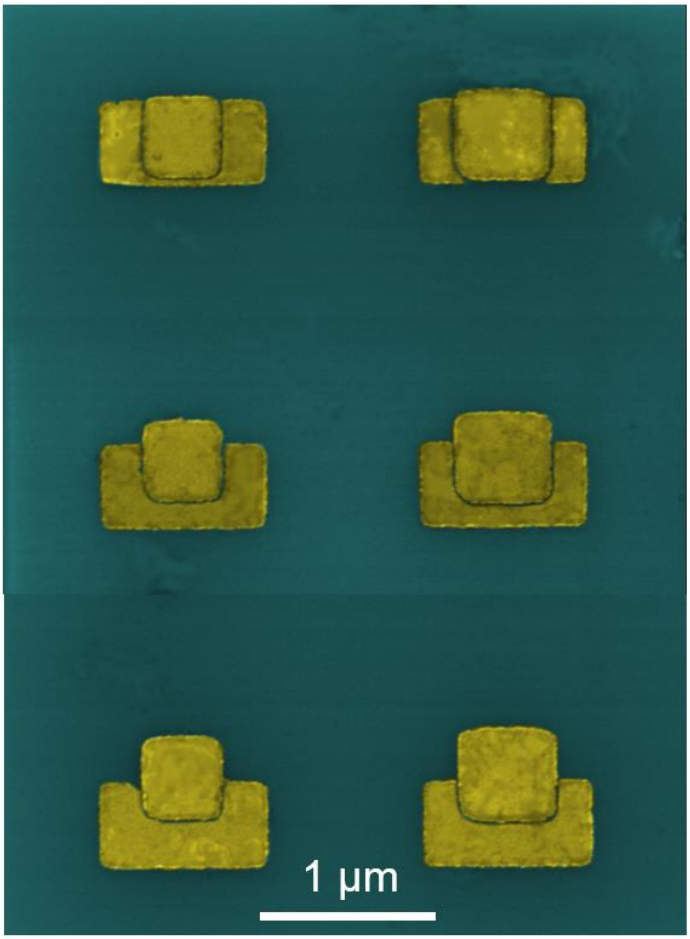

Figure 4.3.1: Offset square patterns fabricated via nanomasking.

The resulting patterns were rectangles with portions missing where they overlapped the squares and nanogaps separating the two shapes. The ability to obtain finer resolution nanostructures was evident for the patterns in which the rectangles and squares were close to completely overlapping. The bottom edge of the rectangles beneath the square was reduced in width for those array patterns in which the two shapes were close to overlapping but were not

perfectly aligned. The surface in these samples can be seen to contain some contamination. It is suspected that the contamination was due to the use of an expired chemical in the wet etch process, so this is not a common issue. This is typically not an issue and will be resolved in future work.

Figure 4.3.2 shows a higher magnification image of one structure in Figure 4.3.1 for which the combination of overlapping geometries was successful in creating a nanostructure (labeled with a width of 30 nm) below the resolution limit of the ESEM used during the two lithography steps that created the square and rectangle patterns themselves.

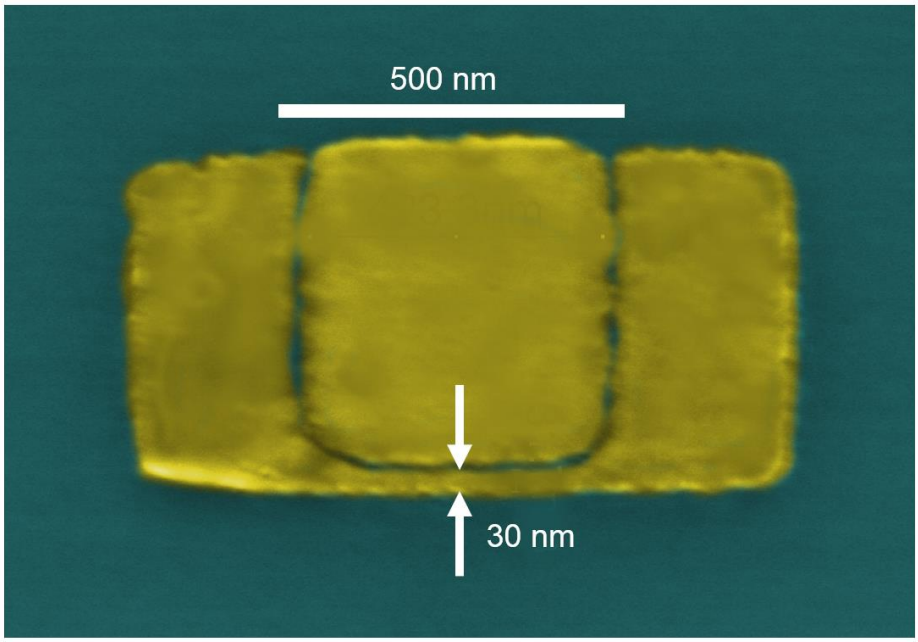

Figure 4.3.2: Single offset square pattern.

This result was a successful indication of the potential for overcoming the lithography resolution limit not only for creating gaps between features, but for creating material structures as well.

Similar to the patterns created as shown in Figure 4.3.1 and Figure 4.3.2, overlapping circle patterns were fabricated. The circles were also offset by different amounts so that the

patterns in which the two circles were closest to overlapping resulted in nanostructures smaller than the ESEM's lithographic capability. The varying degrees of overlapping circles are shown in Figure 4.3.3.

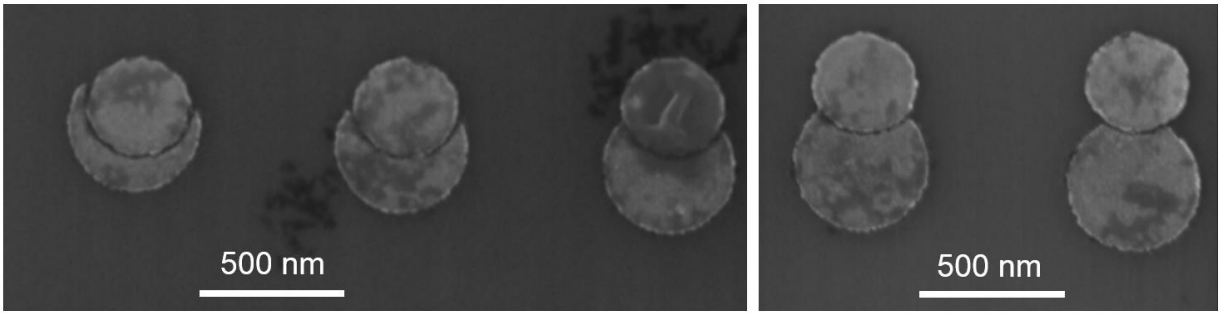

Figure 4.3.3: Offset circle patterns fabricated via nanomasking.

This method of nanomasking with circles was able to produce the unique crescent shapes seen in Figure 4.3.3. If the primary step were chosen to be Cr and thus could be etched, the crescent shapes could be created without the adjacent circles in the final result, as shown in Figure 3.2.3(a_{ii}) – (c_{ii}). Crescent structures such as these could potentially be used as a kind of split-ring resonator for nano-optics applications [130]–[133].

Expanding upon the overlapping geometry method, the method of aligning concentric squares was performed as outlined in Figure 3.2.1 with the final result sketches reproduced for convenience in Figure 4.3.4. Preliminary results were promising even though the alignment of the two square patterns was not ideal. Figure 4.3.4 shows colorized SEM images of concentric square patterns created via nanomasking. The bottom right image contains a nanogap between the primary and secondary Au structures without pushing the limit on the minimum width of the outer ring. The bottom left structure gives a better indication of the capability of the technique. This higher magnification image shows the two patterns separated by a 5 nm gap with the top portion of the outer ring measuring approximately 15 nm.

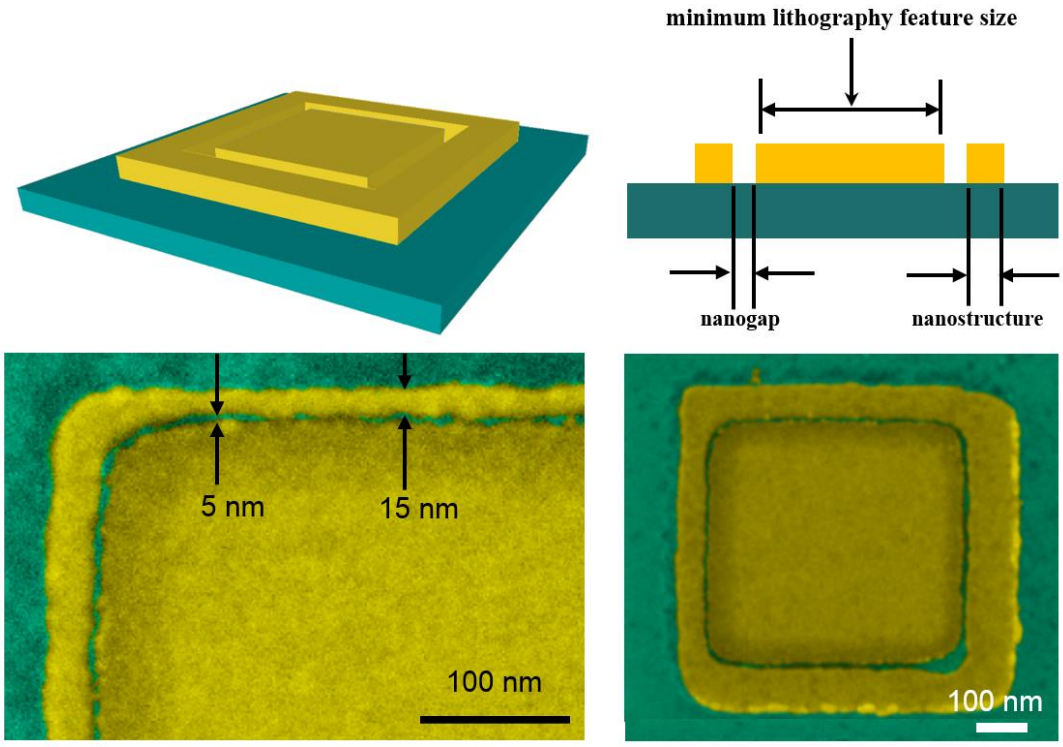

Figure 4.3.4: Concentric square pattern fabricated as shown in Figure 3.2.1 [125].

The resolution obtained in the concentric square patterns in Figure 4.3.4 as well as the other structures shown in Section 4.3 is a positive indication of the capabilities of the nanomasking advances. Nanostructures below the 60 nm observed resolution limit of the ESEM lithography system were fabricated alongside nanogaps also below this limit. Preliminary results were obtained even for samples with non-ideal alignment of primary and secondary patterns. Results were also obtained for both circular and rectangular geometries, demonstrating a greater variety of patterning capabilities.

4.4 Nanomasking and Second Step Blanketing

As discussed in Section 3.3, the nanomasking technique was hypothesized to be capable of producing specific patterns with the characteristic nanogaps without need for the second lithography step. The process of depositing a layer of metal over an entire region of pre-existing

structures with no lithography used to define deposition regions is referred to as blanketing in the remainder of this section. A preliminary test was performed for the checkered square pattern similar to that shown in Figure 3.3.1 with the final result sketches reproduced for convenience in Figure 4.4.1. Also shown in Figure 4.4.1(a) and (b) are SEM images of two such patterns that were fabricated using nanomasking with a larger second pattern to simulate the blanketing of the entire second step. Technically, the process used actually follows the flow shown in Figure 3.3.1(a) – (d) with the second lithography pattern as shown in Figure 3.3.2(a).

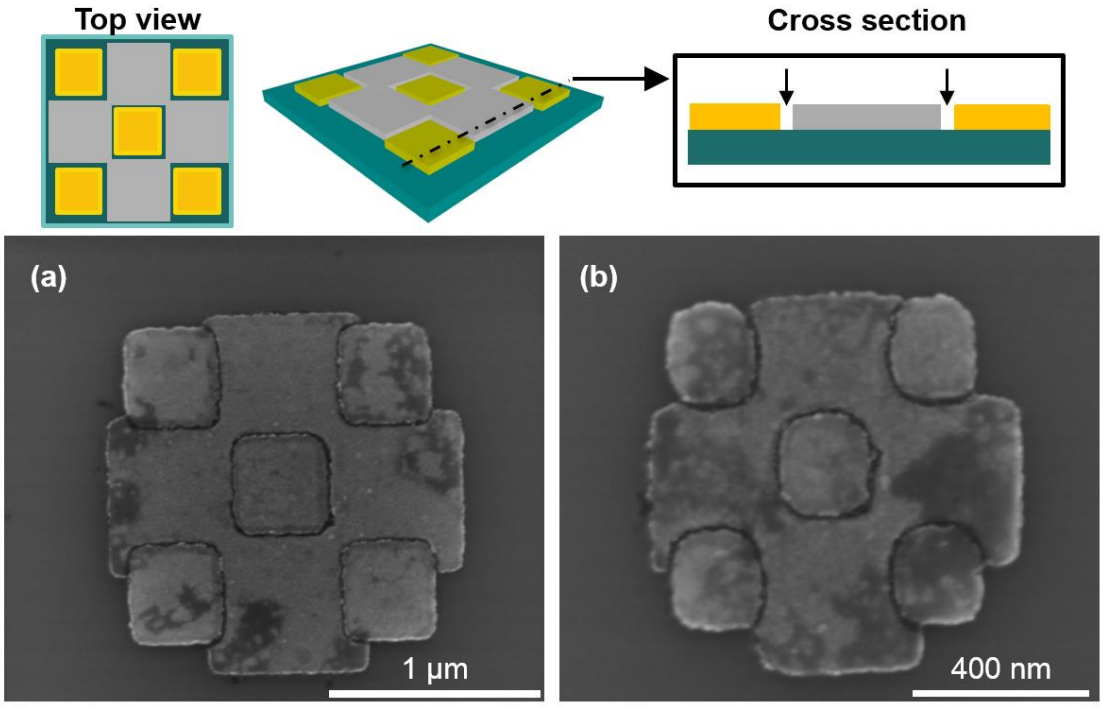

Figure 4.4.1: Checker patterns fabricated as shown in Figure 3.3.1 [124].

Though the second lithography step was not skipped in the production of the structures in Figure 4.4.1, the middle squares demonstrate that blanketing should produce similar results. The middle squares in the pattern were essentially blanketed in that the metal surrounding them was deposited completely over and next to them. A region of squares with metal deposited over the entire area would produce similar results. Another difference in the fabricated samples was that

the squares were spaced slightly farther apart than those in the sketches. This was mostly to prevent the squares from merging together due to the proximity effect during patterning and development.

A similar blanket type process was performed using circles for the primary patterns. In this case, the circles were spaced at different distances as shown in Figure 4.4.2. The second pattern was chosen to allow for a large area of metal deposition over the region of circles, similar to the large cross region used for the squares in Figure 4.4.1. The proximity issue can be seen in Figure 4.4.2(c) where the circles have merged together at the closest points. Though the second lithography step was also performed for these patterns, the middle circles in Figure 4.4.2(a) and (b) demonstrate that depositing metal all around the primary structures still allows for the creation of nanogaps via nanomasking.

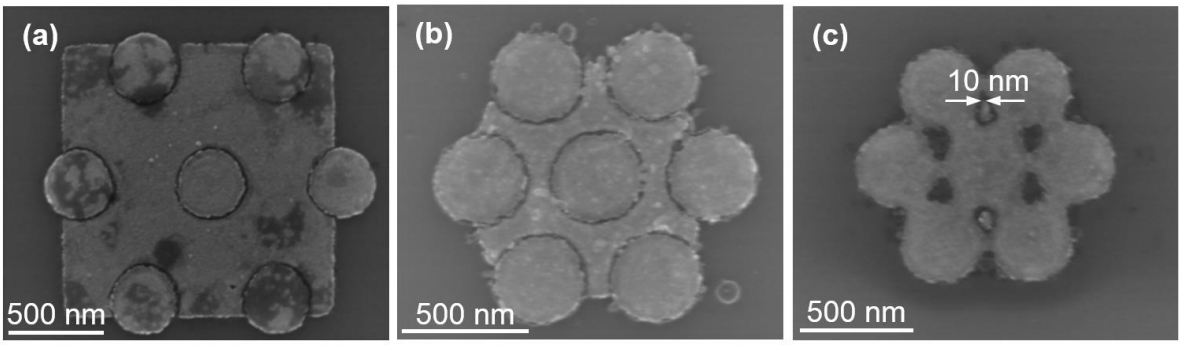

Figure 4.4.2: Circular gap patterns fabricated via blanket nanomasking.

Figure 4.4.2(c) shows one of the limitations of the nanomasking technique under the conditions used. The second evaporation step was unable to uniformly fill in all of the small regions between the circles as the gaps between them was decreased to the distance shown. This was possibly the result of an issue during the second resist lift-off process. This means that it would not necessarily be problematic were the second metal evaporation blanketed over the entire sample versus relying on a second lithography step as in this sample.

Regardless of the absence of the teardrop-shaped structures in four of the six gaps shown in Figure 4.4.2(c), the two structures that appeared exhibit impressive features. The small tips of the teardrop-shaped features taper down to 10 nm in width and potentially even below this.

Figure 4.4.3 shows parallel nanowire patterns that were fabricated via blanketing the entire area with the secondary metal evaporation step after performing the primary nanomasking procedure. The step one nanowires were spaced at different distances.

The top two images in Figure 4.4.3 show wires that were designed to be 100 nm in width and spaced by 300 nm. The wires in the bottom images were also designed to be 100 nm wide, with the left image designed for 200 nm spacing and the right image wires designed for 125 nm spacing. All of the resulting nanowires were separated by nanogaps of approximately 5 – 10 nm width.

The results reported in this section were considered to be a validation of the method of nanomasking in which the second lithography step is eliminated. Instead of a second lithography step, a blanketing evaporation over the entire sample can be used.

It should be noted that there was a visible sidewall roughness for many of the structures and gaps in the SEM images shown in this chapter. The roughness is likely an artifact of the lithography process at this scale (tens of nanometers), and not necessarily due to the nanomasking technique. Future work will investigate this and will likely confirm this suspicion. Most gold nanostructures fabricated using EBL have a similar sidewall roughness (on the order of nanometers). One must keep in mind that this scale involves the controlled simultaneous placement of hundreds and even tens of atoms. It has also been shown that surface roughness is beneficial for plasmonic devices because it helps to create stronger hybrid plasmon modes [93].

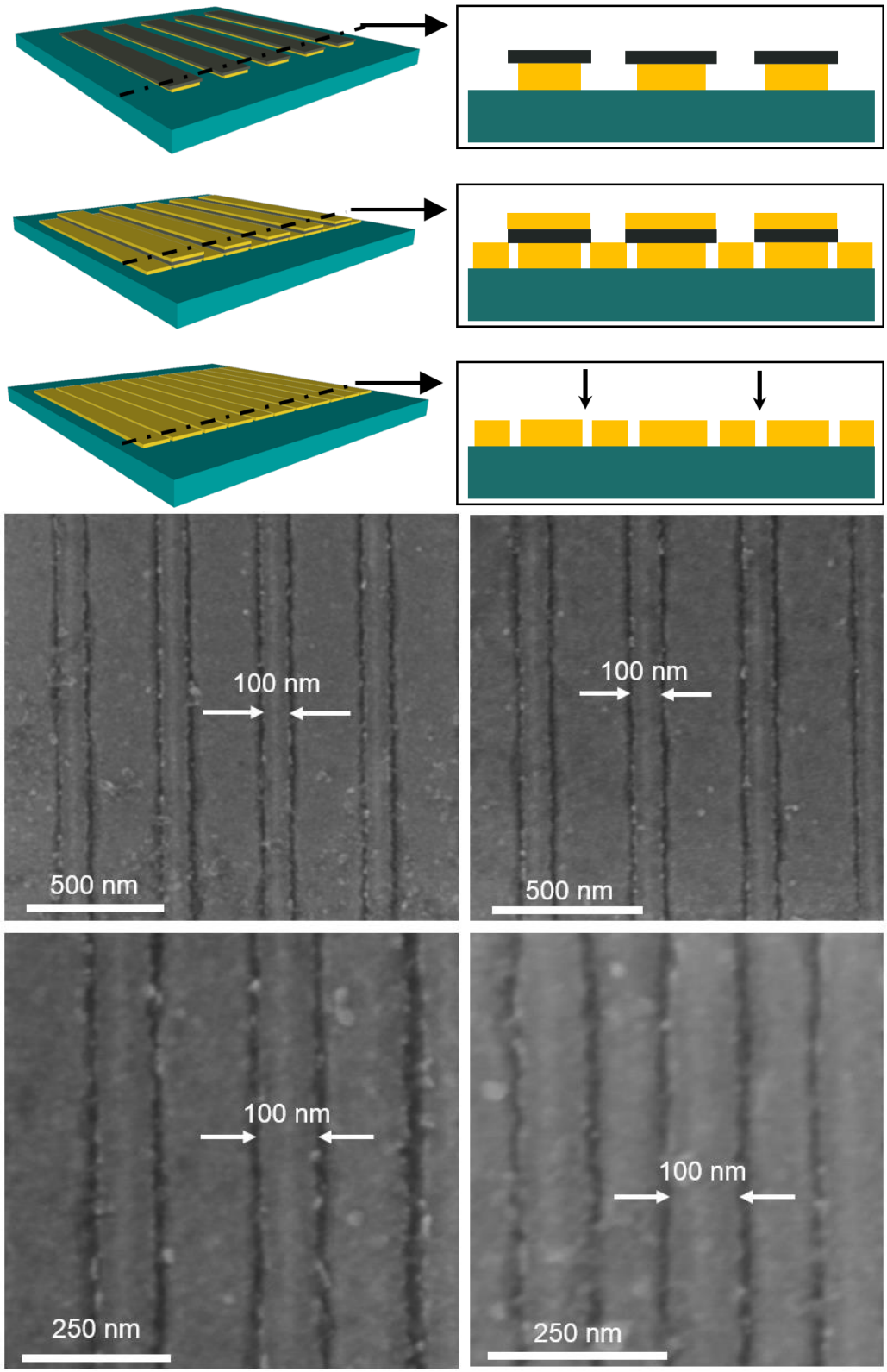

Figure 4.4.3: Parallel nanowires and gaps fabricated via blanket nanomasking.

Chapter 5. OPTICAL SIMULATION

Computational electromagnetic simulations are useful in optimizing the designs used in nanofabrication for the purpose of optical studies. Knowing how specific geometries respond to incident light under different conditions is beneficial for being able to fabricate useful structures for spectroscopy experiments. Due to the time-consuming nature of performing any multi-step nanofabrication process, computational results can reduce the time required for trial and error type fabrication to be used in future experimentation. Simulations are accurate tools for predicting what type of optical response to expect from a sample prior to fabrication.

A finite element method (FEM) simulation software, COMSOL 4.4, was used in this work for the simulation of electric field distributions in the near field of a nanostructure model. This was a three-dimensional concentric square model. The simulation was performed with the intention of understanding the potential for optical enhancement in devices with dimensions capable of being fabricated with the new process.

5.1 Simulation Parameters

As described in detail in Bauman et al. [125], a model was created and simulated. Gold material properties are assigned to the metal portions in all cases while an effective medium, simulation $n_{\text{eff}} = 1.25$, was applied to the surrounding environment to approximate the effect of the substrate. A simulated electromagnetic wave was incident on the device from a direction normal to the surface. The model was designed to be symmetrical, and the polarization direction was aligned with one gap direction and perpendicular to the other. The enhancement was defined as in the simulation discussed in Section 2.3. Thus, the enhancement calculated by the simulations was a unit-less value [118]. The simulation space and perfectly matched layer were

created in the same way as those used in the nanogap optical enhancement simulation described in Section 2.3

The 3D model was created to simulate a structure that was more like those capable of being fabricated via nanomasking as shown in Figure 4.3.4. The inner square width, w_{in}, was designed to be 500 nm, with the outer structure width, w_{out}, at 50 nm and a gap of 5 nm separating the two. This device geometry design is shown in Figure 5.1.1. This model is described in detail in Bauman et al. [125].

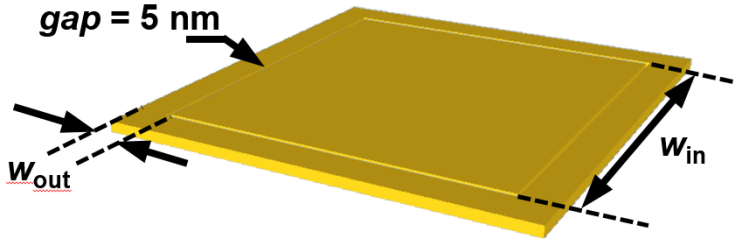

Figure 5.1.1: Device geometry for the concentric squares model [125].

The gap space in this simulation was given the same n_{eff} = 1.25 as the surrounding material. The simulation space and perfectly matched layer (hemispherical shell) were designed as shown in Figure 5.1.2, centered on the concentric squares geometry.

This spherical space was designed in order to provide sufficient space between the sample and the edges of the simulation area. This is key to differentiating between the near and far field electromagnetic radiation in the model. The light was incident on the device with the Poynting vector normal to the surface. This corresponds to the z-direction in Figure 5.2.1 with the light polarized in the x-direction as shown. The coordinate axis is defined relative to the top view Figure 5.2.1(sub-figure (i)) [125].

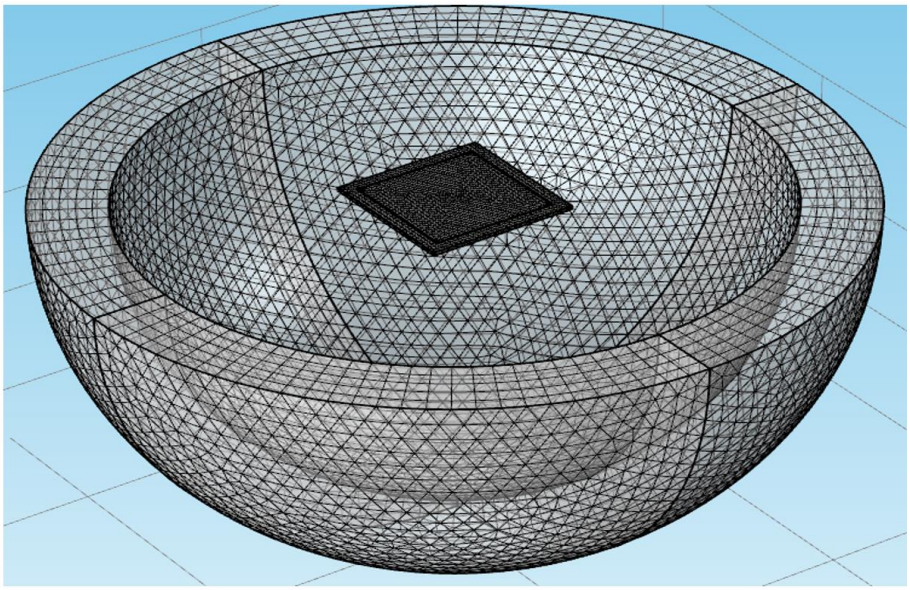

Figure 5.1.2: Sliced view of the bottom half of the simulation space and perfectly matched layer for the concentric squares model.

5.2 Simulation Results

Figure 5.2.1(a) – (e) shows the optical response of the device for different wavelengths of light, ranging from 500 to 900 nm by 100 nm intervals. The electric field distribution was plotted in the color maps (i – iii) where view (i) shows the z-plane. The model shows the field strength in all regions of the device, but cross-sectional slices were taken in order to determine the difference between enhancement in the gaps parallel to light polarization and those perpendicular. The strongest optical enhancement (shown in dark red) was found to occur between the two concentric squares, inside of the 5 nm air gap. The two-dimensional "slices" seen in Figure 5.2.1(ii) and (iii) display the optical enhancement within the gap of the device: (ii) views the nanogap in the x-plane and (iii) views the nanogaps in the y-plane. The light was constantly polarized in x, so it was transverse to the gap in (ii) and along the gap in (iii) since the gaps are orthogonal to each other. The top view (z-plane cross section) gives an indication that the gaps exhibit the highest localized field enhancement on the device. The x and y-plane slices

were indicative of polarization-dependent enhancement. For the device dimensions modeled, the field enhancement was increased with wavelength from 500 to 900 nm (Figure 5.2.1 (a-e)).

As reported in Bauman et al. [125],

> It was observed that the optical response changes within the gaps depending on the light polarization direction. For the wavelengths of 500 nm, 600 nm, and 700 nm, the strongest enhancement was produced when the electric field was polarized transverse to the gap. However, for the 800 nm wavelength, the strongest enhancement was for a polarization longitudinal to the gap. There was approximately equal enhancement for both gaps orientations at 900 nm. This shows the polarization dependence of the plasmonic optical enhancement. For the specified dimensions, maximum optical enhancement ranged from 13 at an incident wavelength of 500 nm to 2137 at the 900 nm incident wavelength. These results also show wavelength dependent results of the plasmonic response. Adjusting the dimensions of the device can allow for control over the optical response to different wavelengths of light, which can be tuned for maximum overall near-field enhancement. These models assumed no surface roughness. The surface roughness on the real devices can further improve the plasmonic enhancement as shown in [93].

These results validate that the 5 nm wide by 500 nm long nanogaps create a hotspot enhancement region along the length of the gap. This simulation provides useful insight into the potential plasmonic enhancement capabilities of the types of structures fabricated in this work, as discussed in Chapter 4. The optical enhancement demonstrated in these computational results exhibits the promise for surface-based light enhancement applications. Future experiments such as dark-field spectroscopy and photoluminescence will be useful in confirming this capability.

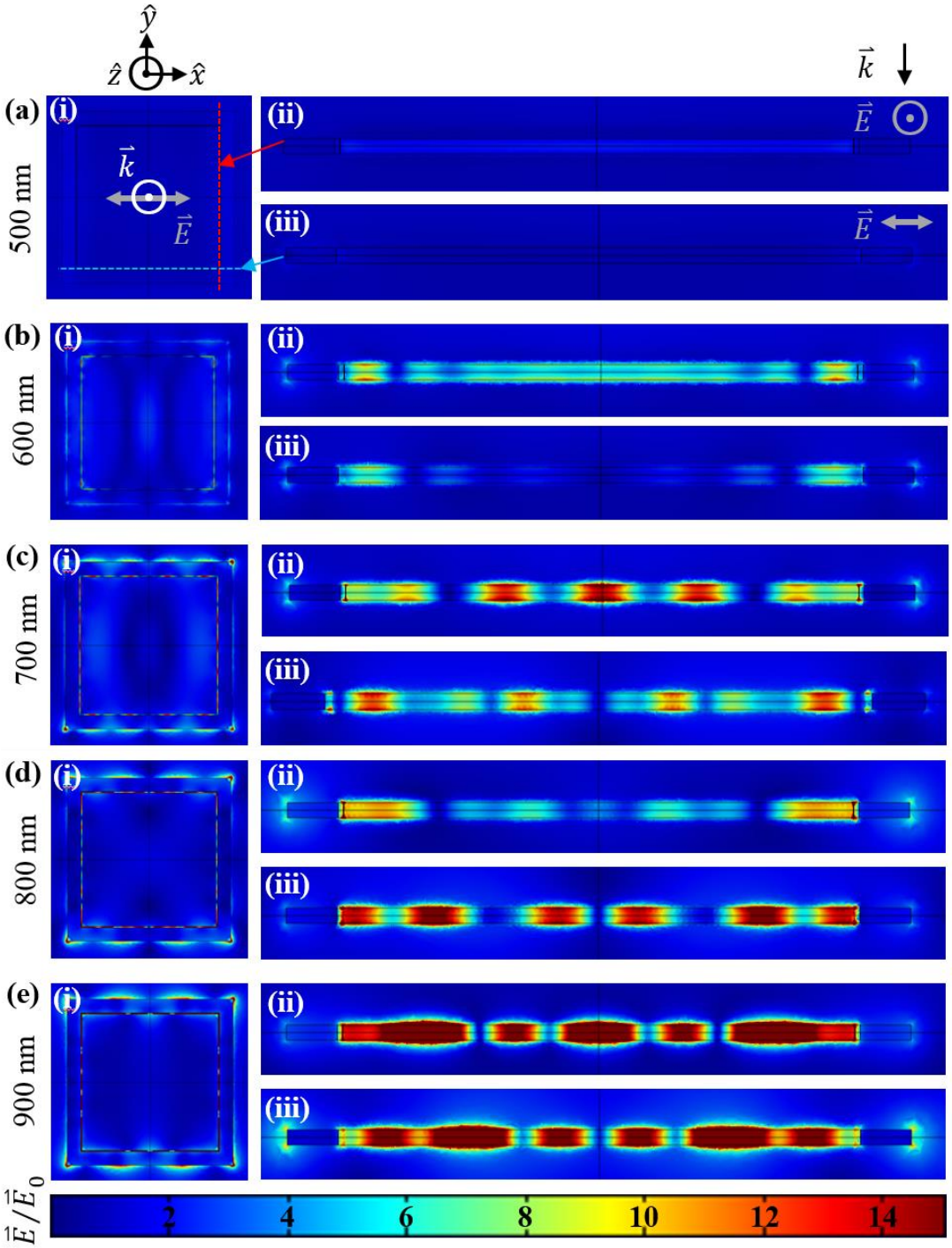

Figure 5.2.1: Electric field distribution for the concentric squares model displaying top views (i) and cross-sectional gap views (ii) and (iii) at different wavelengths (a) – (e) [125].

Chapter 6. CONCLUSION AND FUTURE WORK

In this work, a fabrication technique was developed by which nanogaps and nanostructures were fabricated below the resolution limit of lithography. The versatility of the nanomasking method was first demonstrated through a discussion of various process flows. Processes for simultaneous sub-10 nm gap fabrication were discussed, followed by those for creating sub-lithography resolution nanostructures, and the possibility of eliminating the need for the second lithography step in creating specific patterns. While electron beam lithography was used in this work, the same methodology can be followed using photolithography to obtain similar results. Similarly, deposition methods other than electron beam lithography may allow for successful reproduction of the nanomasking results discussed in this work.

Advanced fabrication results were then successfully demonstrated. The technique was shown to be capable of simultaneously producing multiple nanogaps on the order of 5 nm and nanostructures on the order of 15 nm. This was performed using well established lithography and deposition methods in a new fashion. Various geometries were fabricated including rectangular and circular features, all including these nanoscale features. The potential for obtaining nanogap devices without the need for the secondary lithography process was demonstrated as well.

A computational electromagnetic simulation was performed for one type of device capable of being fabricated. The local enhancement of the electric field upon incident light irradiation was calculated for the concentric squares model in this work. Polarization dependence and wavelength dependence were both observed for the optical enhancement within the device, with a peak enhancement of 2137 for the 900 nm incident field strength.

Reproduction of some of the preliminary results demonstrated in this work will help to further prove the robustness and repeatability of this newly developed style of nanofabrication. The nanomasking technique has the potential to create different types of geometries and thus fabricating new geometries will help to test even more capabilities. Varying steps in the process such as utilizing two different metals for the resulting structures or depositing them at different heights may provide more unforeseen benefits. See Appendix I: Supplemental Information for a brief discussion of these variations on nanomasking fabrication. Future work will also include a thorough study and investigation of the fabrication potential and limitation including a detailed study of gap width roughness.

Performing more electromagnetic simulations and obtaining experimental spectroscopy data for the optical response of the fabricated structures will be useful to understanding the full potential of nanomasking devices.

This work holds potential for benefitting many areas of nanoscience and technology. Continued research into the nanomasking technique will not only benefit applications in plasmonics and nano-optics, but also other areas, such as high-speed electronics, may be able to benefit from devices fabricated using this method [4], [11], [134]–[138]. With continued tests, the feasibility of nanomasking as a mass production capable fabrication technique may be more clearly discerned. Researching various structure geometries for their usefulness in specific applications may be a promising next step for this work.

REFERENCES

[1] C. A. Mack, “Fifty Years of Moore’s Law,” *IEEE Trans. Semicond. Manuf.*, vol. 24, no. 2, pp. 202–207, May 2011.

[2] J. D. Meindl, “Ultra-large scale integration,” *IEEE Trans. Electron Devices*, vol. 31, no. 11, pp. 1555–1561, Nov. 1984.

[3] C. Fiegna, H. Iwai, T. Wada, M. Saito, E. Sangiorgi, and B. Ricco, “Scaling the MOS transistor below 0.1 mu;m: methodology, device structures, and technology requirements,” *IEEE Trans. Electron Devices*, vol. 41, no. 6, pp. 941–951, Jun. 1994.

[4] R. F. Pease and S. Y. Chou, “Lithography and Other Patterning Techniques for Future Electronics,” *Proc. IEEE*, vol. 96, no. 2, pp. 248–270, Feb. 2008.

[5] Q. Cao and S. Han, “Single-walled carbon nanotubes for high-performance electronics,” *Nanoscale*, vol. 5, no. 19, pp. 8852–8863, Sep. 2013.

[6] J. W. Goodman, F. J. Leonberger, S.-Y. Kung, and R. A. Athale, “Optical interconnections for VLSI systems,” *Proc. IEEE*, vol. 72, no. 7, pp. 850–866, Jul. 1984.

[7] D. A. B. Miller, “Rationale and challenges for optical interconnects to electronic chips,” *Proc. IEEE*, vol. 88, no. 6, pp. 728–749, Jun. 2000.

[8] E. Ozbay, “Plasmonics: Merging Photonics and Electronics at Nanoscale Dimensions,” *Science*, vol. 311, no. 5758, pp. 189–193, Jan. 2006.

[9] P. Bharadwaj, B. Deutsch, and L. Novotny, “Optical Antennas,” *Adv. Opt. Photonics*, vol. 1, no. 3, pp. 438–483, Nov. 2009.

[10] L. Tsakalakos, *Nanotechnology for Photovoltaics*. CRC Press, 2010.

[11] H. A. Atwater and A. Polman, “Plasmonics for improved photovoltaic devices,” *Nat. Mater.*, vol. 9, no. 3, pp. 205–213, Mar. 2010.

[12] S. Ghosh, S. GhoshMitra, T. Cai, D. R. Diercks, N. C. Mills, and D. L. Hynds, “Alternating Magnetic Field Controlled, Multifunctional Nano-Reservoirs: Intracellular Uptake and Improved Biocompatibility,” *Nanoscale Res. Lett.*, vol. 5, no. 1, pp. 195–204, Jan. 2010.

[13] O. M. Koo, I. Rubinstein, and H. Onyuksel, “Role of nanotechnology in targeted drug delivery and imaging: a concise review,” *Nanomedicine Nanotechnol. Biol. Med.*, vol. 1, no. 3, pp. 193–212, Sep. 2005.

[14] S. GhoshMitra, D. R. Diercks, N. C. Mills, D. L. Hynds, and S. Ghosh, “Role of engineered nanocarriers for axon regeneration and guidance: Current status and future trends,” *Adv. Drug Deliv. Rev.*, vol. 64, no. 1, pp. 110–125, Jan. 2012.

[15] S. Nie, Y. Xing, G. J. Kim, and J. W. Simons, “Nanotechnology Applications in Cancer,” *Annu. Rev. Biomed. Eng.*, vol. 9, no. 1, pp. 257–288, 2007.

[16] P. Ball, *Made to Measure: New Materials for the 21st Century*. Princeton University Press, 1999.

[17] P. J. F. Harris and P. J. F. Harris, *Carbon Nanotubes and Related Structures: New Materials for the Twenty-first Century*. Cambridge University Press, 2001.

[18] S. A. Wilson, R. P. J. Jourdain, Q. Zhang, R. A. Dorey, C. R. Bowen, M. Willander, Q. U. Wahab, M. Willander, Al-hilli Safaa M., O. Nur, E. Quandt, C. Johansson, E. Pagounis, M. Kohl, J. Matovic, B. Samel, W. van der Wijngaart, E. W. H. Jager, D. Carlsson, Z. Djinovic, M. Wegener, C. Moldovan, R. Iosub, E. Abad, M. Wendlandt, C. Rusu, and K. Persson, “New materials for micro-scale sensors and actuators: An engineering review,” *Mater. Sci. Eng. R Rep.*, vol. 56, no. 1–6, pp. 1–129, Jun. 2007.

[19] C. N. R. Rao, A. K. Sood, K. S. Subrahmanyam, and A. Govindaraj, “Graphene: The New Two-Dimensional Nanomaterial,” *Angew. Chem. Int. Ed.*, vol. 48, no. 42, pp. 7752–7777, Oct. 2009.

[20] R. Valiev, “Materials science: Nanomaterial advantage,” *Nature*, vol. 419, no. 6910, pp. 887–889, Oct. 2002.

[21] G. M. Whitesides, J. P. Mathias, and C. T. Seto, “Molecular Self-Assembly and Nanochemistry: A Chemical Strategy for the Synthesis of Nanostructures,” Dec. 1991.

[22] D. Philp and J. F. Stoddart, “Self-Assembly in Natural and Unnatural Systems,” *Angew. Chem. Int. Ed. Engl.*, vol. 35, no. 11, pp. 1154–1196, Jun. 1996.

[23] G. M. Whitesides and B. Grzybowski, “Self-Assembly at All Scales,” *Science*, vol. 295, no. 5564, pp. 2418–2421, Mar. 2002.

[24] M. Haider, S. Uhlemann, E. Schwan, H. Rose, B. Kabius, and K. Urban, “Electron microscopy image enhanced,” *Nature*, vol. 392, no. 6678, pp. 768–769, Apr. 1998.

[25] J. Goldstein, *Scanning Electron Microscopy and X-ray Microanalysis: Third Edition*. Springer US, 2003.

[26] D. A. Edwards and M. J. Syphers, *An Introduction to the Physics of High Energy Accelerators*. John Wiley & Sons, 2008.

[27] S. Humphries, *Charged Particle Beams*. Courier Corporation, 2013.

[28] J. S. Dunfield and B. J. Taylor, “Selective thin film etch process,” US4793897 A, 27-Dec-1988.

[29] J. D. Plummer, M. D. Deal, and P. B. Griffin, *Silicon VLSI Technology: Fundamentals, Practice and Modeling*. Prentice Hall, 2000.

[30] J. E. Mahan, *Physical Vapor Deposition of Thin Films*. 2000.

[31] M. Leskelä and M. Ritala, "Atomic layer deposition (ALD): from precursors to thin film structures," *Thin Solid Films*, vol. 409, no. 1, pp. 138–146, Apr. 2002.

[32] G. L. Hornyak, H. F. Tibbals, J. Dutta, and J. J. Moore, *Introduction to Nanoscience and Nanotechnology*. CRC Press, 2008.

[33] E. Serrano, G. Rus, and J. García-Martínez, "Nanotechnology for sustainable energy," *Renew. Sustain. Energy Rev.*, vol. 13, no. 9, pp. 2373–2384, Dec. 2009.

[34] W. Lu and C. M. Lieber, "Nanoelectronics from the bottom up," *Nat. Mater.*, vol. 6, no. 11, pp. 841–850, Nov. 2007.

[35] J. Appenzeller, J. Knoch, M. T. Bjork, H. Riel, H. Schmid, and W. Riess, "Toward Nanowire Electronics," *IEEE Trans. Electron Devices*, vol. 55, no. 11, pp. 2827–2845, Nov. 2008.

[36] R. S. Kane and A. D. Stroock, "Nanobiotechnology: Protein-Nanomaterial Interactions," *Biotechnol. Prog.*, vol. 23, no. 2, pp. 316–319, Jan. 2007.

[37] J. Wang, "Nanomaterial-based electrochemical biosensors," *Analyst*, vol. 130, no. 4, pp. 421–426, Mar. 2005.

[38] T. Thio, "Surface-plasmon enhanced photovoltaic device," US6441298 B1, 27-Aug-2002.

[39] T. K. Manna and S. M. Mahajan, "Nanotechnology in the Development of Photovoltaic Cells," in *International Conference on Clean Electrical Power, 2007. ICCEP '07*, 2007, pp. 379–386.

[40] V. E. Ferry, L. A. Sweatlock, D. Pacifici, and H. A. Atwater, "Plasmonic Nanostructure Design for Efficient Light Coupling into Solar Cells," *Nano Lett.*, vol. 8, no. 12, pp. 4391–4397, Dec. 2008.

[41] K. Nakayama, K. Tanabe, and H. A. Atwater, "Plasmonic nanoparticle enhanced light absorption in GaAs solar cells," *Appl. Phys. Lett.*, vol. 93, no. 12, p. 121904, Sep. 2008.

[42] S. Pillai and M. A. Green, "Plasmonics for photovoltaic applications," *Sol. Energy Mater. Sol. Cells*, vol. 94, no. 9, pp. 1481–1486, Sep. 2010.

[43] V. E. Ferry, J. N. Munday, and H. A. Atwater, "Design Considerations for Plasmonic Photovoltaics," *Adv. Mater.*, vol. 22, no. 43, pp. 4794–4808, Nov. 2010.

[44] I. Thomann, B. A. Pinaud, Z. Chen, B. M. Clemens, T. F. Jaramillo, and M. L. Brongersma, "Plasmon Enhanced Solar-to-Fuel Energy Conversion," *Nano Lett.*, vol. 11, no. 8, pp. 3440–3446, Aug. 2011.

[45] J. Yang, J. You, C.-C. Chen, W.-C. Hsu, H. Tan, X. W. Zhang, Z. Hong, and Y. Yang, "Plasmonic Polymer Tandem Solar Cell," *ACS Nano*, vol. 5, no. 8, pp. 6210–6217, Aug. 2011.

[46] A. J. Haes, C. L. Haynes, A. D. McFarland, G. C. Schatz, R. P. Van Duyne, and S. Zou, "Plasmonic Materials for Surface-Enhanced Sensing and Spectroscopy," *MRS Bull.*, vol. 30, no. 05, pp. 368–375, May 2005.

[47] D. R. Ward, N. K. Grady, C. S. Levin, N. J. Halas, Y. Wu, P. Nordlander, and D. Natelson, "Electromigrated Nanoscale Gaps for Surface-Enhanced Raman Spectroscopy," *Nano Lett.*, vol. 7, no. 5, pp. 1396–1400, May 2007.

[48] K. A. Willets and R. P. Van Duyne, "Localized Surface Plasmon Resonance Spectroscopy and Sensing," *Annu. Rev. Phys. Chem.*, vol. 58, no. 1, pp. 267–297, 2007.

[49] J. P. Camden, J. A. Dieringer, J. Zhao, and R. P. Van Duyne, "Controlled Plasmonic Nanostructures for Surface-Enhanced Spectroscopy and Sensing," *Acc. Chem. Res.*, vol. 41, no. 12, pp. 1653–1661, Dec. 2008.

[50] J. M. Baik, S. J. Lee, and M. Moskovits, "Polarized Surface-Enhanced Raman Spectroscopy from Molecules Adsorbed in Nano-Gaps Produced by Electromigration in Silver Nanowires," *Nano Lett.*, vol. 9, no. 2, pp. 672–676, Feb. 2009.

[51] J. B. Herzog, "Optical spectroscopy of colloidal CdSe semiconductor nanostructures," 23-Jun-2011. [Online]. Available: http://etd.nd.edu/ETD-db/theses/available/etd-06172011-075105/. [Accessed: 12-Feb-2015].

[52] D. Natelson, Y. Li, and J. B. Herzog, "Nanogap structures: combining enhanced Raman spectroscopy and electronic transport," *Phys. Chem. Chem. Phys.*, vol. 15, no. 15, pp. 5262–5275, Mar. 2013.

[53] W. Denk and D. W. Pohl, "Near-field optics: Microscopy with nanometer-size fields," *J. Vac. Sci. Technol. B*, vol. 9, no. 2, pp. 510–513, Mar. 1991.

[54] L. E. Brus and J. K. Trautman, "Nanocrystals and Nano-Optics," *Philos. Trans. R. Soc. Lond. Math. Phys. Eng. Sci.*, vol. 353, no. 1703, pp. 313–321, Dec. 1995.

[55] M. Stockman, "Light-emitting devices: From nano-optics to street lights," *Nat. Mater.*, vol. 3, no. 7, pp. 423–424, Jul. 2004.

[56] S. Lal, S. Link, and N. J. Halas, "Nano-optics from sensing to waveguiding," *Nat. Photonics*, vol. 1, no. 11, pp. 641–648, Nov. 2007.

[57] L. Novotny, "Nano-optics: Optical antennas tuned to pitch," *Nature*, vol. 455, no. 7215, pp. 887–887, Oct. 2008.

[58] S. Kemme, *Microoptics and Nanooptics Fabrication*. CRC Press, 2009.

[59] Z.-Y. Li, “Optics and photonics at nanoscale: Principles and perspectives,” *EPL Europhys. Lett.*, vol. 110, no. 1, p. 14001, Apr. 2015.

[60] H. Harutyunyan, “Nonlinear optics: Anti-diffraction of light,” *Nat. Photonics*, vol. 9, no. 4, pp. 213–214, Apr. 2015.

[61] N. Dean, “Colouring at the nanoscale,” *Nat. Nanotechnol.*, vol. 10, no. 1, pp. 15–16, Jan. 2015.

[62] A. W. Topol, D. C. L. Tulipe, L. Shi, D. J. Frank, K. Bernstein, S. E. Steen, A. Kumar, G. U. Singco, A. M. Young, K. W. Guarini, and M. Ieong, “Three-dimensional integrated circuits,” *IBM J. Res. Dev.*, vol. 50, no. 4.5, pp. 491–506, Jul. 2006.

[63] W. Ehrfeld and A. Schmidt, “Recent developments in deep x-ray lithography,” *J. Vac. Sci. Technol. B*, vol. 16, no. 6, pp. 3526–3534, Nov. 1998.

[64] R. K. Kupka, F. Bouamrane, C. Cremers, and S. Megtert, “Microfabrication: LIGA-X and applications,” *Appl. Surf. Sci.*, vol. 164, no. 1–4, pp. 97–110, Sep. 2000.

[65] S. K. Griffiths, “Fundamental limitations of LIGA x-ray lithography: sidewall offset, slope and minimum feature size,” *J. Micromechanics Microengineering*, vol. 14, no. 7, p. 999, Jul. 2004.

[66] M. Altissimo, “E-beam lithography for micro-/nanofabrication,” *Biomicrofluidics*, vol. 4, no. 2, p. 026503, Jun. 2010.

[67] B. Cord, J. Yang, H. Duan, D. C. Joy, J. Klingfus, and K. K. Berggren, “Limiting factors in sub-10nm scanning-electron-beam lithography,” *J. Vac. Sci. Technol. B*, vol. 27, no. 6, pp. 2616–2621, Nov. 2009.

[68] T. H. P. Chang, “Proximity effect in electron-beam lithography,” *J. Vac. Sci. Technol.*, vol. 12, no. 6, pp. 1271–1275, Nov. 1975.

[69] A. N. Broers, A. C. F. Hoole, and J. M. Ryan, “Electron beam lithography—Resolution limits,” *Microelectron. Eng.*, vol. 32, no. 1–4, pp. 131–142, Sep. 1996.

[70] C. Vieu, F. Carcenac, A. Pépin, Y. Chen, M. Mejias, A. Lebib, L. Manin-Ferlazzo, L. Couraud, and H. Launois, “Electron beam lithography: resolution limits and applications,” *Appl. Surf. Sci.*, vol. 164, no. 1–4, pp. 111–117, Sep. 2000.

[71] C. Genet and T. W. Ebbesen, “Light in tiny holes,” *Nature*, vol. 445, no. 7123, pp. 39–46, Jan. 2007.

[72] L. Cao, J. S. White, J.-S. Park, J. A. Schuller, B. M. Clemens, and M. L. Brongersma, “Engineering light absorption in semiconductor nanowire devices,” *Nat. Mater.*, vol. 8, no. 8, pp. 643–647, Aug. 2009.

[73] J. A. Schuller, E. S. Barnard, W. Cai, Y. C. Jun, J. S. White, and M. L. Brongersma, "Plasmonics for extreme light concentration and manipulation," *Nat. Mater.*, vol. 9, no. 3, pp. 193–204, Mar. 2010.

[74] L. Novotny and N. van Hulst, "Antennas for light," *Nat. Photonics*, vol. 5, no. 2, pp. 83–90, Feb. 2011.

[75] A. Manjavacas, J. G. Liu, V. Kulkarni, and P. Nordlander, "Plasmon-Induced Hot Carriers in Metallic Nanoparticles," *ACS Nano*, Jun. 2014.

[76] W. L. Barnes, A. Dereux, and T. W. Ebbesen, "Surface plasmon subwavelength optics," *Nature*, vol. 424, no. 6950, pp. 824–830, Aug. 2003.

[77] V. A. M. and T. F. George, "Optics of Nanostructured Materials," *Meas. Sci. Technol.*, vol. 12, no. 9, p. 1607, Sep. 2001.

[78] L. Pavesi, Z. Gaburro, L. D. Negro, P. Bettotti, G. V. Prakash, M. Cazzanelli, and C. J. Oton, "Nanostructured silicon as a photonic material," *Opt. Lasers Eng.*, vol. 39, no. 3, pp. 345–368, Mar. 2003.

[79] D. S. Wiersma, R. Sapienza, S. Mujumdar, M. Colocci, M. Ghulinyan, and L. Pavesi, "Optics of nanostructured dielectrics," *J. Opt. Pure Appl. Opt.*, vol. 7, no. 2, p. S190, Feb. 2005.

[80] V. E. Ferry, A. Polman, and H. A. Atwater, "Modeling Light Trapping in Nanostructured Solar Cells," *ACS Nano*, vol. 5, no. 12, pp. 10055–10064, Dec. 2011.

[81] V. R. Almeida, Q. Xu, C. A. Barrios, and M. Lipson, "Guiding and confining light in void nanostructure," *Opt. Lett.*, vol. 29, no. 11, pp. 1209–1211, Jun. 2004.

[82] D. R. Ward, N. J. Halas, J. W. Ciszek, J. M. Tour, Y. Wu, P. Nordlander, and D. Natelson, "Simultaneous Measurements of Electronic Conduction and Raman Response in Molecular Junctions," *Nano Lett.*, vol. 8, no. 3, pp. 919–924, Mar. 2008.

[83] D. R. Ward, G. D. Scott, Z. K. Keane, N. J. Halas, and D. Natelson, "Electronic and optical properties of electromigrated molecular junctions," *J. Phys. Condens. Matter*, vol. 20, no. 37, p. 374118, Sep. 2008.

[84] D. R. Ward, F. Hüser, F. Pauly, J. C. Cuevas, and D. Natelson, "Optical rectification and field enhancement in a plasmonic nanogap," *Nat. Nanotechnol.*, vol. 5, no. 10, pp. 732–736, Oct. 2010.

[85] A. Fursina, S. Lee, R. G. S. Sofin, I. V. Shvets, and D. Natelson, "Nanogaps with very large aspect ratios for electrical measurements," *Appl. Phys. Lett.*, vol. 92, no. 11, p. 113102, Mar. 2008.

[86] L. Tong, H. Xu, and M. Käll, "Nanogaps for SERS applications," *MRS Bull.*, vol. 39, no. 02, pp. 163–168, 2014.

[87] Y. Yokota, K. Ueno, and H. Misawa, “Essential nanogap effects on surface-enhanced Raman scattering signals from closely spaced gold nanoparticles,” *Chem. Commun.*, vol. 47, no. 12, pp. 3505–3507, Mar. 2011.

[88] A. W. Clark and J. M. Cooper, “Nanogap Ring Antennae as Plasmonically Coupled SERRS Substrates,” *Small*, vol. 7, no. 1, pp. 119–125, Jan. 2011.

[89] U. S. Dinish, F. C. Yaw, A. Agarwal, and M. Olivo, “Development of highly reproducible nanogap SERS substrates: Comparative performance analysis and its application for glucose sensing,” *Biosens. Bioelectron.*, vol. 26, no. 5, pp. 1987–1992, Jan. 2011.

[90] W. Kubo and S. Fujikawa, “Au Double Nanopillars with Nanogap for Plasmonic Sensor,” *Nano Lett.*, vol. 11, no. 1, pp. 8–15, Jan. 2011.

[91] R. A. Awang, S. H. El-Gohary, N.-H. Kim, and K. M. Byun, “Enhancement of field–analyte interaction at metallic nanogap arrays for sensitive localized surface plasmon resonance detection,” *Appl. Opt.*, vol. 51, no. 31, pp. 7437–7442, Nov. 2012.

[92] H. Im, K. C. Bantz, N. C. Lindquist, C. L. Haynes, and S.-H. Oh, “Vertically Oriented Sub-10-nm Plasmonic Nanogap Arrays,” *Nano Lett.*, vol. 10, no. 6, pp. 2231–2236, Jun. 2010.

[93] J. B. Herzog, M. W. Knight, Y. Li, K. M. Evans, N. J. Halas, and D. Natelson, “Dark Plasmons in Hot Spot Generation and Polarization in Interelectrode Nanoscale Junctions,” *Nano Lett.*, vol. 13, no. 3, pp. 1359–1364, Mar. 2013.

[94] A. García-Martín, D. R. Ward, D. Natelson, and J. C. Cuevas, “Field enhancement in subnanometer metallic gaps,” *Phys. Rev. B*, vol. 83, no. 19, p. 193404, May 2011.

[95] Y. Chen and A. Pépin, “Nanofabrication: Conventional and nonconventional methods,” *Electrophoresis*, vol. 22, no. 2, pp. 187–207, Jan. 2001.

[96] A. Biswas, I. S. Bayer, A. S. Biris, T. Wang, E. Dervishi, and F. Faupel, “Advances in top–down and bottom–up surface nanofabrication: Techniques, applications & future prospects,” *Adv. Colloid Interface Sci.*, vol. 170, no. 1–2, pp. 2–27, Jan. 2012.

[97] Q. Xu, J. Bao, R. M. Rioux, R. Perez-Castillejos, F. Capasso, and G. M. Whitesides, “Fabrication of Large-Area Patterned Nanostructures for Optical Applications by Nanoskiving,” *Nano Lett.*, vol. 7, no. 9, pp. 2800–2805, Sep. 2007.

[98] D. C. Watson, R. V. Martinez, Y. Fontana, E. Russo-Averchi, M. Heiss, A. Fontcuberta i Morral, G. M. Whitesides, and M. Lončar, “Nanoskiving Core–Shell Nanowires: A New Fabrication Method for Nano-optics,” *Nano Lett.*, vol. 14, no. 2, pp. 524–531, Feb. 2014.

[99] S. Davies and B. Khamsehpour, “Focused ion beam machining and deposition for nanofabrication,” *Vacuum*, vol. 47, no. 5, pp. 455–462, May 1996.

[100] A. Lugstein, B. Basnar, J. Smoliner, E. Bertagnolli, and M. Weil, "Advanced nanoscale material processing with focused ion beams," *J. Vac. Sci. Technol. B*, vol. 22, no. 6, pp. 2995–2999, Nov. 2004.

[101] A. A. Tseng, "Recent Developments in Nanofabrication Using Focused Ion Beams," *Small*, vol. 1, no. 10, pp. 924–939, Oct. 2005.

[102] R. M. Langford, "Focused Ion Beam Nanofabrication: A Comparison with Conventional Processing Techniques," *J. Nanosci. Nanotechnol.*, vol. 6, no. 3, pp. 661–668, Mar. 2006.

[103] M. Ito, M. Yagi, K. Morihara, and J.-I. Shirakashi, "Simultaneous fabrication of nanogaps using field-emission-induced electromigration," in *2014 International Conference on Manipulation, Manufacturing and Measurement on the Nanoscale (3M-NANO)*, 2014, pp. 312–315.

[104] R. J. P. Keijsers, O. I. Shklyarevskii, J. G. H. Hermsen, and H. van Kempen, "Thin film mechanically controllable break junctions," *Rev. Sci. Instrum.*, vol. 67, no. 8, pp. 2863–2866, Aug. 1996.

[105] J. M. van Ruitenbeek, A. Alvarez, I. Piñeyro, C. Grahmann, P. Joyez, M. H. Devoret, D. Esteve, and C. Urbina, "Adjustable nanofabricated atomic size contacts," *Rev. Sci. Instrum.*, vol. 67, no. 1, pp. 108–111, Jan. 1996.

[106] T. Li, W. Hu, and D. Zhu, "Nanogap Electrodes," *Adv. Mater.*, vol. 22, no. 2, pp. 286–300, Jan. 2010.

[107] H. Agheli and D. S. Sutherland, "Nanofabrication of polymer surfaces utilizing colloidal lithography and ion etching," *IEEE Trans. NanoBioscience*, vol. 5, no. 1, pp. 9–14, Mar. 2006.

[108] J. Zhang, Y. Li, X. Zhang, and B. Yang, "Colloidal Self-Assembly Meets Nanofabrication: From Two-Dimensional Colloidal Crystals to Nanostructure Arrays," *Adv. Mater.*, vol. 22, no. 38, pp. 4249–4269, Oct. 2010.

[109] A. Dolatshahi-Pirouz, K. Kolind, C. P. Pennisi, M. Duroux, V. Zachar, M. Foss, and F. Besenbacher, "Synthesis of Nano- and Micro-Scale Topographies by Combining Colloidal Lithography and Glancing Angle Deposition (GLAD)," *Adv. Eng. Mater.*, vol. 17, no. 1, pp. 8–13, Jan. 2015.

[110] F. Liu, M. T. Umlor, L. Shen, J. Weston, W. Eads, J. A. Barnard, and G. J. Mankey, "The growth of nanoscale structured iron films by glancing angle deposition," *J. Appl. Phys.*, vol. 85, no. 8, pp. 5486–5488, Apr. 1999.

[111] B. Dick, M. J. Brett, and T. Smy, "Controlled growth of periodic pillars by glancing angle deposition," *J. Vac. Sci. Technol. B*, vol. 21, no. 1, pp. 23–28, Jan. 2003.

[112] M. M. Hawkeye and M. J. Brett, "Glancing angle deposition: Fabrication, properties, and applications of micro- and nanostructured thin films," *J. Vac. Sci. Technol. A*, vol. 25, no. 5, pp. 1317–1335, Sep. 2007.

[113] M. O. Jensen and M. J. Brett, "Periodically structured glancing angle deposition thin films," *IEEE Trans. Nanotechnol.*, vol. 4, no. 2, pp. 269–277, Mar. 2005.

[114] M. T. Taschuk, M. M. Hawkeye, and M. J. Brett, "Chapter 13 - Glancing Angle Deposition," in *Handbook of Deposition Technologies for Films and Coatings (Third Edition)*, P. M. Martin, Ed. Boston: William Andrew Publishing, 2010, pp. 621–678.

[115] M. M. Hawkeye, M. T. Taschuk, and M. J. Brett, "Introduction: Glancing Angle Deposition Technology," in *Glancing Angle Deposition of Thin Films*, John Wiley & Sons, Ltd, 2014, pp. 1–30.

[116] R. B. Abdulrahman, H. Cansizoglu, M. F. Cansizoglu, J. B. Herzog, and T. Karabacak, "Enhanced light trapping and plasmonic properties of aluminum nanorods fabricated by glancing angle deposition," *J. Vac. Sci. Technol. A*, vol. 33, no. 4, p. 041501, Jul. 2015.

[117] W. Zhu, M. G. Banaee, D. Wang, Y. Chu, and K. B. Crozier, "Lithographically Fabricated Optical Antennas with Gaps Well Below 10 nm," *Small*, vol. 7, no. 13, pp. 1761–1766, Jul. 2011.

[118] S. J. Bauman, D. T. Debu, A. M. Hill, E. C. Novak, D. Natelson, and J. B. Herzog, "Optical nanogap matrices for plasmonic enhancement applications," in *SPIE 9163, Plasmonics: Metallic Nanostructures and Their Optical Properties XII*, San Diego, CA, 2014, vol. 9163, p. 91631A–91631A–6.

[119] J. Homola, S. S. Yee, and G. Gauglitz, "Surface plasmon resonance sensors: review," *Sens. Actuators B Chem.*, vol. 54, no. 1–2, pp. 3–15, Jan. 1999.

[120] K. C. Bantz, A. F. Meyer, N. J. Wittenberg, H. Im, Ö. Kurtuluş, S. H. Lee, N. C. Lindquist, S.-H. Oh, and C. L. Haynes, "Recent progress in SERS biosensing," *Phys. Chem. Chem. Phys.*, vol. 13, no. 24, pp. 11551–11567, Jun. 2011.

[121] T. Chung, S.-Y. Lee, E. Y. Song, H. Chun, and B. Lee, "Plasmonic Nanostructures for Nano-Scale Bio-Sensing," *Sensors*, vol. 11, no. 11, pp. 10907–10929, Nov. 2011.

[122] J. Chen, G. Qin, J. Wang, J. Yu, B. Shen, S. Li, Y. Ren, L. Zuo, W. Shen, and B. Das, "One-step fabrication of sub-10-nm plasmonic nanogaps for reliable SERS sensing of microorganisms," *Biosens. Bioelectron.*, vol. 44, pp. 191–197, Jun. 2013.

[123] R. Yu, Q. Lin, S.-F. Leung, and Z. Fan, "Nanomaterials and nanostructures for efficient light absorption and photovoltaics," *Nano Energy*, vol. 1, no. 1, pp. 57–72, Jan. 2012.

[124] J. B. Herzog and D. Natelson, "Systems and Methods for Fabricating Nanostructures and Nanogaps," 62/039,337.

[125] S. J. Bauman, E. C. Novak, D. T. Debu, and J. B. Herzog, “Fabrication of sub-lithography limited structures via Nanomasking technique for plasmonic enhancement applications,” *IEEE Trans. Nanotechnol.*, vol. In press, Jul. 2015.

[126] F. A. Ghelmansarai, “Interdigital photodetector for indirect x-ray detection in a radiography imaging system,” US6373062 B1, 16-Apr-2002.

[127] A. I. Nusir, J. Aguilar, Z. Bever, and M. O. Manasreh, “Uncooled photodetectors based on CdSe nanocrystals with an interdigital metallization,” *Appl. Phys. Lett.*, vol. 104, no. 5, p. 051124, Feb. 2014.

[128] A. M. Hill, A. I. Nusir, P. V. Nguyen, O. M. Manasreh, and J. B. Herzog, “Computational electromagnetic study of plasmonic effects in interdigital arrays,” in *Proc. SPIE 9163, Plasmonics: Metallic Nanostructures and Their Optical Properties XII*, San Diego, CA, 2014, vol. 91633, p. 91633Q.

[129] A. I. Nusir, A. M. Hill, M. O. Manasreh, and J. B. Herzog, “Near-infrared metal-semiconductor-metal photodetector based on semi-insulating GaAs and interdigital electrodes,” *Photonics Res.*, vol. 3, no. 1, p. 1, Feb. 2015.

[130] S. Tretyakov, “On geometrical scaling of split-ring and double-bar resonators at optical frequencies,” *Metamaterials*, vol. 1, no. 1, pp. 40–43, Mar. 2007.

[131] A. W. Clark, A. Glidle, D. R. S. Cumming, and J. M. Cooper, “Nanophotonic split-ring resonators as dichroics for molecular spectroscopy,” *Appl. Phys. Lett.*, vol. 93, no. 2, p. 023121, Jul. 2008.

[132] T. D. Corrigan, P. W. Kolb, A. B. Sushkov, H. D. Drew, D. C. Schmadel, and R. J. Phaneuf, “Optical plasmonic resonances in split-ring resonator structures: an improved LC model,” *Opt. Express*, vol. 16, no. 24, p. 19850, Nov. 2008.

[133] A. W. Clark, A. Glidle, D. R. S. Cumming, and J. M. Cooper, “Plasmonic Split-Ring Resonators as Dichroic Nanophotonic DNA Biosensors,” *J. Am. Chem. Soc.*, vol. 131, no. 48, pp. 17615–17619, Dec. 2009.

[134] Z.-J. Yang, N.-C. Kim, J.-B. Li, M.-T. Cheng, S.-D. Liu, Z.-H. Hao, and Q.-Q. Wang, “Surface plasmons amplifications in single Ag nanoring,” *Opt. Express*, vol. 18, no. 5, pp. 4006–4011, Mar. 2010.

[135] G. F. Walsh and L. D. Negro, “Engineering Plasmon-Enhanced Au Light Emission with Planar Arrays of Nanoparticles,” *Nano Lett.*, vol. 13, no. 2, pp. 786–792, Feb. 2013.

[136] R. Rodríguez-Oliveros and J. A. Sánchez-Gil, “Gold nanostars as thermoplasmonic nanoparticles for optical heating,” *Opt. Express*, vol. 20, no. 1, pp. 621–626, Jan. 2012.

[137] B. C. Stipe, T. C. Strand, C. C. Poon, H. Balamane, T. D. Boone, J. A. Katine, J.-L. Li, V. Rawat, H. Nemoto, A. Hirotsune, O. Hellwig, R. Ruiz, E. Dobisz, D. S. Kercher, N.

Robertson, T. R. Albrecht, and B. D. Terris, “Magnetic recording at 1.5 Pb m(-2) using an integrated plasmonic antenna,” *Nat. Photonics*, vol. 4, no. 7, pp. 484–488, Jul. 2010.

[138] T. J. Davis, “Plasmonics: the convergence between optics and electronics,” in *Proc. SPIE 8923, Micro/Nano Materials, Devices, and Systems*, 2013 vol. 8923, p. 89232R.

Appendix A: Description of Research for Popular Publication

Not Your Grandpa's Nanolithography

Creating a new generation of nanoscale devices

When it comes to creating technology at the nanoscale, improving control over structure geometry and achieving mass production are key. At the University of Arkansas, μEP MS student Stephen Bauman and his major professor Dr. Joseph Herzog have developed a method that provides increased control over the fabrication of many sub-10 nanometer patterns at once which is scalable to a wafer-sized area.

Today, much of the nanotechnology that is useful for semiconductor electronics, LEDs, solar cells, and other applications is created by combinations of bottom-up and top-down fabrication methods. These refer to deposition and growth methods that start from the bottom and build up nanoscale structures of specific materials or starting with blocks or layers of material and essentially chiseling them down with some top-down process to leave the desired structures behind. At this size, and especially below 10 nanometers, many common methods of patterning devices lack sufficient resolution. Bauman says, "Many existing techniques just aren't capable of producing geometries with such fine features or spaces between features. Think of trying to trace an extremely fine pencil sketch with a dry erase marker. You are bound to bunch together some of the lines unintentionally."

Bauman explains that the advanced technique makes use of existing methods in a unique way. By cleverly employing a sacrificial layer of metal in the first of the two steps of the process, the metal is able to provide finer resolution of the resulting features. This allows for a

level of control and simultaneous nanostructure creation that is typically impossible with the previous methods alone. Figure A.1 shows a process flow for the nanomasking technique.

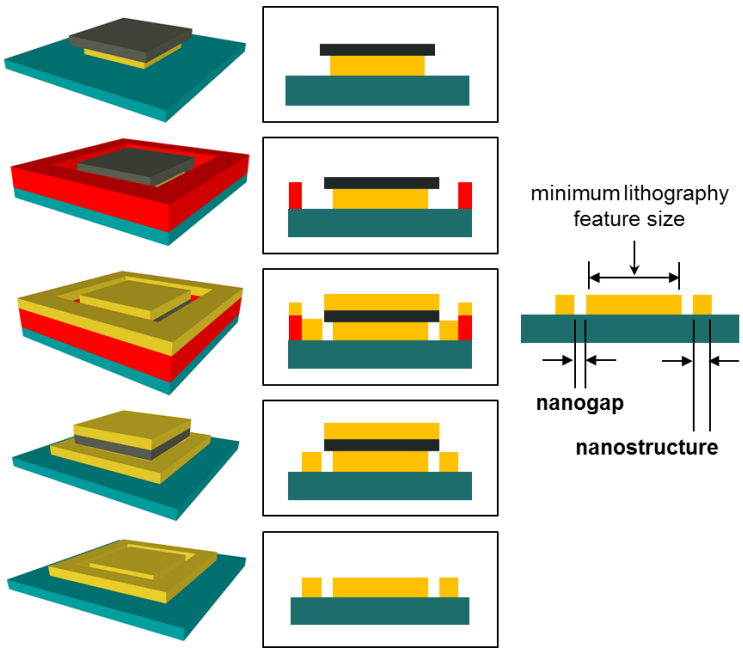

Figure A.1: Nanomasking process flow including sacrificial metal layer (gray) and resulting features [125].

Making use of the University of Arkansas Electron Optics Facility as well as other campus labs for processing, Bauman has successfully demonstrated the feasibility of this advanced technique. He explains, "The sacrificial metal layer acts as an umbrella that shields, or masks, areas of the surface below from subsequent deposition of materials. The width of the umbrella, and thus the masked area, is controllable, therefore the technique allows designers control over the dimensions of the resulting features. This width can be on the order of single nanometers, and that is how this technique overcomes the limitations of the machines used in the other process steps, which is on the order of 60 nanometers."

The nanomasking technique is on the forefront of nanoscale technological innovation. The ability to simultaneously create many sub-10 nanometer features on a substrate holds great potential for many areas of nanotechnology and nanoscience.

Appendix B: Executive Summary of Newly Created Intellectual Property

The following list of new intellectual property items were created in the course of this research project and should be considered from both a patent and commercialization perspective.

1. The two-step method of fabrication called “nanomasking” in which a lithographically patterned metal oxide layer is used as a deposition mask capable of resolution on the order of 10 nm for simultaneously fabricated features.
2. Specific devices fabricated via the nanomasking technique that cannot be easily fabricated via other existing methods and variations on the nanomasking technique including different material combinations, varying material heights and geometries, and the sequence of material deposition.
3. Technological applications such as improved systems for light absorption in sensing, spectroscopy, and photovoltaics made possible by the types of devices capable of being fabricated via nanomasking technique.

Appendix C: Potential Patent and Commercialization Aspects of Listed Intellectual Property Items

C.1 Patentability of Intellectual Property (Could Each Item be Patented)

The three items listed were considered first from the perspective of whether or not the item could be patented.

1. The method of fabrication called nanomasking can be patented. The method is novel, unique, and non-obvious. It improves upon the capabilities of current lithography techniques and has potential to make possible nanofabrication at the mass production scale.
2. Specific devices fabricated via nanomasking technique that cannot be fabricated via other existing methods and variations on the nanomasking technique can be patented with the restriction that they are patented as being fabricated via the novel, unique, non-obvious technique.
3. Technological application made possible by the types of devices fabricated via nanomasking could be patented if developed further.

C.2 Commercialization Prospects (Should Each Item Be Patented)

The three items listed were then considered from the perspective of whether or not the item should be patented.

1. The nanomasking technique should be patented and is currently patent pending.
2. Variations of the nanomasking technique and specific devices capable of being fabricated should be patented and are currently patent pending.
3. A patent should not be pursued for specific technological applications made possible by nanostructures fabricated via the nanomasking technique unless developed further.

C.3 Possible Prior Disclosure of IP

The following items were discussed in a public forum or have published information that could impact the patentability of the listed IP.

1. The nanomasking technique has been discussed in publications and presentations by the author, but only after the previously mentioned patent application was submitted.
2. The devices fabricated via nanomasking technique and variations on the technique have been discussed in publications and presentations by the author, but only after the previously mentioned patent application was submitted.
3. The technological applications making use of devices fabricated via the nanomasking technique have not been specifically discussed in any forum.

Appendix D: Broader Impact of Research

D.1 Applicability of Research Methods to Other Problems

Beyond nanoplasmonics applications, many fields of nanotechnology will benefit from increased control of the fabrication of nanoscale features. Better resolution of feature dimensions will improve many of the existing technologies making use of devices at this small scale. Saving space on integrated circuit chips has been the source of the scaling down process that has allowed for increased processing power in the past three decades. The more control that circuit engineers have over the resolution of lithographic processes, the better they will be able to continue this trend. With increased control over nanoscale fabrication geometry, doors may be opened to new nanotechnologies, areas of nanoscience, and applications that have been limited to this point. The ability to produce many patterns simultaneously over macroscopic areas (cm^2 and greater) will help to make nanoscale fabrication more feasible for mass production scale processes.

D.2 Impact of Research Results on U.S. and Global Society

The impact of increased nanofabrication control on photovoltaics, spectroscopies, sensing, and other areas will potentially have a range of effects on U.S. and global society alike. If nanomasking or further developments of the technique are capable of improving the absorption capability of photovoltaic cells, thin film solar cells could become more feasible economically. If solar cell technology can reach a more economically viable cost to efficiency ratio, more people will have access to this renewable energy source. This would be a great step in the right direction for reducing the societal need for costly fuel sources that are closely tied to the

economic state of the U.S. today. Any technology that provides alternatives to current fuel technology creates the potential for disrupting the energy sector of the U.S. and global markets. This could mean a massive shift in jobs, probably destroying some and creating others. The solar energy market is more likely to remain stable than current fossil markets, as it is a renewable.

Improving the signal strength of spectroscopy and sensing techniques through the use of devices created via nanomasking would be beneficial for research and various technologies. Enhanced spectroscopy signals help in areas of research where samples tend to give off weaker signals or have poorly defined peaks. The ability to detect spectral signals from otherwise difficult or impossible to measure samples will allow researchers to discover new science that may not otherwise be possible. Enhanced signal strength in sensing and detection applications could greatly improve the usefulness of current technologies. This technique could also make it possible to fabricate more efficient detectors in terms of throughput. This could make possible various substance detectors that could help in the agriculture, food, biomedical, and security sectors as well as research and other areas. Improved detection of dangerous or harmful substances will undoubtedly be beneficial to the U.S. and global health and safety.

D.3 Impact of Research Results on the Environment

The impact of the nanomasking fabrication method and any future developments on the environment is potentially quite positive. The potential for improvement of solar cell absorption via plasmonic enhancement means that photovoltaics may become more prevalent in U.S. and global society. The more that solar cell technology begins to pervade the global energy sector, the less reliant humans will be on fossil fuels and nuclear power. This transition from high waste energy sources to renewables is a massive step in the right direction for protecting the

environment. An improved ability to detect harmful substances could also prove beneficial for the environment in waste management, control of agricultural residue, water testing, and other areas.

Appendix E: Microsoft Project for MS MicroEP Degree Plan

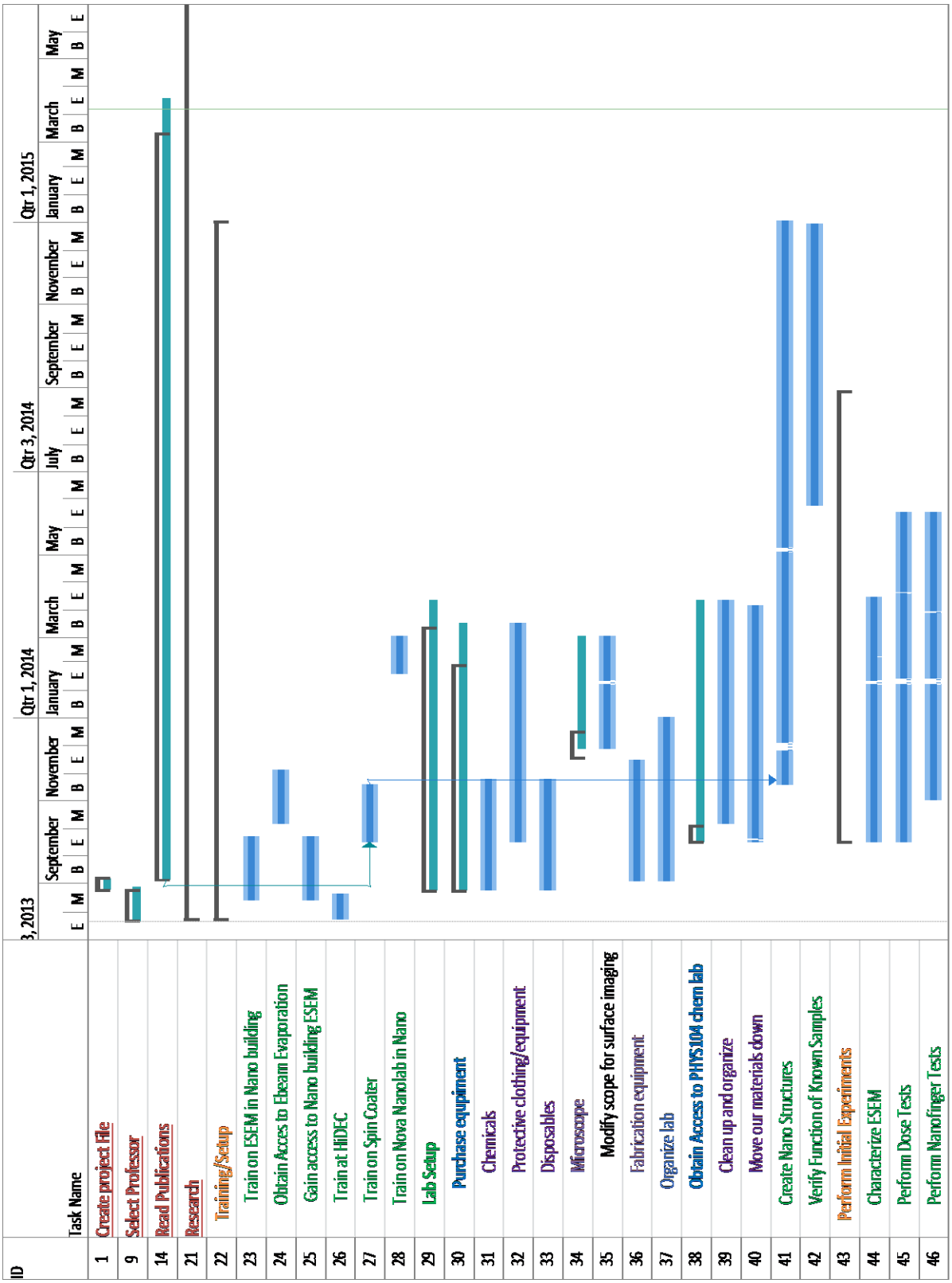

ID	Task Name
46	Perform Nanofinger Tests
47	Perform Alignment Tests with ESEM
48	Perform Etchant Tests
49	Fabricate Nano-gap structures
50	Analyze Results
51	Determine success of fabricating nanc
52	SPIE Conference Presentation
53	Obtain travel funding
54	Prepare Manuscript
55	Prepare Presentation
56	Conference
57	Define New Experiments
58	Plan fabrication designs for nanomask
59	Fabricate Nanostructures via nanoma
60	First step Cr fabrication
61	Different heights/materials
62	Compare PHYS ebeam evaporator to
63	Last Results/Plan Future Work
64	Train on dicing saw
65	Present poster at IAC, INBRE, and Gra
66	Submit manuscript to IEEE Transactio
67	Fabricate with Nanomasking 1st step
68	Characterize nanogaps via spectrosco
69	Compare to simulations
70	Different heights/materials
71	Write Thesis
72	Get outline and formatting finished
73	Chapter 1: Introduction
74	Appendices

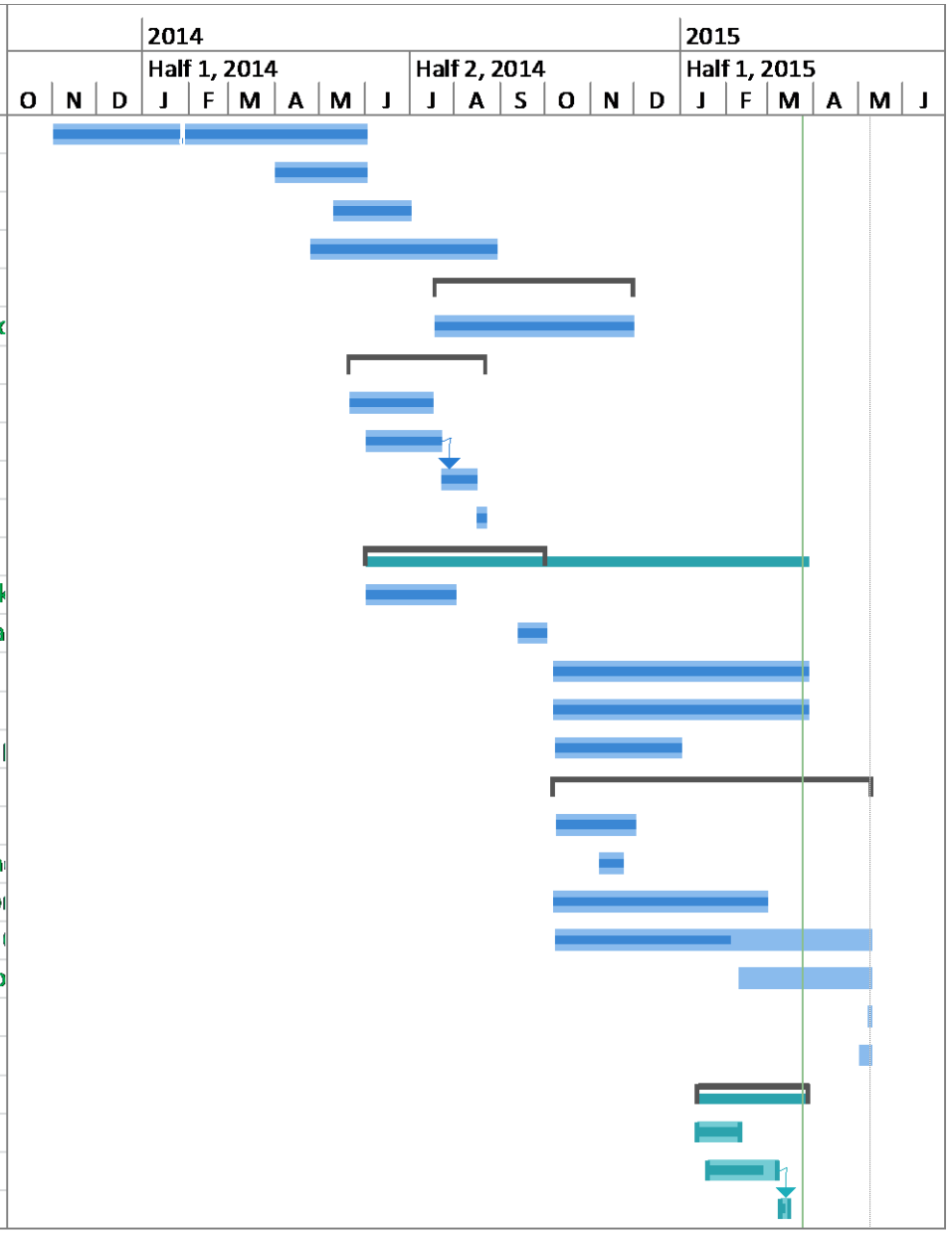

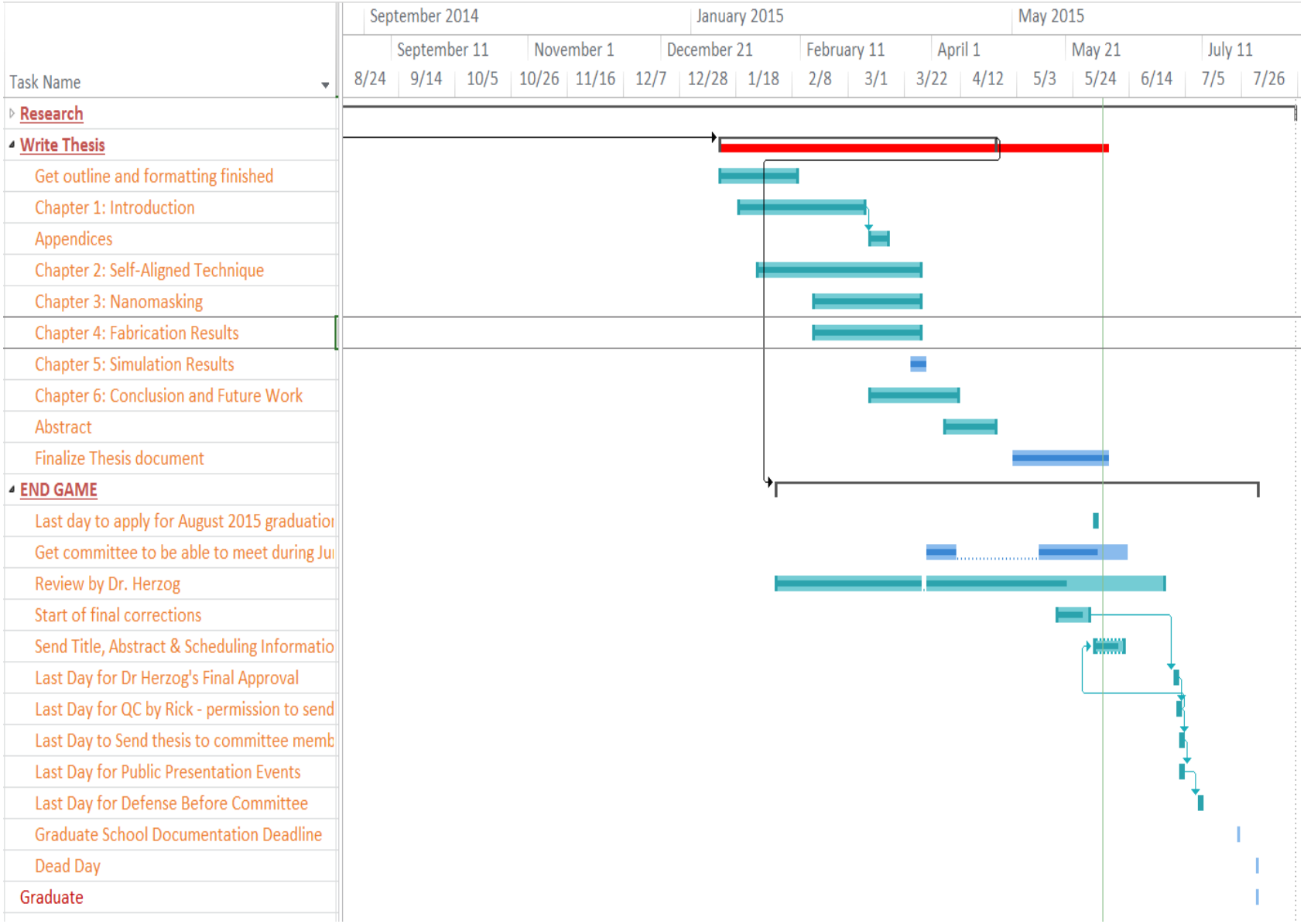
Task Name
Research
Write Thesis
Get outline and formatting finished
Chapter 1: Introduction
Appendices
Chapter 2: Self-Aligned Technique
Chapter 3: Nanomasking
Chapter 4: Fabrication Results
Chapter 5: Simulation Results
Chapter 6: Conclusion and Future Work
Abstract
Finalize Thesis document
END GAME
Last day to apply for August 2015 graduatio
Get committee to be able to meet during Ju
Review by Dr. Herzog
Start of final corrections
Send Title, Abstract & Scheduling Informatio
Last Day for Dr Herzog's Final Approval
Last Day for QC by Rick - permission to send
Last Day to Send thesis to committee memb
Last Day for Public Presentation Events
Last Day for Defense Before Committee
Graduate School Documentation Deadline
Dead Day
Graduate
September 2014
January 2015
May 2015
September 11
November 1
December 21
February 11
April 1
May 21
July 11
8/24
9/14
10/5
10/26
11/16
12/7
12/28
1/18
2/8
3/1
3/22
4/12
5/3
5/24
6/14
7/5
7/26

Appendix F: Identification of All Software Used In Research and Thesis Generation

Computer #1:

Model Number: Toshiba Satellite P55t-A5116
Serial Number: 2E062215S
Location: N/A
Owner: Stephen Bauman

Software #1:

Name: Microsoft Office 2013
Owner: University of Arkansas Fulbright College of Arts and Sciences

Software #2:

Name: Nanopattern Generation System (NPGS) v9 Office Installation
Owner: University of Arkansas Institute for Nanoscience and Engineering

Software #3:

Name: DesignCAD 2000LT with NPGS
Owner: University of Arkansas Institute for Nanoscience and Engineering

Software #4:

Name: Adobe Reader XI v11.0.01
Owner: Stephen Bauman (freeware)

Software #5:

Name: Google SketchUp 8
Owner: Stephen Bauman (freeware)

Software #6:

Name: GNU Image Manipulation Program (GIMP) 2.8.14
Owner: Stephen Bauman (freeware)

Software #7:

Name: Zotero 4.0.21.2
Owner: Stephen Bauman (freeware)

Computer #2:

Model Number: ASUS Essentio Series X18-82071
Serial Number: 150290C00700
Location: PHYS 245
Owner: Dr. Joseph Herzog

Software #1:

Name: COMSOL Multiphysics
Owner: Dr. Joseph Herzog

Software #2:
Name: COMSOL Multiphysics
Owner: University of Arkansas Microelectronics-Photonics Graduate Program

Software #3:
Name: Nanopattern Generation System (NPGS) v9 Office Installation
Owner: University of Arkansas Institute for Nanoscience and Engineering

Software #4:
Name: DesignCAD 2000LT with NPGS
Owner: University of Arkansas Institute for Nanoscience and Engineering

Software #5:
Name: Microsoft Office 2013
Owner: University of Arkansas Fulbright College of Arts and Sciences

Software #6:
Name: MATLAB R2014a (Version 8.3)
Owner: University of Arkansas Department of Physics

Computer #3:
Model Number: N/A (Custom built)
Serial Number: N/A (Custom built)
Location: PHYS 245
Owner: Dr. Joseph Herzog

Software #1:
Name: COMSOL Multiphysics
Owner: Dr. Joseph Herzog

Software #2:
Name: COMSOL Multiphysics
Owner: University of Arkansas Microelectronics-Photonics Graduate Program

Software #3:
Name: Nanopattern Generation System (NPGS) v9 Office Installation
Owner: University of Arkansas Institute for Nanoscience and Engineering

Software #4:
Name: DesignCAD 2000LT with NPGS
Owner: University of Arkansas Institute for Nanoscience and Engineering

Software #5:
Name: Microsoft Office 2013
Owner: University of Arkansas Fulbright College of Arts and Sciences

Software #6:

Name: MATLAB R2014a (Version 8.3)
Owner: University of Arkansas Department of Physics

Computer #4:

Model Number: Dell 3615KL – 04W – B86
Serial Number: 8XRZL51
Location: Nano Room 125
Owner: University of Arkansas Institute for Nanoscience and Engineering

Software #1:

Name: Nanopattern Generation System (NPGS) v9 Microscope Installation
Owner: University of Arkansas Institute for Nanoscience and Engineering

Software #2:

Name: DesignCAD 2000LT with NPGS
Owner: University of Arkansas Institute for Nanoscience and Engineering

Computer #5: Accessed University of Arkansas VLab General Access Computing Lab

Model Number: N/A
Serial Number: N/A
Location: VLab General Access Computing Lab
Owner University of Arkansas IT Services

Software #1:

Name: Adobe Photoshop v?
Owner: University of Arkansas IT Services

Appendix G: All Publications Published, Submitted and Planned

Journal Publications:

- S. J. Bauman, E. C. Novak, D. T. Debu, J. B. Herzog, "Fabrication of sub-lithography limited structures via Nanomasking technique," *IEEE Transactions on Nanotechnology*, accepted for publication May 2015

Planned Publications:

- S. J. Bauman, J. B. Herzog, "Nanomasking lithography technique with Cr evaporation mask"
- S. J. Bauman, D. T. Debu, J. B. Herzog, "Study of proximity effect on pattern width in electron beam lithography"
- S. J. Bauman, J. Mishler, J. B. Herzog, "Study of LER and LWR for nanogap structures created via nanomasking technique"
- J. Mishler, S. J. Bauman, S. Barraza-Lopez, J. B. Herzog, "Band structure computation of diatoms as a photonic crystals"

Conference Proceedings:

- S. J. Bauman, D. T. Debu, J. B. Herzog, "Plasmonic structures fabricated via nanomasking sub-10 nm lithography technique," *SPIE Optics + Photonics Research Conference*, San Diego, U.S.A., August 2015 (accepted)
- M. Sarollahi, J. Mishler, S. J. Bauman, S. Barraza-Lopez, P. Millet, J. B. Herzog, "The significance of the number of periods and period size in 2D photonic crystal waveguides," *SPIE Optics + Photonics Research Conference*, San Diego, U.S.A., August 2015 (accepted)
- S. J. Bauman, D. T. Debu, A. M. Hill, E. C. Novak, D. Natelson, J. B. Herzog, "Optical nanogap matrices for plasmonic enhancement applications," Proc. SPIE 9163, 91631A of the *SPIE Optics + Photonics Research Conference*, San Diego, U.S.A., August 2014

Presentations:

- D. French, S. Bauman, D. Debu, C. Saylor, J. Herzog, "Dark-field Spectroscopy of Plasmonic Nanodevices with Nanometer Scale Features," *Bulletin of the American Physical Society, APS March Meeting 2015, Volume 60 Number 2*, San Antonio, U.S.A., March 2015
- D. Debu, S. Bauman, C. Saylor, E. Novak, D. French, J. Herzog, "Investigation of nanogap localized field enhancement in gold plasmonic structures," *Bulletin of the American Physical Society, APS March Meeting 2015, Volume 60 Number 2*, San Antonio, U.S.A., March 2015
- S. Bauman, D. Debu, E. Novak, J. Herzog, "Nanomasking technique for fabrication of sub-10 nm structures and their plasmonic properties," *Arkansas INBRE Research Conference*, Fayetteville, U.S.A., November 2014
- S. Bauman, J. Blaylock, D. French, D. Debu, J. Herzog, "Fabrication and Characterization of Optical Nanogap Arrays for Plasmonic Enhancement Applications," *Arkansas Institutional Development Award (IDeA) Network of Biomedical Research Excellence (INBRE) Research Conference*, Fayetteville, U.S.A., October 2013

Appendix H: Manuals and Direction Sheets Developed

For the benefit of future researchers in Dr. Herzog's Plasmonic Nano-optics group as well as to supplement the author's lack of perfect memory, direction sheets were developed for the imaging and fabrication processes used during this thesis work. While variable in some aspects, the details of this appendix should at least serve as a guide for the reproduction of results obtained in this thesis work.

H.1 Scanning Electron Microscopy with the FEI Nova Nanolab 200

Scanning Electron Microscopy with the FEI Nova Nanolab 200:

********** The procedure for just imaging is different from the electron beam lithography procedure. One can safely turn on the beam without fear of resist exposure in the case of imaging.**********

- *Gloves!* must be worn whenever the sample or chuck is handled!
- Sign into the logbook.

1. Starting up the FEI System Control Software
    a. Username: user Password: user
    b. Double click the gray box to expand it and move it to the top right of the screen
        i. Click START
        ii. Username: students Password: esemuser1
    What is blue is selected! The FIB and SEM both use the same control panel!
    Never click WAKE UP!
    c. Check CCD screen
        i. Make sure no one has left a sample inside the chamber (contact Mourad if so)
    d. Check for green symbol for ion, electron, and vacuum chambers
    e. Click VENT
- The chamber part turns orange while venting. Black means that it is fully vented.

2. Sample Loading
    a. *Gloves!* for touching the sample/chuck
    b. Insert the chuck into the pin slot in the chamber (may need to loosen the screw slightly)
    c. Align the sample with the door in such a way that you can remember, and such that the Faraday cup is opposite the chamber door.

    d. Use the allen wrench to tighten the screw slightly so that the chuck is held in place
    e. Close the door gently and hold it in place while clicking PUMP to evacuate the chamber
    **Be careful with fingers near the door, as it pull the door closed once pumping begins*
    f. Wait for the Black, Orange, Green chamber icon sequence

3. Exploring the Sample Orientation

a. The beam can be turned on (Beam On → Play/Pause) without fear of messing up the sample

b. It is a good idea to find and focus on the Faraday Cup and confirm that the X and Y directions are as expected and draw a picture of the sample's orientation with X and Y directions labeled.

- Center Click = drag around movement, Double Click = jump to click location
- Beam Shift knobs are easier at higher magnifications
- Shift + Ctrl you can drag screen around
- F5 goes full screen and back

4. Finding the Eucentric Height for Imaging

a. Beam Control → Navigation

b. Use small particles on the sample surface - not down in a scratch - with easily visible contrast to focus the beam at at least 1000X magnification.

c. After the sample is in focus, the Z FWD icon will measure the true distance of the sample from the bottom of the electron column.

d. Look at CCD and enter 5 mm as the Z value. This moves the sample up.

Be ready to hit Escape and/or click cancel if the sample comes too close to the column!

e. Continue focusing and moving the sample to 5 mm up to at least 8000X magnification.

f. For high resolution focus, the stigmator will need to be adjusted as well.

5. High Resolution (Immersion) Mode Imaging

- Must be at the eucentric height and at least 1200X magnification in order to use hi-res mode.
    - Don't leave the scope in immersion mode when you zoom back out.

*****Hi-Res mode uses a strong magnet close to the sample, so no ferrous materials (like stainless steel) or liquid should be used without discussing it with Mourad!*****

6. Two-Computer Network

- There is a switch that changes between the two computers. The images taken via the Nova should be saved onto the one whose *screen is on the left* and *tower is on the right on the floor*, where they can be saved onto a USB drive.
    - Take an image and Save As .tif16 normally. Use .jpg to save the colored measurements.
    - Path: sdb-d000 (C: Shared Folder/sjbauman)

7. Checkout procedure

a. Set magnification to minimum

b. Bring the stage height Z to 28, set x=0 and y=0

c. Set Voltage to 15 kV and Spot Size to 2.2 nC

d. Turn off the beam (HV)

e. Press Vent and wait until the stage door opens with a gentle pull.

f. Remove the sample. Hold the door closed and press Pump button. Wait until the vacuum indicator is Green

g. Close the microscope user interface

h. Log off computer

i. Sign out of the logbook.
j. Don’t forget your USB drive!

H.2 Scanning Electron Microscopy with the FEI XL30 ESEM

Scanning Electron Microscopy with the FEI XL30 ESEM:

********** The procedure for just imaging is different from the electron beam lithography procedure. One can safely turn on the beam without fear of resist exposure in the case of imaging.**********

- *Gloves!* must be worn whenever the sample or chuck is handled!
- Sign into the logbook.

1. Starting up the Computer
    a. Username: guest Password: esemuser1
    b. ESEM control interface is located in C: → xl → mc → mctrl
        i. Username: students Password: esemuser1
    c. Check for "Vac OK" (~10^{-6} up to 10^{-4})
    d. Click VENT
    e. Click CCD in Detectors to see inside the chamber
        i. Make sure no one has left a sample inside the chamber (contact Mourad if so)
    f. Boot the NPGS computer to get its calibration started
        Username: ebluser Password: ebluser1

2. Sample Loading
    a. *Gloves!* for touching the sample/chuck
    b. Be sure that the stage is not screwed down all the way so that the working distance can be made to be 10 mm without exceeding the stage limits.
    c. Insert the chuck into the pin slot in the chamber (may need to loosen the screw slightly)
    d. Align the sample with the door in such a way that you can remember, and such that the Faraday cup is opposite the chamber door.
    e. Use the allen wrench to tighten the screw slightly so that the chuck is held in place
    f. Close the door gently and hold it in place while clicking PUMP to evacuate the chamber
**Be careful with fingers near the door, as it will pull the door tightly closed once pumping begins*
    g. While waiting for the vacuum to pump down to "Vac OK", begin working with NPGS

3. Nano Pattern Generation System (NPGS) Software
    a. Computer should be performing calibration - minimize this window.
    b. Open NPGS from the desktop
Note The A/B switch can be switched to B and then NPGS can be used to go between SEM and NPGS control. NPGS can be used to obtain images that can be saved via USB.

4. Exploring the Sample Orientation
    a. The beam can be turned on (10.0 kV button) without fear of messing up the sample
    b. It is a good idea to find and focus on the Faraday Cup and confirm that the X and Y directions are as expected and draw a picture of the sample's orientation with X and Y directions labeled.
- There are two beam control modes using the mouse. The crosshair centers on a double-clicked location. The target moves in the direction of the cursor during a left click held down. Use them interchangeably for efficiency

5. Finding the Eucentric Height for Imaging

Spot Size: 3, Accelerating Voltage: 10 or 15 kV

a. The sample should be at a distance of ~20-28 mm from the electron column, as the previous user should have moved the stage to this height.

b. Use small particles on the sample surface - not down in a scratch - with easily visible contrast to focus the beam at at least 1000X magnification.

c. After the sample is in focus, the Z FWD button will measure the true distance of the sample from the bottom of the electron column.

d. Switch the detector to CCD and enter 10 mm as the Z value. This moves the sample up.

Be ready to hit Escape and/or click cancel if the sample comes too close to the column!

e. Continue focusing and moving the sample to 10 mm up to at least 8000X magnification.

f. For high resolution focus, the stigmator will need to be adjusted as well.

6. Saving Images

Black Desktop with NPGS software:

a. From the NPGS menu, go to the Digital Imaging window

b. With the ESEM under NPGS control, take a new image using the desired parameters

c. Save the image to the appropriate desktop folder

d. Save the image to your USB drive

White Desktop with MCtrl software:

a. Using the In/Out → Image menu option, give the image an appropriate title

b. Save the image to the appropriate desktop location

c. Use Nero to burn the saved images to a CD

7. Checkout procedure

a. Set magnification to minimum

b. Bring the stage height Z to 28mm, set x=0 and y=0

c. Set Voltage to 10.0 kV and Spot Size to 3

d. Turn off the beam (HV) and switch to CCD detector

e. Press Vent and wait until the stage door opens with a gentle pull.

f. Remove the sample. Hold the door closed and press Pump button. Wait until the vacuum indicator is "Vac OK"

g. Close the microscope user interface

h. Log off and turn off ESEM screen monitor. Turn off the NPGS computer

i. Sign out of the logbook.

j. Don't forget your USB drive or CD!

H.3 Electron Beam Lithography with FEI XL30 ESEM for Nanomasking Process

Sample Preparation:

- *Gloves!* must be worn and tweezers used at all times when handling the sample!
- Obtain pre-cut sample chip(s)

1. Sample Cleaning

If Not Already Coated with Resist Or To Apply New Resist	**If Already Coated with Resist**
Turn on the hotplate to 180ºC (~3.7 on knob) to start it heating up	Just clean with IPA
Soak the chip in Acetone for at least 10 minutes. Sonicate the chip in the large petri dish for at least 2 minutes of the soaking	Dry with Nitrogen
Rinse the chip with Isopropanol (IPA) and blow dry with Nitrogen	Skip to Number 4.
Secure the sample on the spin-coater with the vacuum on	
Center the sample on the spin-coater	
Test that the spin-coater will spin for 40 seconds at 3000 rpm	

2. Spin-Coating
    a. Set up the spin-coater to run at 3000 rpm for 40 seconds
        i. Vacuum must be on
        ii. Control button must be pressed
        iii. Turn Time 1 down to zero and Time 2 so that it will spin at Speed 2 for 40 seconds
        iv. Speed 2 should be around 37 so that it spins at 3000 rpm
    b. Apply A4 PMMA 495 (Cover the sample using ~3 drops)

    Note Make sure that the PMMA is free of air bubbles as it is applied with a pipette

    c. Some other resists may require a different chuck to be used. Pressing START will start the actual spinning process
4. Post Bake
    a. Cure on the hotplate at 180ºCfor 2 minutes
    b. Cover the sample with glass, but leave room for air circulation
    c. Check to see if the sample appears very clean under the OMAX microscope. If not, repeat step 1.
        i. Turn off the hotplate when done
5. Apply Silver Dust (Optional)
    a. Dab a very small amount on the long edges of the sample with a broken wooden q-tip
6. Mounting on the Chuck
    a. For small chip, use PMMA to glue to center of larger chip and heat on the hot plate to dry glue
    b. Align chip(s) on the SEM chuck and tighten washers to hold the samples in place
    c. With the scriber, scratch number into the corner(s) in such a way that it will face right-side up on the ESEM screen.

d. Blow the sample with Nitrogen to help remove particles from the scratching

Electron Beam Lithography with the XL30 ESEM:

********** The procedure for just imaging is different from the electron beam lithography procedure. One must be careful during the lithography procedure not to treat the sample the same as if he/she was viewing the sample. Shooting a beam of electrons at the sample to view it will expose the resist, so one must be aware of where the beam is on the surface at all times!**********

- *Gloves!* must be worn whenever the sample or chuck is handled!
- Sign into the logbook.

1. Starting up the Computer
   a. Username: guest Password: esemuser1
   b. ESEM control interface is located in C: → xl → mc → mctrl
   c. Username: students Password: esemuser1
   d. Check for "Vac OK" (~10^{-6} up to 10^{-4})
   e. Click VENT
   f. Click CCD in Detectors to see inside the chamber
   g. Make sure no one has left a sample inside the chamber (contact Mourad if so)
   h. Boot the NPGS computer to get its calibration started
   i. Username: ebluser Password: ebluser1
   j. Minimize the window that pops up. It is initializing the software that controls the ESEM

2. Sample Loading
   a. *Gloves!* for touching the sample/chuck
   b. Be sure that the stage is not screwed down all the way so that the working distance can be made to be 7 mm without exceeding the stage limits.
   c. Insert the chuck into the pin slot in the chamber (may need to loosen the screw slightly)
   d. Align the sample with the door in such a way that you can remember, and such that the Faraday cup is opposite the chamber door.
   e. Use the allen wrench to tighten the screw slightly so that the chuck is held in place
   f. Close the door gently and hold it in place while clicking PUMP to evacuate the chamber
      **Be careful with fingers near the door, as it will pull the door tightly closed once pumping begins*
   g. While waiting for the vacuum to pump down to "Vac OK", begin working with NPGS

3. Nano Pattern Generation System (NPGS) Software
   a. Computer should be performing calibration - minimize this window.
   b. Open NPGS from the desktop
   c. Select desired Project folder
   d. DesignCAD Software
      All commands must be done with the NPGS dropdown menu (even SAVE)
      - Layers and Line Styles are important. Dashed lines will be "area-dose" filled polygons
      - NPGS can do different dosages by color (useful for arrays)

Note The A/B switch can be switched to B and then NPGS can be used to go between SEM and NPGS control. NPGS can be used to obtain images that can be saved via USB.

4. Exploring the Sample Orientation

Viewing the sample exposes it!!!

- The beam should not be turned on until you are confident that the sample is out of the way. It is good to move the stage so that the beam will be off the chuck on the side of the Faraday Cup.

a. Start at (X,Y) = (0,0). Moving to (12,000,0) μm will bring the edge of the sample with the Faraday Cup near to the beam for our round chuck (~1" diameter).
b. The beam can be turned on (10.0 kV button) when this confidence is established.
c. It is a good idea to find and focus on the Faraday Cup and then carefully explore the edges of the sample. Confirm that the X and Y directions are as expected. The NPGS software run files will move in the same directions as the SE view in the ESEM control software.
d. Draw a picture of the sample's orientation with X and Y directions labeled.

5. Finding the Eucentric Height for Lithography

Spot Size: 1, Accelerating Voltage: 30 kV

a. The sample should be at a distance of ~20-28 mm from the electron column, as the previous user should have moved the stage to this height.
b. Use small particles on the sample surface - not down in a scratch - with easily visible contrast to focus the beam at at least 1000X magnification.
c. After the sample is in focus, the Z FWD button will measure the true distance of the sample from the bottom of the electron column.
d. Switch the detector to CCD and enter 7 mm as the Z value. This moves the sample up.

Be ready to hit Escape and/or click cancel if the sample comes too close to the column!

e. Continue focusing and moving the sample to 7 mm up to at least 8000X magnification.
f. For high resolution focus, the stigmator will need to be adjusted as well.

6. Checking the Beam Current

- Spot size and accelerating voltage affect the beam current. This then affects the dose.

a. Go to maximum magnification at the hole in the center of the Faraday Cup
b. Replace the Sample Crash Detector BNC cable with the Ammeter BNC
c. Turn on the ammeter and push ZCHK
d. Record beam current value. (Should be ~10 pA)
e. Zoom back out to find the scribed sample corner and center the beam on the corner.
f. If possible, rotation alignment will help to make sure that X and Y align with the sample edges.

7. NPGS Run Files

- Run files move in the same XY directions as the SE screen when imaging

a. Need the first step to turn the ESEM to External Mode
b. Need a secondary step to bring up the comment window before movement/writing steps

c. Based on the known orientation of the sample, a move step will bring the beam away from the corner of the sample to the desired writing location prior to writing the pattern.
   - NPGS can be made to write patterns in an array, varying dose for each step (used for dose test)
   - The dose percentage can be controlled, and entering the beam current value in the main NPGS window calibrates based on the measured current and the desired run file current to get the correct dose.
   - NPGS moves back to the center of the array (where it started the array from) afterwards.

d. Make another move at the end of the write to bring the beam back to the sample corner.
   - Command → Calibrate DACS can often fix an NPGS run error

8. Checkout procedure
   a. Set magnification to minimum
   b. Bring the stage height Z to 28 mm, set x=0 and y=0
   c. Set Voltage to 10.0 kV and Spot Size to 3
   d. Turn off the beam (HV) and switch to CCD detector
   e. Press Vent and wait until the stage door opens with a gentle pull.
   f. Remove the sample. Hold the door closed and press Pump button. Wait until the vacuum indicator is "Vac OK"
   g. Close the microscope user interface
   h. Log off and turn off ESEM screen monitor. Turn off the NPGS computer
   i. Sign out of the logbook.
   j. Don't forget your USB drive or CD!

Chemical Development of the Exposed Sample:

- Work under a fume hood!
- For multiple samples, use separate developer for each

1. Pour enough Developer (3:1 IPA: MIBK) and IPA into the respective dishes to cover the sample with dish tilted.
2. Developer bath first for 40 seconds

Keep grip on the chip with the tweezers while dunking it

a. Move the sample back and forth while dunking.

2. Do a quick IPA dunk
3. Dry with Nitrogen gun
4. Store sample safely

Electron Beam Evaporation:

- E-beam evaporation is more precise than thermal evaporation (2 nm vs 20 nm)
- We use Four 9's Gold (99.99% purity)
- 14 Å Titanium at 1 Å/s (allow 40 Å before sample shutter opened to ensure stable rate)
  140 Å Gold at 2 Å/s (allow 50 Å before sample shutter opened to ensure stable rate)

14 Å Silicon dioxide at 0.3 Å/s (allow 20 Å before sample shutter opened to ensure stable rate)

140 Å Chromium at 1 Å/s (allow 30 Å before sample shutter opened to ensure stable rate)

Dr. Manasreh's (Angstrom Engineering Nexdep Evaporator) in BELL	**Nanofab Lab R2D2 (Edwards Auto 306 Evaporator) in PHYS**
Yahia controls the machine 1. Pumping down the chamber a. The vacuum chamber takes ~8 hours to pump down to the required level (~2.7E-7 Torr) b. Thus, bring the desired samples to the lab the day prior to evaporation so that they can be mounted and the chamber will have time to evacuate. 2. Evaporation System Process Control a. Required parameters are input into the system to control the machine automatically for each material desired to evaporate i. Evaporation Rate ii. Layer Thickness iii. Sample Temperature iv. Sample Rotation Speed b. When the shutter opens after ramping up the power on the gold sample, record important system parameters such as: i. Beam Current ii. High Voltage iii. Power iv. Rate v. Vacuum level	Closely follow the typed procedure in the lab. • Obtain N2 from Nano building before beginning anything else • Turn on N2 first • *Only turn the crucible stage clockwise!* • Write down crucible position # • Push down R2's head after pressing cycle • Pressing RUN opens the shutter and starts evaporating the sample then stops when the thickness is reached • The current knob that gets turned to 10 mA is very sensitive! • Record information in the logbook

PMMA Lift-Off:

1. Place the sample(s) in a vial of Acetone after evaporation (need at least 10 minutes to soak)
2. In the lab (fume hood with a layer of clean room wipes), add IPA to the small petri dish to be able to submerge the sample
3. Get the small Acetone petri dish and add a small amount of Acetone
4. Have the Nitrogen tank opened up and ready to use
5. Swirl the sample around in the vial to help remove PMMA and metal
6. Use a filter to collect any loose metal in the vial.
7. Place the sample into the petri dish and add the vial Acetone to the organic waste container.
8. Spray the sample with the Acetone squeeze bottle for 10 seconds
9. Dunk the sample in IPA
10. Blow dry the sample with Nitrogen gas
11. Look at the sample under an optical microscope to make sure the lift-off was successful
12. When the filter paper has dried, place it in the "Used Metal from E-Beam Evaporation" jar.

2nd Lithography Step (If Applicable):

---

1. See **Sample Preparation**
2. See **Electron Beam Lithography with the XL30 ESEM** through Step 7
3. Only moving the stage across the sample surface with the **beam blanked**, find the top cross from the first lithography step and use it along with the bottom cross to get a coarse rotation alignment. **It is useful to use the MCtrl software to save locations such as the Faraday Cup and the Crosses. This is carried out in the maximized Stage control panel.
4. Center and focus on the center cross
5. Use the Align Runfile along with the 2nd step of the previously designed pattern to align and write

   During alignment:
   - @ = Enable Auto-Align, # = Disable Auto-Align
   - A = Auto Contrast, ? = Help, ← → = Contrast Adjust
   - [Y], you do want to recalculate matrix before continuing each step. This tells the software to actually move the sample based on where you told it the alignment patterns were.

<u>Note</u> Focusing Dots:
Focusing dots are a method for achieving the best focus possible prior to drawing an e-beam lithography pattern. A focusing dot is created by setting the SEM to "spot" mode which disables rastering of the electron beam and thus sends a focused stream of electrons to a single point on the sample. The electron beam damages the resist and creates a "dot" of damaged resist that can be seen when the SEM is returned to imaging mode. The dot can be used to improve the current focus of the microscope as well as correct any astigmatism. Creating multiple focusing dots allows for successive improvements in focus until the limits of the focusing electrons are reached, typically requiring 3-5 focusing dots. At the best focus a focusing dot will appear to be 25 nm or smaller in diameter.

Chromium Etch:

*****DANGER wear protective gear (lab coat, chemical apron, 2 pairs of gloves)*****
1. Dilute 20 mL of Cr-7 (Cyantek) or CEP-200 in 40 mL DI water in a Petri dish and stir (1:2)
2. Hold small beaker in sonicator with etchant and water surface at equal levels
3. Place sample face down into the beaker and sonicate for 1 minute
4. Rinse sample in DI water by flowing DI water continuously over sample for 1 minute
5. Rinse in IPA
6. Dry with N_2 for 10 seconds

Buffered Oxide Etch

DANGER! HF Acid! Wear lab coat, chemical apron, 2 pairs of gloves, arm sleeves, face shield

1. Prepare a buffered oxide etch (BOE) with an etch rate of 100 nm/min SiO_2
2. Place sample in BOE for 2-3 seconds
3. Rinse in DI water
4. Rinse in IPA
5. Dry with N_2 for 10 seconds

H.4 NPGS/DesignCAD Help and Troubleshooting

For all issues or questions, the NPGS Manual is usually quite helpful and contains much of the information to which Nabity will refer you if you ask him for help. Be sure to check the documentation early on if some problem exists or you have a question. He prefers if you have looked at the manual prior to asking his help, as is often the case with people who write manuals for just that purpose.

Basic Controls:

- Most controls must be run through the NPGS dropdown menu within DesignCAD
    - Keyboard shortcuts match those listed in the dropdown menu
    - Ctrl + i is useful for checking and changing Layer, Color, and Linetype of selected entities
        - DesignCAD won't let you change these properties if the DesignCAD window is maximized.
- Polyfill command must be used to create a polygon (squares, triangles, etc)
    - Vertices are important. A polygon with 2 vertices will be closed as if the vertices are opposite corners. If a polygon with greater than 2 vertices is started and not closed, Polyfill will close the polygon by connecting the two end points. If vertices are too close to lines such that it is impossible for the ESEM to write the pattern to such detail, it will not write the pattern. (See ShowPoints)
        - Vertices that are placed very close together (i.e., less than the "Line Spacing") or <u>when the changes in the perpendicular distance from the original sweep side between successive vertices is less than the "Line Spacing"</u>.
        - Depending on the version of DesignCAD you are using, you may be able to use 'Ctl-Shift' while in the Point Select mode to delete vertices from an existing polygon.
- Line types are crucial to obtaining the correct sample exposure
    - Dashed lines are used to fill in a polygon in a serpentine fashion. (Line type 1 = serpentine fill) **We typically use this line type**
    - Dotted lines fill in from one side (Line type 5 = one sided fill)
    - Solid lines are just written as lines by the ESEM (Line type 0 = single pass of the beam)
- Circle types are also crucial
    - Dashed line type fills in circles
    - The line type 4 can be used for filled circles, wide circles, and wide arcs. When these entities are designed with a line type of 4, the sweep will be from the inside towards the outside of the structure. When the default line type is used, the normal writing direction is from the outside towards the inside. *This feature is typically used in FIB milling applications, where the direction of the sweep can be very important*.

NPGS with DesignCAD:

- The CheckAll function in the NPGS drop down menu allows for duplicate patterns to be detected and subsequently deleted if desired. This helps prevent overexposure of areas where only one pattern should exist.
- The ShowPoints function in the NPGS drop down menu allows for the program to tell how many vertices a shape has. If there are more than the expected number
    - If you use the 'ShowPoints' function in DesignCAD and select the alignment windows in your L14 alignment pattern, you will see that many of the windows have unnecessary vertices. Closer inspection of the actual DC2 file shows that the extra points basically fall along the edge of the window, but often have small deviations from the edge. These small deviations can result in filled polygons that cannot be filled by NPGS.
- Save/everything via NPGS menu not File/SaveAs
- Filenames can only be so long or else NPGS won't be able to run the file
- Alignment
    - Alignment can be done with just one alignment window containing one alignment mark, but it can only do XY shifts, and not rotation alignment. This is better than trying to use two windows when only one alignment mark was written, however. The window that can't find the mark will cause rotation issues and the alignment will progressively worsen for each time a window can't "see" a mark it is supposed to.
    - Registration (Alignment) marks = Polyfilled Line type 4
        - These are the actual shapes to which one aligns
    - Alignment windows = Line type 0
        - These are the windows in which the SEM scans to find the alignment marks
        - Don't use Polyfill to make these polygons. Just draw them and check to make sure they are solid lines

Necessary software etc:

- One must install the DesignCAD software as well as the NPGS software on the desired computer. There is an NPGS version used to control the SEM (lab version). Make sure to install the office version on the desired computer.

1) Log into Win8 as an Administrator.

2) Install NPGS v9.

3a) Turn off any active virus scanning.

3b) Install DesignCAD LT 2000 into the "\NPGS\DC2000LT" which was created in step 2.

3c) Delete the "\NPGS\DC2000LT\encrypt.exe" file. This file is safe, but it is unnecessary and most virus scanners will incorrectly warn that it is potentially dangerous.

3d) Turn on virus scanning, if disabled in 3a

4) Return to your normal login and set the desktop theme to 'Classic'. This should avoid problems when running DC LT2k.

5) Run NPGS and DesignCAD and check if it works. You may need to set the entire \NPGS directory structure to be accessible in your login.

6) Go to http://support.microsoft.com/kb/917607 and install the Microsoft support for WinHlp32. This allows the popup help in the Run File Editor to work correctly.

- For computers with touchscreens, there is a required touchscreen disable batch file that must be installed in order to run the program successfully. I recommend replacing the NPGS desktop shortcut with a shortcut to this batch file and then changing its icon to the NPGS icon.
    - The batch file is locate under SJBauman Plasmonics/Labs and Procedures/NPGS
- It is a good idea to download some updates from the NPGS website. This may require the help of Nabity in order to gain access to certain files.
    - http://www.jcnabity.com/download.htm

Follow the instructions on the page in order to complete the update that allows for the use of the CheckAll function and other updates. An email from Nabity contained the following regarding the download page:
You can also download the latest update to NPGS v9.1 from www.jcnabity.com/download.htm which will include the new CheckAll.bsc for every supported version of DesignCAD.
Here is the info for downloading the latest release of NPGS.

You can now download the latest update to NPGS v9.1 from www.jcnabity.com/download.htm.

Appendix I: Supplemental Information

I.1 Additional Design Capabilities

The following is a brief discussion of additional potential design capabilities of the nanomasking technique as mentioned in Chapter 6. The images are included in the U.S. patent application number 62/039,337 [124]. The first, Figure I.1.1, depicts nanomasking for the fabrication of structures of differing heights with the same metal. This height variation may provide unique and interesting plasmonic effects, resulting in additional potential uses for the fabrication technique.

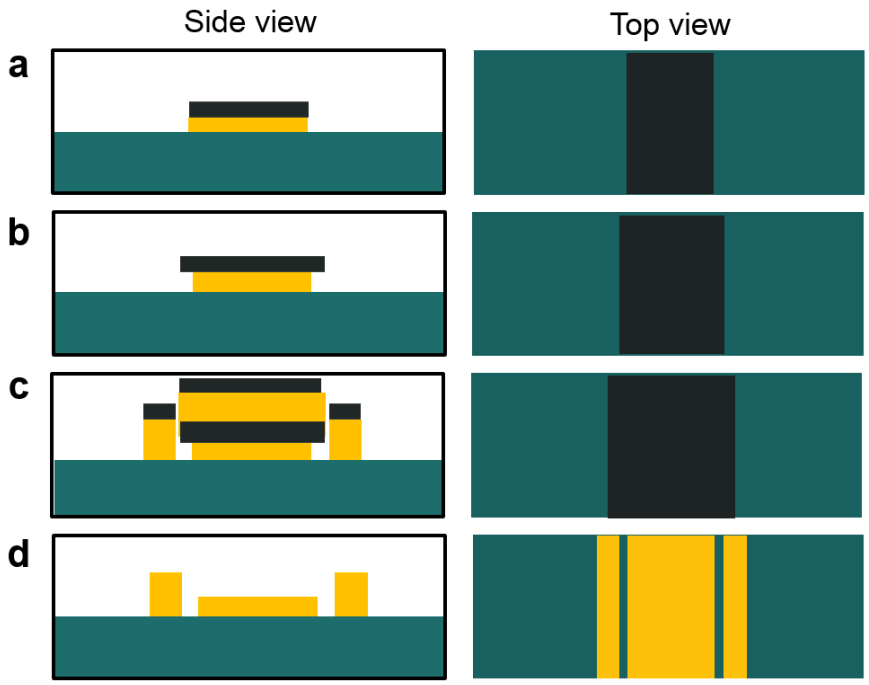

Figure I.1.1: Sketch of the nanomasking process used to create nanogap structures with different heights [124].

The second image, Figure I.1.2, depicts the technique being utilized for the creation of nanogap devices using different metals in subsequent deposition steps. This may allow for unique interactions that would not occur with structures made from the same materials. These

heterogeneous nanodevices will be another demonstration of the versatility of the advanced technique.

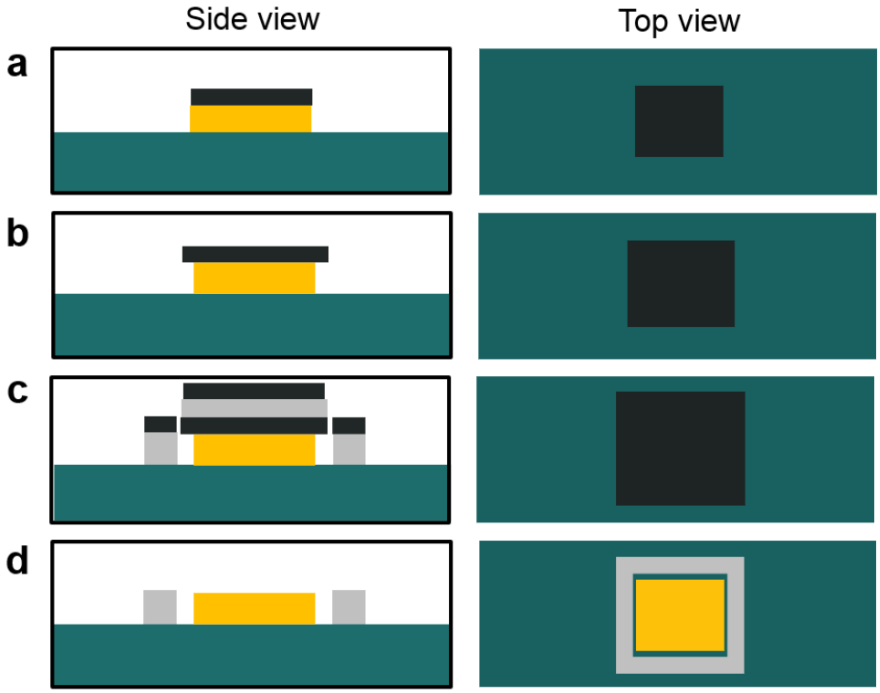

Figure I.1.2: Sketch of the nanomasking process used to create nanogap structures with different materials [124].

The next potential variation of fabrication included in the future work to be tested is a logical extension of the previously mentioned concepts. One might expect that it should be possible to combine height variation and two-material nanomasking. This concept may provide a combination of the unique effects obtained via these two methods alone. A sketch of this variation is shown in Figure I.1.3.

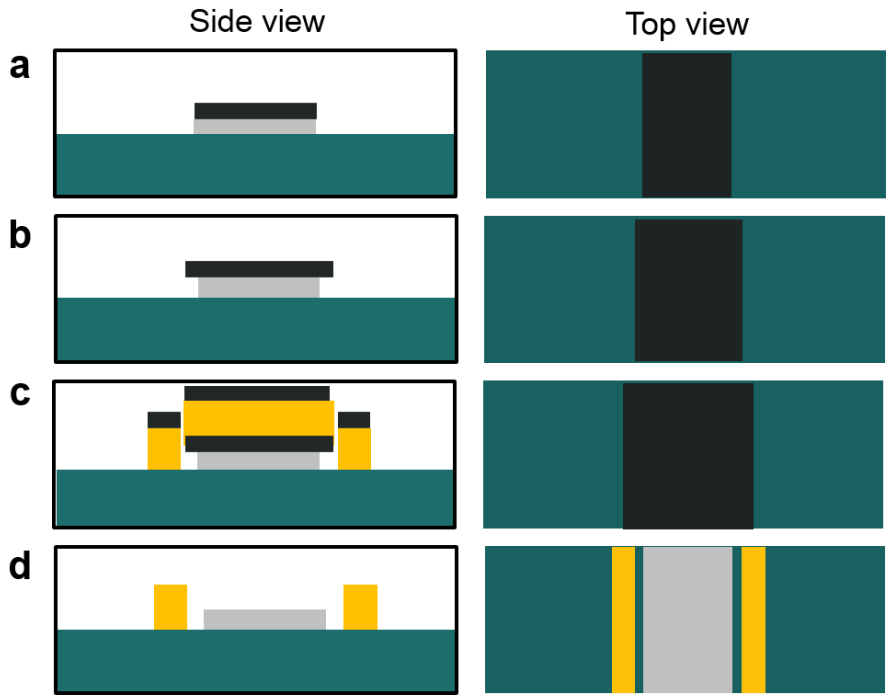

Figure I.1.3: Sketch of the nanomasking process used to create nanogap structures with different heights and materials [124].

As previously stated, these variations remain to be tested for feasibility in the laboratory. Future work in the development of the technique will incorporate tests of these methods.

I.2 Optical Simulation Details

The following is a more detailed description of the parameters used in the creation of the computational electromagnetic simulation for the calculation of the optical enhancement in a gap structure. The data obtained from this simulation is discussed in Section 2.3 and plotted in Figure 2.3.1.

Quoted from Bauman et al. [118],

> The geometry of the device is built in the center of a circular 2D simulation space. This circle is comprised of two layers: the perfectly matched layer (PML) and the far field domain. The far field domain is the inner layer of the circle with a radius of 800 nm. This space, the environment through which the incident electromagnetic wave propagates before and after it interacts with the device, is filled with the material parameters of air with an effective medium of n_{eff} =1.25. This approximates substrate effects the geometry

of which is not included in the model, similar to prior work. The resulting scattered or transmitted light then propagates towards the outer boundary of the far field domain. At this point, the PML absorbs the electromagnetic radiation. The PML is a 300 nm thick layer of the circle that begins where the far field domain ends. The purpose of this is to absorb the light that has already interacted with the device so that it will not scatter back into the simulation space. This provides a truncation point for the computational region and reduces noise, producing accurate results.